DEVELOPMENT OF MOLECULARLY IMPRINTED FLUORESCENCE SENSOR CHIPS

by

Muersha Wusiman

B.A., Istanbul University, 2019

A THESIS SUBMITTED IN PARTIAL FULFILLMENT OF

THE REQUIREMENTS FOR THE DEGREE OF

MASTER OF APPLIED SCIENCE

in

THE FACULTY OF GRADUATE AND POSTDOCTORAL STUDIES

(Chemical and Biological Engineering)

THE UNIVERSITY OF BRITISH COLUMBIA

(Vancouver)

April 2022

The following individuals certify that they have read, and recommend to the Faculty of Graduate and Postdoctoral Studies for acceptance, the thesis entitled:

Development of Molecularly Imprinted Fluorescence Sensor Chips

submitted by Muersha Wusiman in partial fulfillment of the requirements for

the degree of Master of Applied Science

in Chemical and Biological Engineering

Examining Committee:

Dr. Fariborz Taghipour, Chemical and Biological Engineering, UBC
Supervisor

Dr. Vikramaditya G. Yadav, Chemical and Biological Engineering, UBC
Supervisory Committee Member

Dr. Jane Hill, Chemical and Biological Engineering, UBC
Supervisory Committee Member

Abstract

In recent years, molecularly imprinted fluorescence sensors have received significant attention because of their high sensitivity and selectivity. However, the commonly applied liquid-phase molecularly imprinted fluorescence sensing platform has many drawbacks, making it unsuitable for practical in-field applications. In this study, the first of its kind, portable zinc oxide (ZnO)-based molecularly imprinted fluorescence sensor chips were developed to overcome the limitations of liquid fluorescence sensors.

The fluorescence sensing material was prepared with biocompatible ZnO quantum dots (QDs) and tailor-made synthetic receptor molecularly imprinted polymer (MIP). Fluorescence sensor chips were formed using a facile thin-film coating method and the sensor signals were detected with a portable fluorescence detector. The combination of these materials enabled the development of green molecularly imprinted fluorescence sensor chips that are not restricted by complex immobilization process and detection procedure.

A frequently studied herbicide 2,4-dichlorophenoxyacetic acid (2,4-D) was targeted at the first stage of fluorescence sensor development to examine the detection ability of ZnO QDs, the performance of the physical immobilization method, and the reliability of the portable detector. After obtaining a high sensor sensitivity (0.0233) and a good linear correlation (0.98) for 2,4-D measurement, efforts were made to adapt the sensing material to detect algae bloom toxin microcystin-LR (MCLR) to prove the capability of the sensor to perform water analysis. The solid fluorescence sensor was able to distinguish MCLR concentration as low as 1µg/L with good selectivity. Finally, to further demonstrate the flexibility of the developed system, biological analyte lactate was targeted for developing bio-sensor chips. Sensor selectivity was optimized by

employing two different MIPs to compete with the commonly used enzyme-based sensors. The final sensor achieved a sensitivity of 0.0217 with a correlation coefficient of 0.97 for lactate in phosphate-buffered saline (PBS). The ability of the sensor to exhibit a linear sensing range for 0–30 mM of lactate with good selectivity indicated its applicability for sweat analysis.

The high performance, target-flexibility, and portability of the fluorescence sensor chips demonstrated in this study can pave the way for developing lab-on-chip image-based sensing devices for environmental analysis and health monitoring applications.

Lay Summary

Determination of drinking water safety and monitoring of body function can be realized with fluorescence sensors. However, the limitations on the workspace, equipment and operators are limiting the commonly used liquid-phase molecularly imprinted fluorescence sensors for their practical in-field applications. This study aimed to develop a new solid sensing platform that incorporates an easy yet robust thin-film coating with a portable fluorescence detector to overcome the drawbacks of liquid sensors. The viability and the potential of the proposed system were revealed with the successful measurements of herbicide 2,4-dichlorophenoxyacetic acid (2,4-D), algae bloom toxin Microcystin-LR (MCLR) and biochemical lactate. The wide-range applicability, portability, and easy operation method of the sensing platform will facilitate the application of fluorescence sensors in real life for various purposes.

Preface

This research presented here was conducted under the supervision of Professor. Fariborz Taghipour in the Photo-reaction Engineering research group in the Chemical and Biological Engineering (CHBE) Department at the University of British Columbia (UBC). I, Muersha Wusiman, was responsible for conducting the literature review, identifying the knowledge gap, constructing and evaluating hypotheses, defining objectives, designing experimental protocols, performing experiments, compiling and interpreting results, and writing this thesis. The followings are the list of publications from this project in academic journals, to the date of submitting this thesis:

A version of **CHAPTER 3** will be submitted to a scientific journal:

- Muersha Wusiman and Fariborz Taghipour, Development of Solid-Phase Molecularly Imprinted Fluorescence Sensor for the Detection of Organic Contaminants in Water.

A version of **CHAPTER 4** will be submitted to a scientific journal:

- Muersha Wusiman and Fariborz Taghipour, Solid-Phase Molecularly Imprinted Fluorescence Sensor for Lactate Measurement in Sweat.

Table of Contents

List of Figures

List of Symbols

Roman		
C	Concentration	Mol lit-1
F	Fluorescence intensity	a.u.
Ksv	Stren–Volmer constant	Lit Mol-1
S	The slope of the calibration curve	Lit Mol-1
Greek		
σ	Standard deviation	Unitless

List of Abbreviations

2,4-D	2,4-Dichlorophenoxyacetic acid
2,4-DCP	2,4-Dichlorophenol
AA	Ascorbic acid
APTES	(3-Aminopropyl)triethoxysilane
APTES-MIP	Silica-based imprinted polymer
ATP	Adenosine triphosphate
CTAB	Cetrimonium bromide
DI	Distilled water
ELISA	Enzyme-linked immunosorbent assay
FT-IR	Fourier transform infrared spectroscopy
GC	Gas chromatography
Glyphosate	N-(phosphonomethyl)glycine
HPLC	High-performance liquid chromatography
IUPAC	International Union of Pure and Applied Chemistry
MCLR	Microcystin-LR
MCPB	4-(4-Chloro-2-methylphenoxy)butanoic acid
MIP@Pin-BAc	Molecularly imprinted poly(indolylboronic acid)

MIPs	Molecularly imprinted polymers
MOH	Metal hydroxide
MS	Mass spectroscopy
NIPs	Non-imprinted polymers
PBS	Phosphate-buffered saline
PET	Photo-induced electron transfer
PNP	Para-nitrophenol
QDs	Quantum dots
RET	Resonance energy transfer
SERS	Surface-enhanced Raman scattering
TEM	Transmission electron microscope
TEOS	Tetraethyl orthosilicate
UA	Uric acid
UV	Ultraviolet
UV-LED	Ultraviolet light-emitting diode
UV-VIS	Ultraviolet-visible spectroscopy
WHO	World Health Organization
ZnO@MIP	Molecularly imprinted fluorescence sensor incorporated with ZnO quantum dots
ZnO@PMIP	Molecularly imprinted porous fluorescence sensor incorporated with ZnO quantum dots

Glossary

Al^{3+}	Aluminum ion
Cd^{2+}	Cadmium ion
CdS	Cadmium sulfide
CdSe	Cadmium selenide
CdTe	Cadmium telluride
Cu^{2+}	Copper ion
$FeCl_2$	Iron (II) chloride
H_2O_2	Hydrogen peroxide
Hg^{+}	Mercury ion
K	Potassium
Li	Lithium
LiOH	Lithium hydroxide
Na	Sodium
NaOH	Sodium hydroxide
Pb^{2+}	Lead (II) ion
Si	Silicon
ZnO	Zinc Oxide

Acknowledgements

I would like to express my enduring gratitude to all who helped, supported, and encouraged me. First and foremost, I would like to thank my supervisor, Dr. Fariborz Taghipour, who has selflessly offered support, mentorship, guidance, inspiration, and encouragement during my studies. I thank him for giving me the opportunity to learn, to grow and to realize my dream; I am especially grateful for his patience and motivation that allowed me to cope with the challenges and improve myself under his supervision.

I would also like to express my sincere gratitude to Dr. Hill and Dr. Yadav, who have served on my thesis examination committee.

I would like to thank my friends and colleagues, in particular Mahyar Montazeri, Nastaran Taleghani, Sahar Sakhie, and Ghazal Ghurbani, Shalina Nurly for their continuous input and immense assistance, friendship, and support. Also, I would like to thank the current and previous members of the Photo-reaction Engineering research group at CHBE.

Last, but certainly not least, my special thanks to my mother who has always inspired me with her hard work and resilience; my father who has dedicated his life to the family and has always encouraged me to embrace the challenges; my sister who has taught me a different perspective of life and has always kept my company. Their support, prayers and love were always with me throughout all these years, providing the fuel for me to keep on fighting. I am forever in debt for their love and support.

The research presented in this thesis was supported by the Natural Sciences and Engineering Research Council (NSERC) of Canada.

To the almighty GOD for protection, strength, health, and guidance.

To my parents, my sister, and my friends; for all sacrifices.

And to all the people who suffer from genocide, human rights violation, and oppression, may GOD help us all.

Chapter 1: Introduction

1.1 Sensors

Sensors can be defined as devices that produce signals for detection and quantification purposes. There are three basic elements of sensors: (i) recognition elements that bind with the target with specificity, (ii) transducers that convert the binding to readable signals, (iii) detectors that can read, record, and convert the signal generated by the transducer to meaningful information. The purpose of sensor development is to detect the target with an accuracy comparable to sophisticated equipment while overcoming their limitations.

Sensors can be classified according to a few aspects. For example, according to the purpose, sensors can be sorted as chemical, biological and physical sensors; according to the type of transducer, sensors can be classified as electrical, optical, electrochemical, mechanical, and thermal sensors; according to the receptor molecules sensor can be categorized as enzyme-based, antibody-based or synthetic receptor-based sensors. The choice of the receptors and the transducer are largely depending on the target and the purpose of detection; different combinations can be made to fulfill different needs.

1.2 Fluorescence Sensors

Fluorescence sensors belong to the family of optical sensors that generate luminescence signals. Luminescence is defined by the International Union of Pure and Applied Chemistry (IUPAC) as the emission of radiation from an electronically or vibrationally excited species not in thermal equilibrium with its environment.[1] Photoluminescence is the light emission with the absorption of photons. There are two types of photoluminescence: fluorescence and

phosphorescence; fluorescence occurs when the emission takes place shortly after the photoexcitation and stops when the excitation source is switched off whereas phosphorescence shows a delay in the emission process and continue to emit light after the photoexcitation is seized.[2]

Fluorescence is commonly used for assays, in vivo, in vitro imaging, chemical and biological sensing. The sensing process with fluorescence involves the interaction between the analyte and the fluorescence probe that either decreases the fluorescence intensity by quenching mechanism or increases the fluorescence intensity by removing a pre-existing quenching effect. Both the reduction and the enhancement in the fluorescence intensity of the fluorescence probe are proportional to the concentration of the analyte so the changes in the fluorescence intensity can, in turn, be used to calculate analyte concentration.[3] Measurements using fluorescence emission provide a few advantages such as easy detection method, high sensitivity, high resolution and non-destructive detection.[4]

1.2.1 QDs

Quantum dots (QDs) are semiconductor crystalline nanomaterials comprised of hundreds to thousands of atoms. In contrast to the bulk semiconductors, QDs have diameters of 1–10 nm. This small size imparts QDs with unique electrical and optical properties by the quantum confinement effect. Upon excitation, QDs generate electron-hole pairs and emit fluorescence light upon their recombination. When the size of the QDs changes, the bandgap also varies inverse proportional to the size and leads to the emission of various fluorescence colours (Fig. 1-1).[5,6] Apart from size-tunable bandgap, bright emission, broad excitation and narrow emission band, resistivity to photobleaching and chemical degradation made QDs more favourable than organic dyes to develop fluorescence sensors. Compared to QDs, organic dyes suffer from low quantum yield,

short fluorescence lifetime and little resistivity to the chemical environment which are critical factors when designing fluorescence sensors.

Quantum confinement was observed for the first time with CdS nanocrystal in 1983.[7] Until today, Cd-based semiconductors such as CdS, CdSe, CdTe are still the most commonly used QDs. The wide-range application of these Cd-based QDs is mainly due to the established synthesis process and standardized characterization protocols. The high demand facilitated the commercialization of various Cd-based QDs for sensing applications.[4] However, the negative impact of these QDs on the environment and health is causing a shift of research attention from Cd-based QDs.[8]

Zinc oxide (ZnO) QDs are desirable candidates for new generation fluorescence sensor development with biological and environmental compatibility. The wide bandgap and large exciton binding energy enable ZnO QDs to be one of the brightest emissive QDs with a quantum yield (the ratio of the number of photons emitted to the number of photons absorbed) of up to 60%.[9] ZnO QDs can be easily prepared by sol-gel process using zinc precursor and metal hydroxide (MOH) solution. The emission colour of the ZnO QDs can be tuned by varying the ratio of zinc precursor to MOH,[9] the choice of metal hydroxide (Na, K, Li),[10] and the selection of the solvent (methanol, ethanol and hexanol).[11] Although, ZnO nanoparticles have been exhaustively exploited for light-emitting devices, photocatalytic reactions, solar cells and gas sensors, ZnO QDs are rarely used to develop fluorescence sensors. The employment of ZnO QDs as the fluorescence unit could open up new opportunities for the development of green fluorescence sensors.

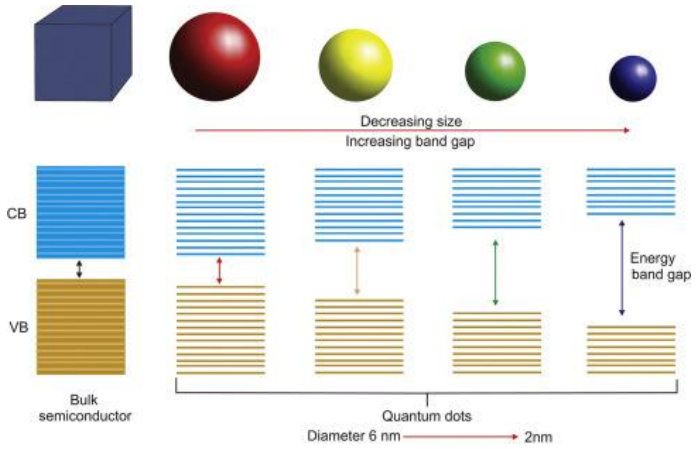

Figure 1-1: schematic representation of the valance band and conduction band structures of bulk molecules and QDs in various sizes, Reprinted and adapted with permission from Sumanth Kumar, D.; Jai Kumar, B.; Mahesh, H. M. Quantum Nanostructures (QDs): An Overview. *Synthesis of Inorganic Nanomaterials* 2018, 59–88. Copyright © 2018 ELSEVIER.

1.3 Receptors

Receptors are important parts of sensors that can recognize and bind with the target molecule; the binding process would trigger the transducer to generate sensor signals. Receptors are responsible for the accuracy of the sensors by showing high selectivity to the target molecule that eliminates false-positive and false-negative responses. Enzymes, antibodies and aptamers are the commonly used biological receptors. Enzymes are proteins that catalyze chemical reactions. Their high selectivity and capability to facilitate chemical reactions have made them one of the most popular receptors for sensor development. Antibodies are proteins produced by the immune system that are responsible for recognizing and neutralizing harmful substances called antigens. Antibodies are renowned for their high target recognition ability; their affinity to the antigen is often described as a lock and key recognition. Since both enzymes and antibodies are natural receptors that are not available for every target molecule, efforts were made to expand the

applicability of biological receptors. Aptamers are synthetic biological receptors consisting of oligonucleotides or peptides. The sequence of the nucleotides or peptides is selected experimentally by their binding capability to a specific target molecule. Even though aptamers extended the application range of bioreceptors, they are expensive to acquire, difficult to produce and sensitive to environmental conditions. Furthermore, the incorporation of the biological receptors with transducers greatly impairs their activity thus reducing the sensor performance.

1.3.1 MIPs

To create synthetic chemical receptors that mimic the target recognition ability of biological receptors, molecularly imprinted polymers (MIPs) were developed. These synthetic polymers are templated throughout polymerization during which they gain target recognition. Because of the similar recognition mechanism and performance of MIPs to antibodies, they are often described as synthetic antibodies. Apart from the comparable specificity and selectivity to the biological receptors, MIPs offers advantages of high stability, low cost and wide-range applicability.

As depicted in Fig. 1-2, the imprinting process contains three steps: (1) polymerization process of the monomer, cross-linking agent and the template (target) molecule, (2) binding between the template molecule and the monomer during the polymerization (3) formation of template-specific molecular cavities (imprinted sites) with the removal of the template molecules from the polymer. When the MIP is exposed to the template (target) molecule, they can re-bind to the imprinted sites that match their molecular size, shape and functional group.[12] Since the selectivity of MIPs relies on the imprinted sites formed by the addition of the target molecule during the polymerization, MIPs are potentially applicable to recognize any type of molecule that does not inhibit the polymerization and stays stable under the polymerization condition. The key

is to combine a suitable monomer and cross-linking agent with the target molecules so the molecule can be included in the polymer.

MIPs have been exploited in numerous applications such as drug delivery,[13] solid-phase extractions,[14,15] chemical and biological reagent purification,[16–18] but its main application area is in sensor development. MIPs have been incorporated with electrical, electrochemical, quartz crystal microbalance, fluorescence, and surface plasmon transducer and have been widely used in the detection of pesticides,[19–21] gases, [22–24] biochemicals,[25–27] pharmaceuticals, [28–30] and many more.

Figure 1-2: Schematic representation of imprinted sites formation process including the initiation of the polymerization, binding of the template to the monomer and the formation of the imprinted sites. Reprinted and adapted with permission from Belbruno, J. J. Molecularly Imprinted Polymers. *Chemical Reviews* 2018, *119* (1), 94–119. Copyright © 2018 American Chemical Society.

1.4 Molecularly Imprinted Fluorescence Sensors

The combination of fluorescent material and the MIPs forms molecularly imprinted fluorescence sensors (MIFSs). The formation of MIFSs can be realized by adding the fluorescent molecule (e.g. QDs) during or after the polymerization process; the final sensing material exhibit the high sensitivity of the fluorescence molecules and the high selectivity, target flexibility of the

MIPs. Benefiting from these advantages, MIFSs have been successfully applied for the detection of (1) ions including Hg^{+}, Cu^{2+}, Pb^{2+}, Al^{3+},[31–33] (2) water contaminates including 2,4-D, bisphenol A and atrazine,[34–36] (3) biomarkers like dopamine, glucose and Hepatitis viruses,[37–39] (4) pharmaceutical and food additives like aspirin, Rhodamine 6G and melamine,[40–42] and many more.

Despite the advantages, the real-life application of the MIFSs is not as well exploited as the electrochemical sensors. One of the major drawbacks of the MIFSs reported in the literature is the lack of a facile and robust method to transform the liquid sensing materials to the solid phase, so the common detection is realized in the liquid phase that is restrained by the workspace, location and the detection equipment. In this research, I present a straightforward way to form MIFS chips that address the abovementioned challenges. The proposed approach, the first of its kind, has the potential of forming a portable, sensitive, selective, and target-flexible fluorescence sensing platform.

1.5 Thesis Layout

This research was conducted through theoretical and experimental work to achieve the development of MIFS chips. This thesis provides information on the theory, methodology, experiments, discussion and conclusion of the research as well as some future recommendations on the subject. The structure of the thesis is as follow:

Chapter 1 is the introduction on the fluorescence sensors and molecularly imprinting technology which is the basis of this research.

Chapter 2 presents the literature review of the working mechanism, applications and challenges of the existing molecularly imprinted fluorescence sensors. The knowledge gap is identified, and research objectives are stated based on the knowledge gap.

Chapter 3 represents the development of the MIFS chips to detect water contaminants 2,4-D and Microcystin-LR (MCLR). This chapter reports the first combination of a physical coating technique with a portable spectrophotometer to obtain portable MIFS chips. The fluorescence sensors were first developed to detect 2,4-D, a commonly studied target molecule for fluorescence sensor development. Then, efforts were made to adapt the sensing material to a new target MCLR to demonstrate the target flexibility of the system. Finally, the advantages and capabilities of the developed system were established by comparing them to the commonly used liquid fluorescence sensors.

Chapter 4 represents the attempts of developing MIFS chips for lactate detection. Two different monomers were used to form lactate MIFSs to compete with the recognition of enzyme-based sensors. The sensor was first studied with lactic acid in deionized (DI) water samples to demonstrate the capability of the sensor to measure lactic acid. Then, efforts were made to detect lactate in phosphate-buffered saline (PBS) to evaluate the applicability of the sensor to be used for sweat analysis.

Chapter 5 includes a summary and the conclusions of the research as well as future recommendations for the fluorescence sensors development. The demonstration of an easy, cost-effective, and portable fluorescence detection system developed in this thesis is expected to open new opportunities for portable fluorescence sensors.

Chapter 2: Literature Review

2.1 Fluorescence Sensors

Fluorescence sensors belong to the family of optical sensors that detect a target molecule with the changes in the fluorescence intensity. Fluorescence-based sensing in general offers a short response time, high sensitivity and straightforward detection method compared to the commonly used electrochemical sensors. Fluorescent materials such as QDs, metal-organic framework, carbon materials, rare-earth materials and fluorescent proteins can be used as the transducer of fluorescence sensors. Target detection is achieved by "fluorescence turn off" which is the reduction in the fluorescence emission through quenching, "fluorescence turn on" which is the enhancement in the fluorescence intensity by removing a quencher, and "ratiometric fluorescence signal" which is the simultaneous existence of two or more fluorescent molecules in different wavelength and each subject to a turn on or turn off signals.

Among fluorescent molecules, QDs are more favourable for sensor formation. Diverse combinations of elements from II-VI or III-V groups and carbon materials can be used to prepare QDs. The most commonly used and commercialized QDs are Cd-based QDs like CdTe, CdSe and CdS with the established synthesizing approach and standardized protocols. However, the Cd^{2+} ions released from this type of quantum dots are raising concerns because of their high toxicity to the cells and tissues. It was reported that there is a direct relation between cellular death by DNA damage and the amount of released Cd^{2+}. The accumulation of the Cd-based QDs on the cell surface can also impair cell functions. As a result, their wide range of applications and commercialization are under debate.[43,44] To replace the Cd-based QDs, "green" QDs have been developed and used for fluorescence sensors. For example, carbon QDs, graphene QDs and ZnO

QDs are the environmentally and biologically friendly alternatives that offer a quantum yield comparable to that of Cd-based QDs'.

2.1.1 Fluorescence sensor working mechanism

To develop a fluorescence sensor, the emissive molecule must generate some changes in the fluorescence signal when introduced to the target molecule; as mentioned above, these can be turn on, turn off and ratiometric signals. Independent of the signal type, fluorescence sensors follow two main working mechanisms: resonance energy transfer and photoinduced electron transfer. The three types of sensor signals shown to the target molecules are based on these working mechanisms and shaped by the environmental conditions.

2.1.1.1 Resonance energy transfer

The Resonance energy transfer (RET) occurs when there is an overlap between the donor's (fluorescence molecules') emission band and the acceptor's (quencher's) absorption band. In the fluorophore, the electrons on the highest-occupied orbital absorb ultraviolet (UV) radiation and are elevated to the lowest-unoccupied orbital (Fig. 2-1A). When the energy gap overlaps between the fluorophore and the quencher, the excess energy from the fluorophore is absorbed by the quencher instead of being released as visible light, so the fluorescence intensity of the molecule is reduced. Apart from the spectral overlap, RET requires a distance of 30 – 60 Å between the fluorophore and the quencher and a specific orientation between them.[45,46]

2.1.1.2 Photoinduced electron transfer

Photoinduced electron transfer (PET) takes place when there is a complex formed between the fluorophore and the quencher. Similar to RET, the electrons of the fluorophore on the highest-occupied orbital absorb UV radiation and are elevated to the lowest-unoccupied orbital; when there is a complex exist, the excited electrons are directly transferred to the complex forming excess electrons on the complex (Fig. 2-1B). These excess electrons are then returned to the fluorophore's highest-occupied orbital and the excess energy of the excited electrons is consumed during the transition. Because the excited electrons return to their ground state by means of the complex molecule instead of a direct route, the emission of the visible light is inhibited. The inhibition reduces the fluorophore's emission intensity, and the degree of quenching is dependent on the amount of transferred electrons.[47]

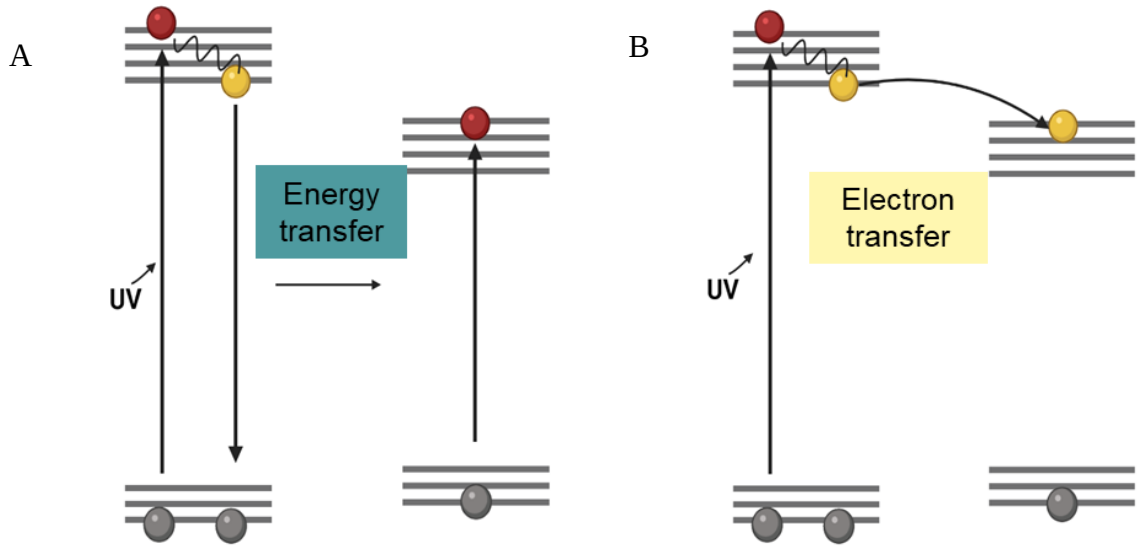

Figure 2-1: Molecular orbital schematic for (A) resonance energy transfer and (B) photoinduced electron transfer working mechanisms of fluorescence sensors.

2.2 Molecularly Imprinted Fluorescence Sensors

Fluorescence sensors are often combined with receptor molecules such as enzymes, antibodies, aptamers and MIPs to increase sensor selectivity and specificity. Enzymes, antibodies and aptamers are biological receptors used for fabricating sensors for biochemical, clinical and environmental applications.[48–51] Despite their capability in molecular recognition, biological receptors suffer from low stability and short lifetime; the slightest change in the temperature, PH or chemical environment may reduce their activity. Moreover, bioreceptors are accompanied by high cost and difficulties to combine with other materials; the immobilization or conjugation process of bioreceptors results in significate loss in the biomolecular activity.

In comparison, the MIFSs formed with the combination of fluorescent molecules and synthetic chemical receptor MIPs can offer more robust target recognition. The recognition ability of MIPs is originated from the imprinted sites that are formed by the polymerization of functional monomers in the presence of template molecules. These imprinted sites match the target molecule with their functional group, molecular size and shape thus impart MIPs with recognition ability comparable to biological receptors. One of the major advantages of MIPs is their wide-range applicability; since the selectivity is obtained by the templated polymerization, the alteration of the template with the right combination of the monomer can tailor the recognition of the MIPs to the specific target molecule.

2.3 MIFS Sensor Detection Means

The MIFS sensors are used in the liquid or solid phase for target detection. For liquid sensors, the synthesized sensing materials are dissolved in an appropriate solvent for fluorescence measurements. The liquid MIFSs are extensively studied and applied for the detection of various

materials with high sensitivity and selectivity. However, there are a few disadvantages regarding liquid phase detection: (1) liquid sensors require a complex preparation process, (2) samples are diluted when added to the liquid phase causing a limitation in the mass transfer efficiency, (3) constant mixing is required to prevent sedimentation which might cause an experimental error, (4) signal read-outs are dependent on sophisticated fluorescence spectrophotometers, (5) liquid spills and mishandling of cuvette may lead to experimental errors. Therefore, the liquid sensors are limited for lab use only.

Solid-phase fluorescence sensors are formed by immobilizing the liquid sensing materials on solid substrates. Transformation to the solid phase makes the handling of the sensing material and the detection of the target molecules easier than the liquid phase. The thin sensing layer can enhance the surface reaction that enables a short response time without any external heating or agitation. More importantly, solid fluorescence sensors can be used with little sample preparation and detected via portable spectrophotometers or cellphones rather than the large size, expensive spectroscopies thus realizing the goal of on-site, real-time detection.[52] Despite the great features, the majority of MIFSs sensors are used in the liquid phase because of the challenges with the transformation of the liquid sensing materials to the solid phase.

2.4 Solid MIFS Formation Method

Developed methods for immobilizing sensing layers can be classified into two main categories: physical immobilization and chemical immobilization. Chemical immobilization requires chemical bond formation between the sensing material and the solid substrate through covalent binding or cross-linking; physical immobilization includes adsorption or entrapment of the sensing material to the solid substrate without any chemical bond.

2.4.1 Chemical Attachment

The chemical immobilization method, especially covalent attachment is mainly used to obtain solid MIFS. Chen et al. developed MIFS test strips by the binding between MIP coated QDs and the methacrylate polyimide substrates.[53] The polyimide substrate was first functionalized with methacrylate groups which is the same functional group that exists on the MIPs-QDs composites, then the methacrylate groups on the MIPs and the solid substrate were polymerized again to immobilize the MIPs. Hartz et al. immobilized the MIPs to a quartz chip using molecular glue; [54] the quartz substrate was first treated with piranha and incubated in polyethylene imine for 1 h. The surface-modified quartz was then immersed in MIPs solution for another 1 h to glue the sensing material to the quartz surface. Paper is another popular substrate to immobilize fluorescence sensing materials. The most prevalent method is to functionalize paper with amino functional groups, then use the covalent binding of the amino groups with the carboxyl group of the QDs (e.g., CdTe) to link the QDs to the paper.[32,55,56] The polymerization is then conducted on the paper surface with an appropriate monomer and cross-linking agent. Solid fluorescence sensors formed this way are time-consuming and labour-intensive; the covalent linking process requires a long period (e.g., 12 h) of immerging the paper to the QDs solution and each of these papers requires a separate washing process to eliminate template molecules. Moreover, the selection of QDs is limited to Cd-based QDs that are most available for carboxyl functionalization and the selection of solid substrates is reduced to papers that are more prone to be functionalized. These limitations considerably hinder the practicality of sensors prepared by the covalent linking process for sensing applications.

2.4.2 Physical Attachment

Contracting the chemical attachment method, the physical coating does not require a bound formation, so the attachment process is more straightforward and time-efficient. The typical physical coating includes drop coating, spray coating, spin coating, and blade coating. Drop coating is the easiest coating method that only needs a drop of the material on the substrate, the solid layers are then formed by evaporating the solvent (Fig. 2-2A). Drop coating was used to developed solid-phase MIFS for detecting sesamol in sesame oil.[57] Despite the easy procedure, drop coating might resolve in a non-uniform layer with a weak attachment which leads to inconsistency of the sensor. Spray coating uses a spray of particles or droplets to deposit material onto a substrate (Fig. 2-2B). The formed coating layers exhibit a strong bonding and a uniform layer; this technique can be applied for coating various materials in either hot or cold conditions. It is commonly used for obtaining a protection layer against erosion, fabricating cathodic or anodic materials for electrochemical cells and producing catalytic beds. The disadvantage of spray coating is the need for repeated spraying to obtain optimum layer thickness. Spin coating is a procedure to deposit a uniform and thin layer on a solid substrate. The deposition process is conducted while the solid substrate is spinning at a low speed, and after the deposition, the speed is increased to spread the material by centrifugal force to form a uniform layer, as depicted in Fig. 2-2C. Spin coating is often used for the deposition of nanomaterials and semiconductors including carbon nanotubes, QDs, and graphene, to generate electrodes, solar cells, thin-film transistors and sensors. Like spray coating, the disadvantage of spin coating is its lack of material efficiency; 95– 98% of the material is splashing off from the surface and only 2–5 % of the material is attached according to the rotation speed. Blade coating is a technique used to form thin films with adjustable thickness. As shown in Fig. 2-2D, a sharp blade is placed at a fixed distance from the solid substrate and the

coating solution is placed in front of the blade. With the addition of the coating solution, the blade is moved in-lined with the surface to create a wet film. Then, the substrate is heated to evaporate the solvent. Blade coating works best with an automated system that regulates the distance between the blade and the substrate which is critical for the thickness and the distribution of the material. It is open to experimental errors when operated manually.

Using physical coating methods to generate films or layers of sensing materials can effectively reduce the time and workload compared to the chemical attachment method and provide features such as adjustable coating area and thickness. Since there is no need to create chemical bonds, the restrictions on the solid substrates and functional groups are lifted so the physical methods are flexible on both the solid substrates and the deposition materials. However, despite the aforementioned advantages of the physical coating techniques, there are no examples of using them except for drop coating to develop solid-phase fluorescence sensors. The wide range of applications of these physical coating methods in the area of sensor development, solar cells formation, and catalyst preparation indicates that they are viable methods for immobilizing chemical materials without impairing their properties. Therefore, they have a great potential to be applied to form solid-phase MIFSs.

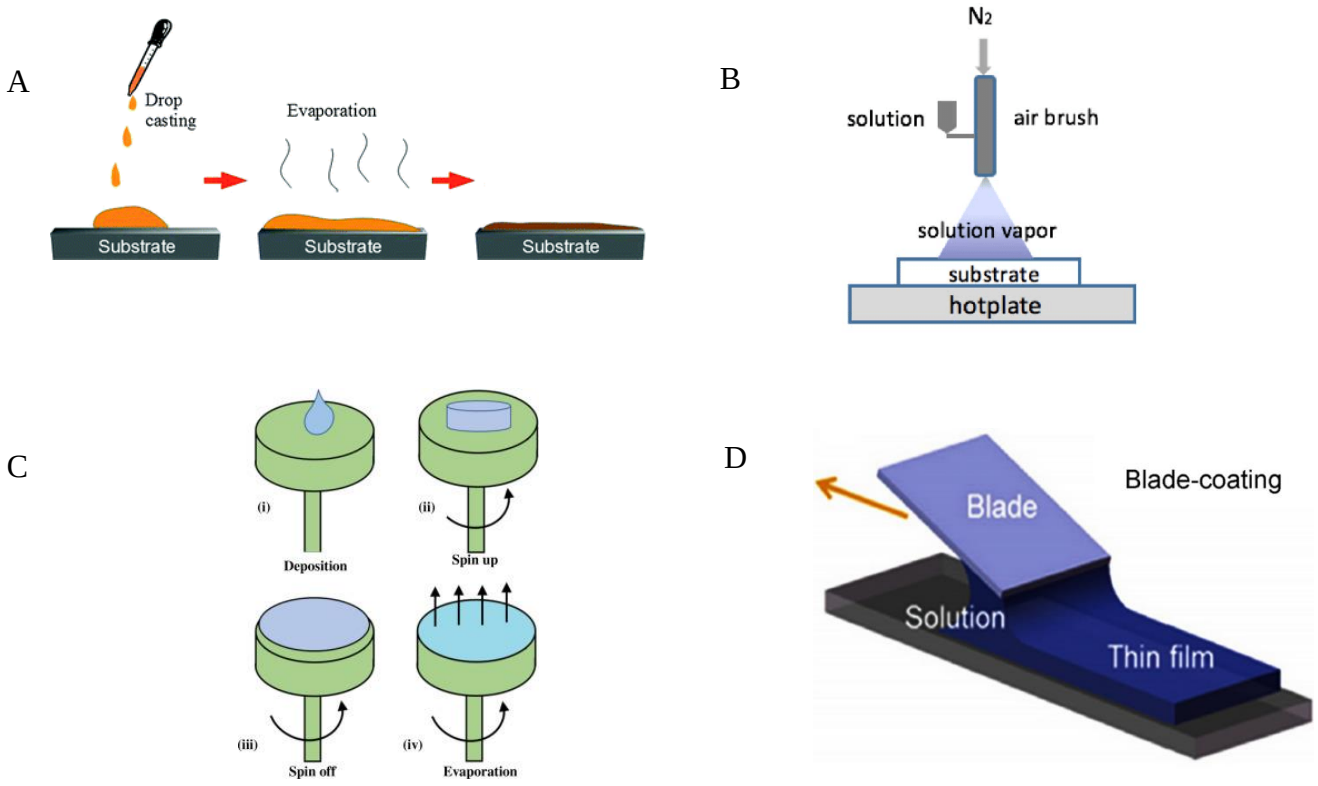

Figure 2-2: Schematic representation of various physical coating methods including drop coating (Kajal, P.; Ghosh, K.; Powar, S. Manufacturing Techniques of Perovskite Solar Cells. *Energy, Environment, and Sustainability* 2018, 341–364. Copyright © 2018, Springer Nature Singapore Pte Ltd.), spray coating (Jha, S.; Wang, X. H.; Faber, H. Touch Sensor Application of Spray Deposited ZnO Films. *IEEE International Symposium on Industrial Electronics* 2017, 1412–1416. Copyright © 2017, IEEE), spin coating (Yilbas, B. S.; Al-Sharafi, A.; Ali, H. Surfaces for Self-Cleaning. *Self-Cleaning of Surfaces and Water Droplet Mobility* 2019, 45–98. Copyright © 2019 Elsevier Inc), and blade coating (Abbas, Z.; Khaliq, S. Variation of Coating Thickness in Blade Coating Process of an Upper-Convected Jeffery's Fluid Model. *Iranian Polymer Journal (English Edition)* 2021, *1*, 1–13. Copyright © 2021, Iran Polymer and Petrochemical Institute).

2.5 2,4-D Detection

2,4-D is a well-known plant growth regulator that controls the spread of broadleaf weeds. The high selectivity and promising endocrine-disrupting activities shown by 2,4-D have made it one of the bestselling herbicides. Due to its wide-range application and water-solubility, 2,4-D is often detected in water resources and dairy products.[58,59] 2,4-D can be absorbed through the skin, inhalation and gastrointestinal tract and cause endocrine-disrupting activities, lymphomas and certain cancer.[60,61] The World Health Organization (WHO) has limited the maximum concentration of 70 μg/L as the maximum permissible concentration of 2,4-D in drinking water.[62]

The wide range of use and the harm for human health and economic development have made 2,4-D a popular target for sensor development. Various sensors including electrochemical sensors, immunoassays, surface plasmon sensors and fluorescence sensors have been reported for the highly sensitive and selective measurements of 2,4-D.[34,63–70] For measurements via fluorescence sensors, the mesoporous fluorescence sensor developed by Mengfan Jia et al.[71] and the ratiometric fluorescence sensor developed by Xiaoyan Wang et al.[72] showed high sensitivity and selectivity in detecting 2,4-D. However, both sensors were confined to liquid phase detection. Microfluidic chips developed by Zhong Zhang et al.[34] were capable of performing field tests, but the sensor sensitivity was lower than that of the liquid sensors and the immobilization process was too complicated to be widely applied. Previous successful measurements of 2,4-D with fluorescence sensors formed the foundations for fluorescent detection and the limitations of these studies are demanding for more efficient and sensitive 2,4-D measurements in the solid phase.

2.6 MCLR Detection

MCs are a group of cyclic heptapeptides belonging to the family of cyanobacterial toxins that are produced during the period of algae bloom formation.[73,74] MCLR is a type of MCs with five invariant amino acids and leucine and arginine as the variable amino acids. Due to the cyclic structure consisting of seven amino acids, the volume of MCLR can reach about 2.63 nm^3 with a molecular length of 1.9 nm.[75–77] The acute toxicity and high water solubility made MCLR one of the great dangers for humans, aquaculture and wildlife. It was reported that about 23 million salmon in Chile[78] and a few hundred elephants in northwest Botswana[79] died because of cyanobacteria. Evidence showed that MCs can cause damage to organs including the kidneys, lungs, reproductive system, and brain.[80–83] As a result of these significant health impacts, the WHO established a limit of 1 µg/L of MCLR in drinking water.[84]

The current detection of MCLR relies on analytical techniques such as high-performance liquid chromatography (HPLC),[85,86] mass spectroscopy,[87] and enzyme-linked immunosorbent assays (ELISA)[88,89]. Even though these techniques provide accurate MCLR amount determination but the requirements for expensive laboratory equipment, time-consuming preparations and high cost are limiting their wide-range application and continuous monitoring of MCLR concentration. Therefore, cost-effective, convenient, and highly responsive sensors are needed for MCLR measurement. Sensors reported for the detection of MCLR contain receptors like antibodies, aptamers and MIPs and the transducers include electrical, electrochemical, optical materials.[90–97] However, there is only one study that reported the successful detection of MCLR with a fluorescence sensor;[76] the study revealed the advantages of using fluorescence sensors for MCLR analysis but required the preparation of liquid test samples and the use of fluorescence spectroscopy equipment. This result shown by Qi et al.[76] is encouraging for the development of

portable fluorescence sensor chips to monitor MCLR concentrations with a convenient visual method.

2.7 Lactate Detection

Lactate is a biochemical formed by anaerobic glycolysis and its concentration is highly relevant for several important reasons.[98] For athletes, the concentration of lactate is used to evaluate their performance by tracking the adenosine triphosphates (ATPs) generating pathway;[99,100] For the patient in intensive care, high lactate concentration is linked to the possibility of shock, kidney, liver diseases and heart failure.[101–103] For manufacturers, lactate concentration is measured to assess the quality of food products such as dairy, alcoholic and non-alcoholic beverages.[104] Despite the various benefits of monitoring lactate concentrations, lactate detecting equipment is not as well-developed as glucose detectors.

Various methods, including HPLC, electrophoresis and biosensors have been used for lactate measurement.[105–108] Among these methods, detection through biosensors is more efficient and convenient compared with conventional laboratory equipment and various biosensors have been reported for detecting lactate in blood,[109,110] sweat,[111,112] and tears.[113,114] Lactate biosensors typically use the enzymatic reaction between lactate and lactate oxidase, the electrons transferred during their reaction are used to generate sensor response. However, immobilizing enzymes cause significant loss in enzyme activity and enzyme-based sensors are vulnerable to temperature and PH. In addition, the activity of enzymes gradually decreases with time even in the most suitable conditions.[111,115] Therefore, using alternative sensing mechanisms and appropriate receptors is the key to obtaining stable sensors.

Fluorescent sensors offer higher sensitivity, specificity, and straightforward detection methods. The direct quenching mechanisms of fluorescent sensors including PET and RET enable target detection without an intermediate such as enzymes. Despite the great offers, no study reports the detection of lactate using MIFS, to the best of our knowledge. However, the studies that reported highly sensitive and selective detection of glucose,[38,116] dopamine,[39,117–121] and ascorbic acid[67] that are similar to lactate in terms of functional group and molecular nature shows the great potential of using MIFSs for lactate measurement.

2.8 Knowledge Gap and Research Question

Based on the literature review above, the formation of MIFS based on the combination of MIPs and QDs can resolve several limitations of biological receptors-based sensors. The application of green QDs like ZnO can effectively reduce the health and environmental concerns raised by the Cd-based QDs while offering a comparable quantum yield and sensor sensitivity. The transformation of MIFS to the solid phase can eliminate the preconditions of the inconvenient liquid sensors. In addition, the formation of solid sensors not only reduces the redundant sample preparation but also offers much better mobility in the sensing process. Instead of the time-consuming and labour-intensive chemical attachment method that requires Cd-based QDs, the employment of physical attachment methods can greatly reduce the effort and time needed to produce sensors chips and offer a wide range of selection on the sensing materials and the solid substrate. Moreover, the fluorescence sensing chips can be analyzed using a portable detector to pave the way for real-time and on-site detection with fluorescence sensors. Benefiting from the flexibility of MIPs and the high sensitivity of ZnO QDs, the sensing regime can be applied to detect a wide range of target molecules.

Despite all the advantages of MIFS chips formed with physical coating methods along with their combinations with a portable detector, no study in the open literature has reported the development of such a sensing system and its application for measuring chemical contaminants in water, or biomarkers in sweat. In particular: i) ZnO QDs have not been explored extensively despite their advantages; ii) physical coating methods have rarely been used for immobilizing fluorescence sensors; iii) MCLR and lactate have not been measured using fluorescence sensors chips. The first step towards filling these knowledge gaps was the development of a ZnO QDs based molecularly imprinted fluorescence sensor to detect 2,4-D, a molecule that has been frequently studied to develop fluorescence sensors. Subsequently, a solid sensing platform was established by studying the design and operating parameters. The applicability of the thin-film coating method was evaluated by comparing the sensing performance of the solid and liquid sensors. In the next step, the flexibility of the developed sensing platform was tested by measuring MCLR with some adjustments on the sensing material. Finally, the feasibility of this sensing platform to be utilized as a biosensor was evaluated by measuring lactate in PBS. The following research questions were stated for the development of ZnO QDs based MIFS chips.

Question 1: Can the ZnO QDs based MIFS detect 2,4-D?

Question 2: Can MIFS chips be formed with physical coating methods?

Question 3: How will the MIFS chip perform compared to the liquid sensor?

Question 4: Can the developed solid sensing platform measure water contaminant MCLR?

Question 5: Is the solid sensing platform applicable for biofluid analysis such as detecting biomarker lactate?

Question 6: Can ZnO QDs base MIFSs measure lactate in the saline environment?

2.9 Objectives

The main objective of this research was to evaluate the feasibility of developing ZnO QD-based MIFS chips with thin-film coating for the sensitive and selective detection of chemical and biological model target molecules. The overall objective was achieved through attaining the following sub-objectives:

1. Investigate the viability of applying ZnO QDs as the sensing material for MIFSs and develop a synthesis protocol that enables a highly responsive ZnO@MIP sensing platform.
2. Develop MIFS chips by transforming ZnO@MIP sensing solution from liquid to solid phase with a thin-film coating method.
3. Evaluate the performance of the ZnO@MIP sensor chips for measuring two distinct chemical contaminants, 2,4-D and MCLR in water.
4. Evaluate the performance of the ZnO@MIP sensor chips for measuring lactate as a model biomarker in PBS.

Chapter 3: Development of Solid-Phase Molecularly Imprinted Fluorescence Sensor for the Detection of Organic Contaminants in Water

3.1 Introduction

As discussed in the literature review section, the MIFSs formed with the combination of QDs and MIPs are advantageous in many aspects compared to other types of sensors. One of the key applications of these MIFSs could be the fast and easy detection of both synthetic and natural toxic contaminants in water. MIFSs usually detect molecules in the liquid phase; even though the sensor performance is appreciable, the complex sensing procedure and the dependency on the fluorescence spectrophotometers along with other disadvantages are restraining the liquid MIFSs for lab use only. As an alternative, the liquid sensor can be transformed to the solid phase and coupled with a portable spectrometer to realize target detection without the limitations of testing location and equipment.

One of the approaches to obtain solid sensors is using the covalent attachment between the sensing material and a solid substrate.[32,55,56,122,123] The most common method is the bond formation between amino-functionalized paper and the carboxyl functionalized CdTe QDs.[32,55,56] Forming solid fluorescence sensors this way is time-consuming and labour-intensive. Moreover, the covalent binding process greatly limits the choice of QDs and the solid substrate. In contrast, physical coating methods like spin coating do not require functionalization on the solid substrate and do not limit the choice of sensing materials. The immobilization is therefore completed in a simple and time-efficient way. To the best of our knowledge, despite its advantages, the spin coating has not been used to transfer liquid MIFSs to the solid phase. Therefore, in this research,

I investigated the viability of solid MIFS formation with spin coating and the development of a portable sensing platform for water contaminant detection.

Since the physical coating method does not restrict the choice of sensing material and the solid substrate, biologically and environmentally compatible ZnO QDs were used as the fluorescent sensing unit to generate MIFSs. The liquid phase fluorescence material was immobilized on quartz by spin coating because quartz substrates' UV transmissivity allows the radiation from the back side, in addition to the front of the immobilized sensing layer. The measurements of fluorescence signals were realized with a portable light detector to impart the sensor with mobility. Two water contaminants, 2,4-D and MCLR, were selected as the model target molecules for the evaluation of the sensing platform. These target molecules were selected to represent contaminants with different structures and origins: 2,4-D represents synthetic molecules with small sizes and MCLR represents biomolecules with larger sizes. The sensor and the sensing concept were first optimized for measuring 2,4-D, and the performance of the solid sensor was evaluated and compared with the liquid sensor. With the feasibility and advantages of the proposed sensor proven by 2,4-D detection, the sensor was further adapted to measure MCLR in the solid phase to demonstrate the flexibility and comprehensiveness of the developed sensing system. The application of the new platform is also believed to solve the challenges regarding the detection of 2,4-D and MCLR mentioned in the literature review. The developed solid sensing platform, the first of its kind, showed the capability to detect water contaminants with good sensitivity and selectivity, thus opening new opportunities for portable fluorescence sensor development.

3.2 Methodology

Sensing materials were synthesized using ZnO QDs and an APTES based polymer, adaptations and optimizations were made in the specific synthesis method according to the target molecule. For both 2,4-D and MCLR target molecules, imprinted and non-imprinted sensors were prepared using a similar method, except for the addition of the template molecule. Several characterization methods were applied to examine the structure, composition, and optical properties of the sensing materials.

3.2.1 Materials and Synthesis

Zinc acetate dihydrate, lithium hydroxide (LiOH), 3-aminopropyltriethoxysilane (APTES), tetraethyl orthosilicate (TEOS), ammonia solution 2M in ethanol, cetrimonium bromide (CTAB), 2,4-dichlorophenoxyacetic acid (2,4-D), 4-(4-chloro-2-methylphenoxy)butanoic acid (MCPB), N-(phosphonomethyl)glycine (glyphosate), para-nitrophenol (PNP), 2,4-dichlorophenol (2,4-DCP) were purchased from Sigma-Aldrich (Ontario, Canada). Microcystin-LR (MCLR) was purchased from Cedarlane Labs (Ontario, Canada).

3.2.1.1 Synthesis and Functionalization of ZnO QDs

ZnO QDs were prepared and functionalized according to the previously reported methods[124–126] with some modifications. 0.549 g of zinc acetate dihydrate was added to 50 ml absolute ethanol and refluxed at 78 °C to obtain a clear solution. 0.2395 g LiOH was added to 30 ml ethanol and mixed until fully dissolved. The fully dissolved LiOH was drop-wisely added to the cooled zinc acetate solution at room temperature under a nitrogen stream and the solution was kept for 1 h at 60 °C to complete the reaction. The final turbid solution was centrifuged at 13000 rpm for 20 min

to collect the QDs particles. The collected QDs were dispersed in 20 ml absolute ethanol for functionalization, and then 400 μL APTES was added drop by drop under continuous stirring followed by the addition of 300 μL DI water. The mixture was allowed to react at room temperature for 2 h.

3.2.1.2 Synthesis of ZnO@MIP and ZnO@NIP

For 2,4-D sensor, 0.7 g of APTES functionalized QDs were dispersed in 20 ml ethanol, 160 μL of APTES and 20 mg 2,4-D were added to the mixture and stirred for 30 min. Then, 200 μL of TEOS and 200 μL ammonia solution were added to the mixture and kept for 22 h in the dark to complete the polymerization. The non-imprinted polymer (NIP) was prepared using the same procedure without the addition of 2,4-D. The prepared polymers were collected and washed with an ethanol–acetonitrile (8:2) mixture and absolute ethanol until no template molecule was detected by UV-Vis spectroscopy.

For the MCLR sensor, 400 μL of 50 mg/ml L-arginine solution was added to the APTES and QDs solution and stirred for 30 min. Then, 1.6 ml of 0.2 M CTAB and 0.2 ml of 0.2 M NaOH were added and stirred for another 30 min. Finally, 200 μL of TEOS and 200 μL ammonia solution were added to the mixture and stirred continuously for 16 h in the dark. The NIP was prepared using the same procedure without the addition of L-arginine. The product was washed three times with the ethanol–acetonitrile (8:2) mixture and three times with absolute ethanol to remove L-arginine and CTAB.

3.2.1.3 Solid-Phase Sensor Preparation

The spin coating of the stock solution was completed according to the previous research[127] with some modifications. 200 μL of the stock solution was added to the quartz chip dropwise while rotating the chip at 500 rpm. The speed was then increased to 1000 rpm for 30 s. The coated quartz chips were heated for 3 min at 80 °C to fully evaporate the solvent. Then, the procedure was repeated 3 times to obtain optimum sensing layer thickness.

3.2.2 Characterization and Evaluation Methods

Fluorescence measurements of the liquid sensor were performed using Fluorescence Spectrometer (Cary Eclipse; Agilent Technologies, Inc., California, USA), measurements of the solid sensor were performed using a portable spectrometer (USB2000+; Ocean Insight, Orlando, USA) with 310 nm UV irradiation (High Power: 2×2 Series; Violumas, California, USA). The morphology was evaluated using the transmission electron microscope (TEM; Hitachi H7600; Hitachi, Tokyo, Japan) and high-resolution TEM (Tecnai G20; FEI, Oregan, USA). Absorption properties were recorded using UV-Visible Spectrophotometer (Cary 100; Agilent Technology, Inc., California, USA). Fourier transform infrared (FT-IR) spectra were obtained using the Frontier FT-IR Spectrometer with attenuated total reflectance (PerkinElmer Inc., Waltham, MA, USA). The Shared Instrument Facility and Bioimaging Facility at the University of British Columbia provided the characterization instruments.

The liquid sensor was prepared by dissolving an appropriate amount of sensing material in ethanol and the fluorescence emission was recorded with 310 nm excitation under medium working voltage. For sensor performance evaluation, 10 μL of 2,4-D samples in various concentrations were added and mixed for 10 min before measurements.

The performance of the solid sensor was evaluated by measuring the fluorescence intensity before and after the addition of 10 µL samples in various concentrations. To reduce experimental errors, the solid sensor was placed in a fixed solid-sample holder which allows 45 ° of excitation and measurement respectively to reduce the interference of ultraviolet light-emitting diode (UV-LED) radiation (Fig. 3-1). Several sets of experiments were performed three times to obtain error bars and tables representing a confidence interval (CI) of 95% (equivalent to a significance level of $\alpha = 0.05$) were generated using student's t-distribution for the samples.

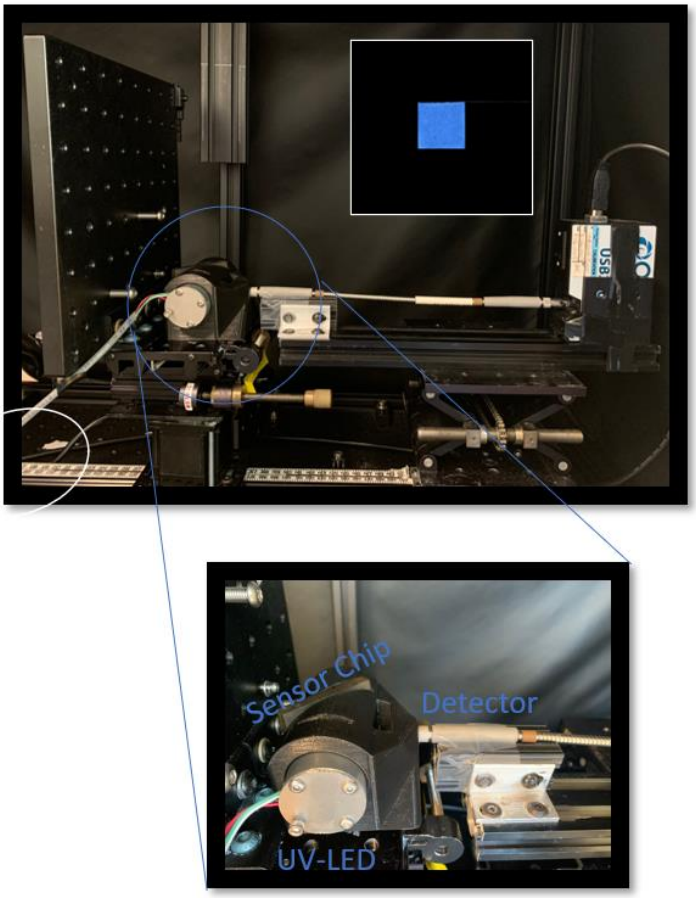

Figure 3-1: Setup of portable detector for fluorescence measurement and a close-up picture of detection arrangement. The solid sensor was placed in a fixed solid-sample holder which allows 45 ° of UV-LED excitation

and detector measurement. The inset of the upper figure shows the fluorescence signal of the sensor chip when UV-LED is on.

3.3 Results and Discussions

The morphology and the topography of the sensing material were examined using TEM and the chemical compositions were determined using FT-IR spectra. The effect of several design and operating parameters were studied in both the liquid and solid phases for 2,4-D sensor development. The optimized sensor was evaluated with regard to sensor sensitivity and selectivity for 2,4-D detection. Furthermore, the sensor was adapted for MCLR detection and assessed for sensitivity and selectivity.

3.3.1 Preparation and Characterization of ZnO@MIPs

The preparation and measurement process of the ZnO-based MIFS (ZnO@MIP) is illustrated schematically in Fig. 3-2A. The MIFS was formed with sensing material ZnO QDs, monomer APTES and template molecule 2,4-D. After washing the template molecule, the liquid ZnO@MIP sensing material was spin-coated on quartz to generate sensor chips. For the measurement, the sensor chip was excited using a UV-LED at 310 nm, and the fluorescence intensity was detected using a portable spectrophotometer.

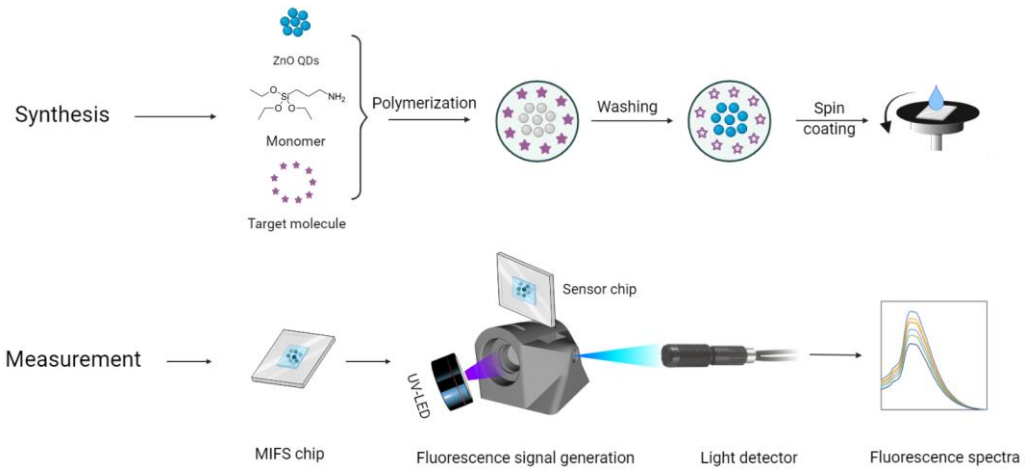

Figure 3-2: Schematic representation of ZnO@MIPs sensor synthesis and measurement process. The sensing material is formed with ZnO QDs and MIPs. After washing the template molecule, the liquid ZnO@MIPs sensing material was spin-coated on quartz to generate solid fluorescence sensors. Then, the sensor chip was excited using a UV-LED and the fluorescence signal was detected using a light detector to acquire the fluorescence spectra.

The TEM images of the QDs indicated that they were well dispersed and ranged from 3 to 5 nm in diameter (Fig. 3-3A). The high-resolution TEM images of QDs after polymerization (Fig. 3-3B) revealed that the QDs were aggregated to form bigger nanoparticles. These molecules were interconnected spherical nanoparticles that contained QDs within their structures (Fig. 3-3C), with uniform distribution and dispersion of QDs inside the MIP (Fig. 3-3D). Comparing the images before and after polymerization, we can conclude that the size of the particle increased from a few nanometers to approximately 200 nm due to these silicon-based polymer coating layers. These polymer layers compose a protective shell for the QDs and impart sensors with target recognition ability.

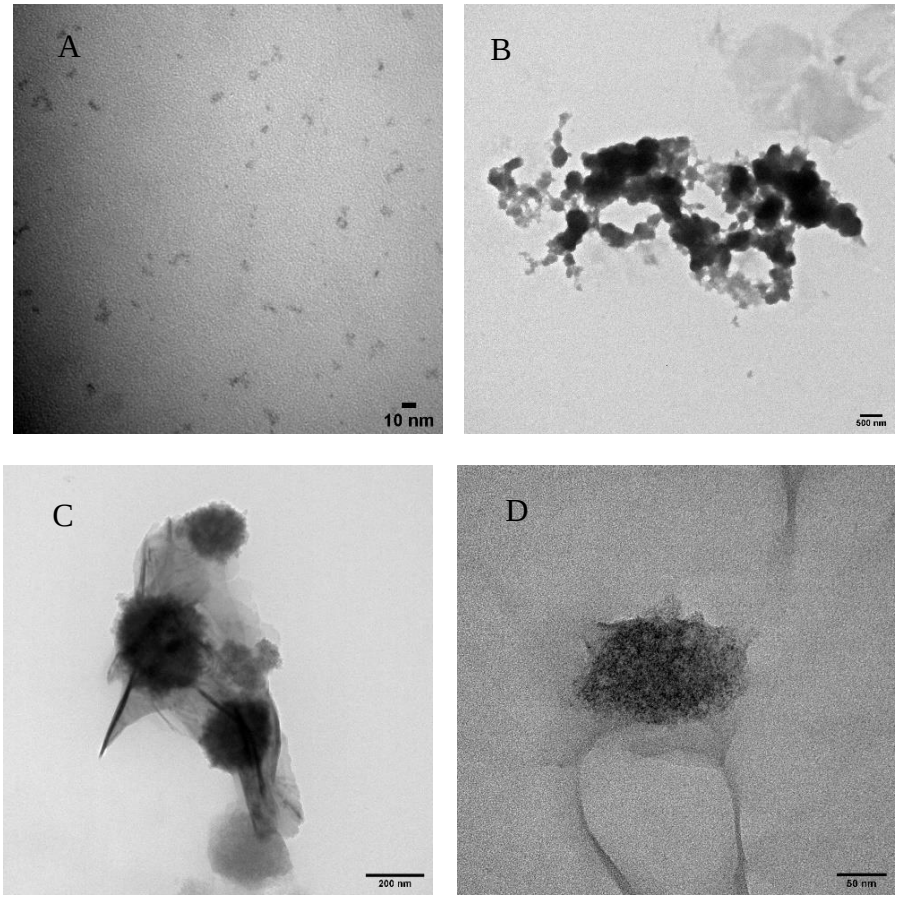

Figure 3-3: TEM images of (A) ZnO QDs and (B, C) high-resolution TEM images of ZnO@MIP showing the spherical shape of the molecule and (D) the QDs embedded inside the MIP.

The FT-IR spectra of ZnO QDs and the ZnO@MIP are shown in Fig. 3-4. The shared absorption peaks for QDs and ZnO@MIP at 1506 cm^{-1} and 1424 cm^{-1} were attributed to the C-H and O-H bonds respectively. These groups are most likely to be the residue of acetate from the QD synthesis.[128] Also, the shared peaks at 866 cm^{-1} and 672 cm^{-1} were assigned to C-H vibration; especially, the peak at 672 cm^{-1} was thought to be the C-H group belonging to alcohols that resulted from the repeated washing with ethanol. The asymmetric stretching appeared for ZnO@MIP

compared with bare ZnO at 1006 cm^{-1} and 1050 cm^{-1} were due to the stretching of Si-O-Si bond which showed the successful formation of imprinted polymer on the surface of QDs.[129,130]

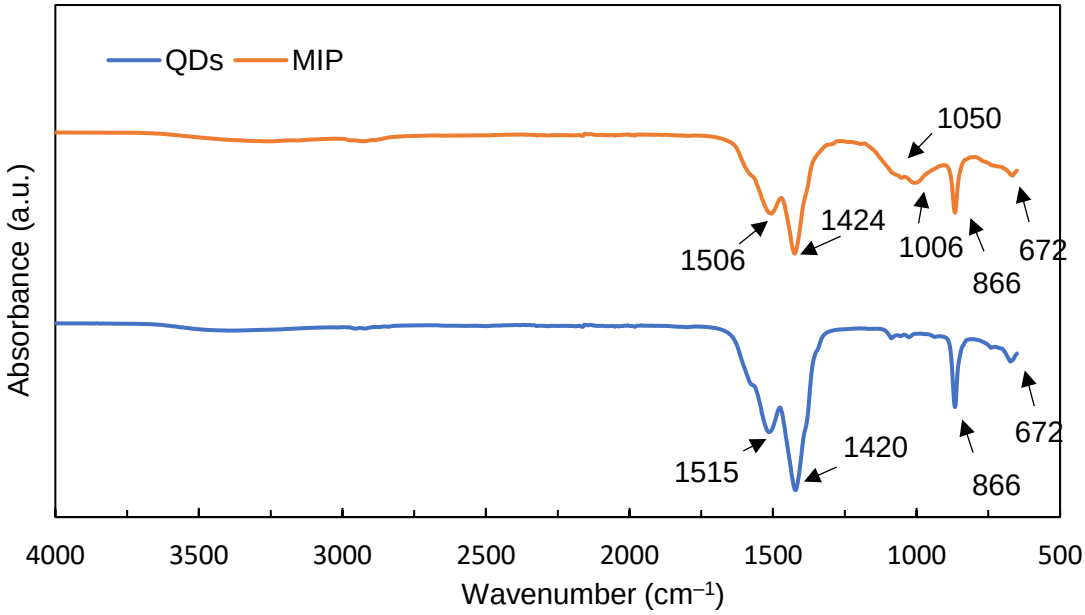

Figure 3-4: FT-IR spectra of ZnO QDs and ZnO@MIP.

3.3.2 Formation of the Liquid-Phase Sensing Platform

Determining the optimum synthesis procedure and sensing conditions to enhance sensing performance was critical, especially since this was the first study to apply ZnO@MIP for measuring 2,4-D, to the best of our knowledge. Therefore, parametric studies were conducted for both liquid and solid phase sensors to compare their best sensing capabilities. Material synthesis factors such as template amount and the sensor solvent affect both liquid and solid phase detection, so they were studied first. Then, phase-specific factors such as polymer solution concentrations and sensing layer thickness were studied in the respective phases. The fluorescence quenching (response) of the sensors in both phases was evaluated using the Stern–Volmer equation:

$$F_0/F = 1 + K_{SV} * C_q \quad (1)$$

Where F_0 and F are the fluorescence intensity before and after the addition of the target molecule, respectively, Cq is the concentration of the target molecule and the Stern-Volmer constant K_{sv} is the sensitivity of the sensor.[40–42] The units of fluorescence intensity and the concentrations are arbitrary units (a.u.) and micromolar (μM), respectively.

3.3.2.1 Evaluating the Effect of Template Amount

To enhance sensor sensitivity and reach the optimum polymer structure, the template amount was varied with the same amount of monomer and the cross-linking agent. Template amount is the amount of target molecule added during polymerization; since these molecules create target-specific imprinted sites, this amount is directly related to the number of imprinted sites. More templates create more imprinted sites that may enhance sensor sensitivity. However, a high amount of template might result in monomer binding with the template molecules rather than binding with another monomer; this preference for monomer binding might affect the thickness of the polymer layer and the stability of the imprinted sites. This two-sided effect of the template molecules was proved by the experimental results shown in Fig. 3-5A, when the template amount was increased from 10 to 20 mg, the sensor response increased, but when the template amount was further increased to 30 mg, the response decreased to a value even lower than the 10 mg imprinted polymer. This behaviour can be explained by the fact that when the template amount was lower, there were fewer imprinted sites to which the 2,4-D could bind; however, when the template amount was higher, which increased the number of imprinted sites, it was harder to maintain these cavities, so the recognition ability of the polymer was impaired. Therefore, considering the higher

sensitivity and consistency, 20 mg of 2,4-D, corresponding to the 1:8:10 ratio of the template: monomer: cross-linking agent (mg: µL: µL) was added to create imprinted sites.

3.3.2.2 Determination of Polymer Solvent and Concentration

To obtain a molecularly imprinted fluorescence sensor, the prepared polymer must first be dissolved and then be used as a liquid sensor or to be transformed to the solid phase. Therefore, appropriate choices should be made concerning the polymer solvent and the concentration of polymer solution. The previously defined 20 mg imprinted polymer was dissolved in water and absolute ethanol to investigate the effect of solvent and 1, 5, 7 g/L of polymer solutions with the predefined solvent were prepared to investigate the effect of the polymer concentration. As anticipated, ZnO@MIP showed an almost four times higher response to 2,4-D when dissolved in ethanol (Fig. 3-5B), which was the solvent we used to prepare the MIP. The solvent can influence the emission wavelength and intensity by altering the environment surrounding the QDs.[131] When the polymer was dissolved in DI water, the amount of active QDs probably reduced because of the quenching effect of DI water on ZnO QDs which would cause a lower sensor sensitivity. Another reason might be that the rebinding efficiency of the target molecule was reduced when dissolved in DI water. When the MIP is dissolved in a different solvent than the solvent used for the imprinting process, the Vander Waals forces resulting from dipole moment and hydrophilic/hydrophobic interactions may change, and the binding affinities of the molecule to the imprinted sites might be reduced as a result.[132] Therefore, ZnO@MIP showed a higher sensitivity when the solvent was identical for the rebinding and imprinting processes.

To study the effect of polymer concentration, different amounts of ZnO@MIP were dissolved in ethanol and tested with 2,4-D. It was noted that when the amount of the quencher was

the same, a smaller amount of the sensing material displayed a higher degree of quenching (Fig. 3-5C); thus, the response of 1 g/L was higher than the responses of 5 and 7 g/L ZnO@MIP solutions. When the concentration was lower than 1g/L, the ZnO@MIP solution was not able to maintain consistency in the sensor response; thus the polymer concentration was fixed as 1 g/L to obtain a more sensitive and consistent response.

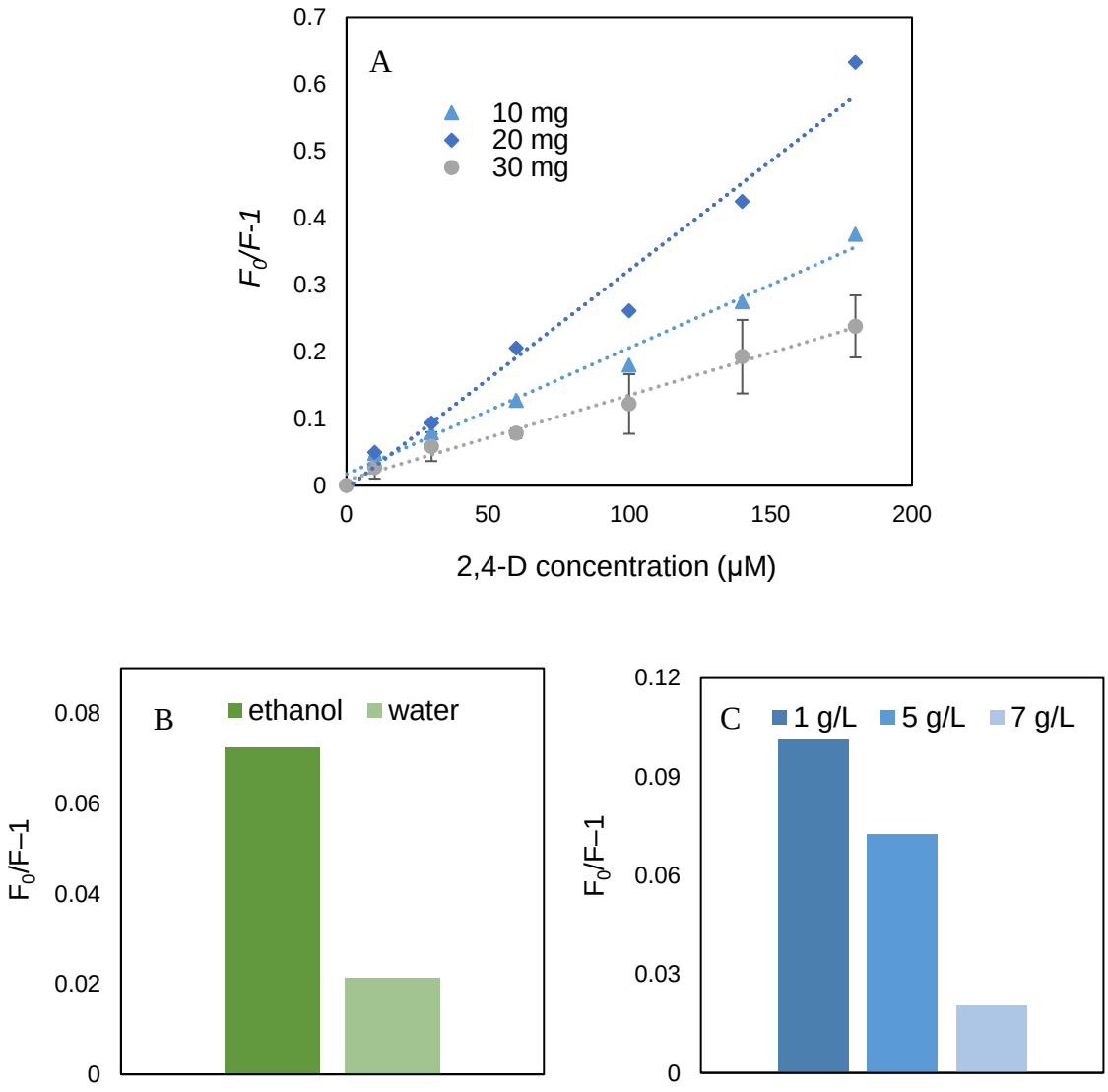

Figure 3-5: Effect of (A) the template amount, (B) the polymer solvent, and (C) the polymer concentration on the performance of the liquid sensor.

3.3.3 Liquid Phase Sensing Performance

The liquid phase ZnO@MIP sensor formed using the abovementioned parameters was further evaluated in its ability to detect 2,4-D. Fig. 3-6A shows the changes in the fluorescence spectra of liquid ZnO@MIP with the addition of 2,4-D. The reduced fluorescence intensity with the addition of 2,4-D revealed the quenching of QDs, but the degree of quenching was not significant enough to differentiate between different concentrations. The Stern–Volmer plot of the liquid sensor (Fig. 3-6B) shows that although quenching took place with the addition of 2,4-D, sensor sensitivity was low, and the difference in the sensor response to subsequent changes in the concentration was often not statistically significant (considering the size of the error bars). In addition to this low sensitivity, the volume/concentration change of the liquid samples, the limited mass transfer rate and the need for a spectrophotometer manifested as the disadvantages of the liquid sensor.

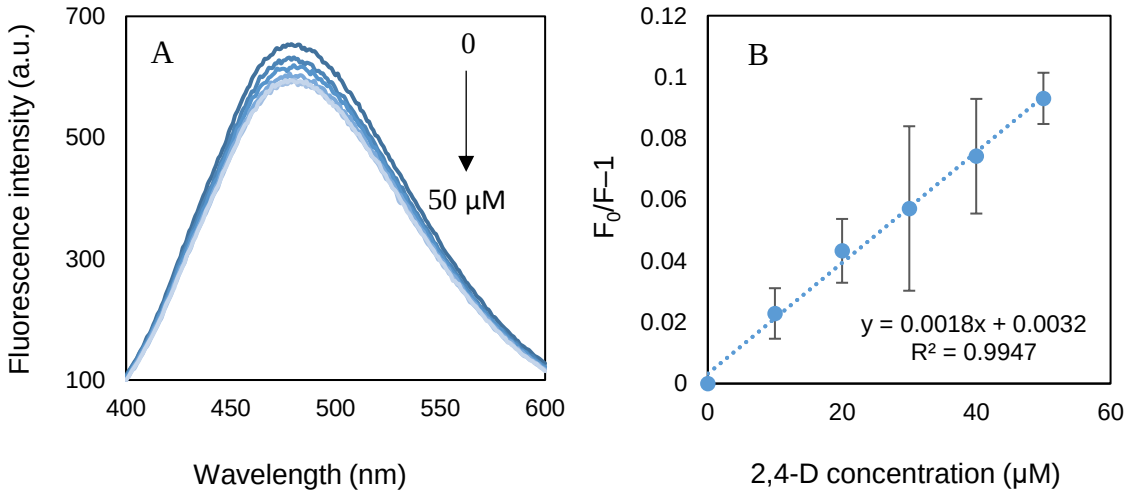

Figure 3-6: Response of ZnO@MIP liquid sensor to 2,4-D represented with (A) fluorescence spectra and (B) Stern–Volmer plot.

3.3.4 Formation of the Solid-Phase Sensing Platform

Formation of solid sensing layers prevents sample dilution and makes it possible to detect sensor response using portable spectrophotometers. This in turn overcomes the workspace and equipment limitations of the liquid sensors and realizes on-site, real-time sensing applications. Among the various methods used for forming solid sensing layers, physical coating methods including blade coating, spin coating and drop coating[133] were proved to be better than the time-consuming, labor-intensive covalent coating method. In addition, physical coating techniques do not require a specific solid substrate in contrast to the covalent binding method so there are no limitations for selecting the solid substrate. Considering the convenience of designing lab-on-chip devices and that quartz chips allow UV irradiation from both the front and back, the sensing material was immobilized on quartz using various coating methods. Among different physical coating methods, spin coating was used for further solid sensor preparation due to its ability to form a uniform, consistent thin layer with a strong attachment.

3.3.4.1 Study of Coating Parameters

The physical parameters of the coating method need to be evaluated for immobilizing the sensing material to obtain the highest sensor response. In addition to the coating area and coating layer, a few variables that affect the quenching efficiency, including the QDs' properties were also evaluated.

The first parameter to be determined for the solid sensor was the coating area; the area of coating should be confined to the area that can be detected by the spectrophotometer while embedding enough sensing materials to show sensor response. For the sensing areas tested from 0.5 to 3.5 cm^2, the highest response was recorded with the sensing area from 1 to 2 cm^2 and the

response was reduced for the area higher than 2 cm^2 and the area lower than 1 cm^2 (Fig. 3-7A). The low response shown by the large coating area was likely because the detector could not record the quenching that took place outside of its viewing area. For the coating area smaller than 1 cm^2, the amount of sensing materials deposited on the chip was limited (e.g., smaller than the detector's viewing area), so the overall sensor response was low. To achieve a high degree of quenching while maintaining a more convenient coating process, a 1 cm^2 square-shaped coating area was selected for the sensor preparation.

Sensor sensitivity and the range of detection are dependent on the amount of sensing material; too many sensing materials might result in lower sensitivity and too few sensing materials might narrow the linear range of detection.[134] To this purpose, the fluorescence response of sensors prepared with various layers of coating was measured. The number of coating layers was used to adjust the amount of sensing materials on the quartz. As shown in Fig. 3-7B, the sensor sensitivity decreased slightly with increasing layers of coating from 1 to 3 and 5 (*Ksv* of 0.045, 0.037, 0.031, respectively), which could be attributed to higher binding efficiency of 2,4-D when the coating layer was thinner. However, the high responsive one-layer coated sensors failed to display a uniform layer and a constant sensor performance due to the formation of empty spots and scratches. Therefore, three layers of coating, corresponding to an average 1.7 μm of coating thickness, were used for solid sensor formation because of the comparable high sensitivity and better repeatability.

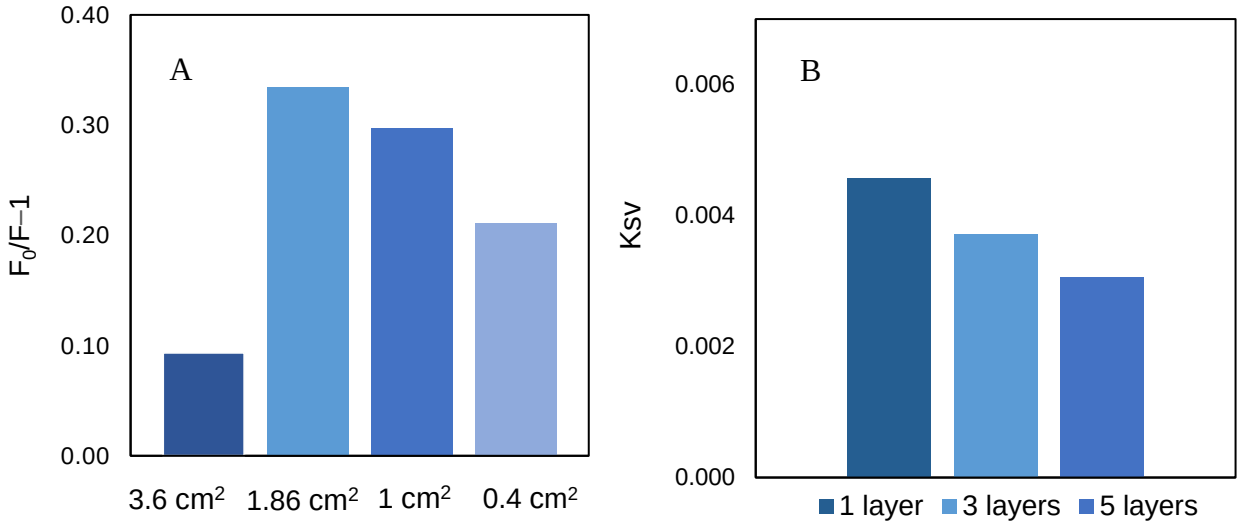

Figure 3-7: (A) Effect of the sensing layer coating area on fluorescence quenching (B) effect of the number of layers on the sensor sensitivity.

3.3.4.2 Evaluation of QD Size and Quantity

In spite of their many advantages, ZnO QDs have rarely been used for MIP sensor development, so, we needed to examine the effect of various ZnO QDs' properties on the sensor response. One of the unique properties of QDs is their size-dependent emission wavelength.[135] To see the impact of the QDs size on the sensor sensitivity, imprinted polymers prepared with blue and yellow ZnO QDs were tested against 2,4-D. As shown in Fig. 3-8A, with the addition of a blank solution, yellow emissive QDs showed an enhancement while blue QDs showed a diminution in the fluorescence intensity; also, sensor sensitivity was improved almost ten times with the blue emissive QDs. It is assumed that the opposite behaviour towards the blank solution is due to the discrete solvent relaxation effect of ZnO QDs in different sizes.[131] For yellow QDs, adding DI water caused an enhancement in the fluorescence intensity with the synergic effect of

DI water on the emission. The lower sensitivity of yellow emissive ZnO@MIP can then be interpreted as the equilibrium on the increasing fluorescence intensity due to water and decreasing fluorescence intensity due to 2,4-D. For blue QDs, both DI water and 2,4-D caused quenching so the response to 2,4-D was enhanced partially due to the response to DI water. Therefore, highly responsive blue ZnO QDs were more suitable for ZnO@MIP sensor development.

The amount of QDs added during the polymerization directly controls the number of active response units in the polymer and the thickness of the polymer shell; a larger amount of QDs may provide more active sites to respond to the target but the polymer layer might become too thin to maintain its imprinted sites and to contain QDs. If the polymer layer is too thick, the diffusion of the target to the imprinted sites might be limited and the response time would be prolonged.[136] Therefore, it is important to balance these two effects by adjusting the amount of QDs. The sensitivity of the sensors were 0.0053, 0.0166 and 0.008 for ZnO@MIP prepared with 0.4, 0.7 and 0.9 g of QDs, respectively (Fig. 3-8B). Adding 0.9 g of QDs resulted in a higher response for lower concentrations but failed to maintain the response for the higher concentrations; this behaviour may have resulted from poorly formed imprinted sites that had limited capacities to bind with 2,4-D. However, ZnO@MIP prepared with 0.4 g of ZnO QDs showed a highly consistent sensor response, but the magnitude of the response level was lower than the other two because of the insufficient response unit within the polymer. Therefore, the addition of 0.7 g of ZnO QDs was preferred because of the balance between sensor sensitivity and the stability of the imprinted sites.

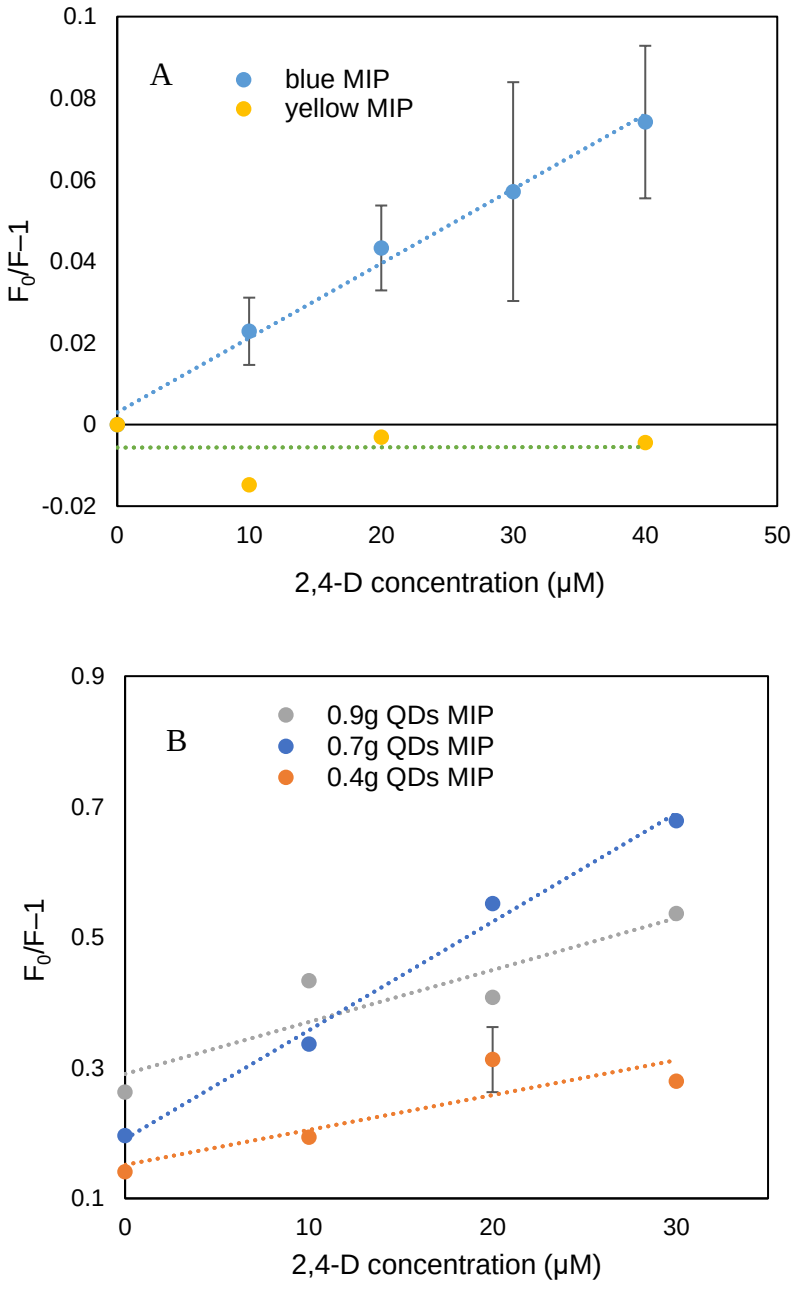

Figure 3-8: Effect of ZnO QDs' (A) size and (B) amount on the sensor response to 0–30 µM of 2,4-D.

3.3.5 Evaluation of Sensor Emission Stability and Response Time

Based on our previously described evaluation of several key design parameters, we successfully formed the ZnO@MIP solid sensors. But before using the solid sensor to detect 2,4-D, the fluorescence emission stability of the sensor had to be evaluated. The fluorescence emission should be stable over time so any changes in the fluorescence are solely dependent on the addition of the target chemical. Before the addition of 2,4-D, the fluorescence intensity of the solid sensor remained steady at around 40000 a.u., when measured every 10 min for 1 h (Fig. 3-9), which indicated a stable emission of the solid sensing layer. After adding 2,4-D, the sensor's fluorescence intensity dropped intensely in the first 10 min and gradually flattened afterwards which suggested that the sensor was capable of showing response in 10 min after the target addition.

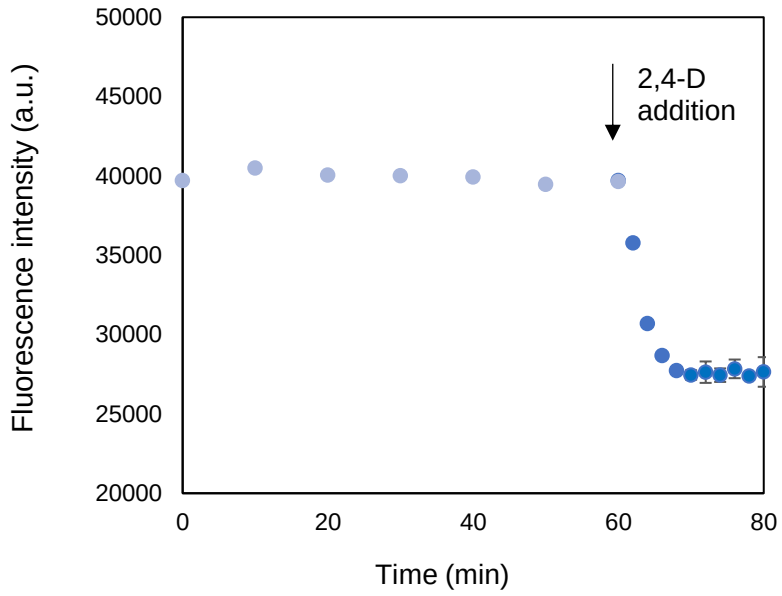

Figure 3-9: Measurements of the fluorescence intensity before and after the addition of 2,4-D. The fluorescence intensity was measured every ten min before the sample addition and measured every two min after the sample addition to obtain the trend of fluorescence change.

3.3.6 Assessment of Solid-Phase Sensor Performance

Under the optimum conditions, the ability of the ZnO@MIP solid sensor to detect 2,4-D was further evaluated by recording its response to 0 to 40 μM of 2,4-D. The response of ZnO with nonimprinted polymer (ZnO@NIP) was recorded in the same way to compare the sensor behaviour with and without imprinted sites. Fig. 3-10A shows the changes in the ZnO@MIP fluorescence spectra with 2,4-D addition; the fluorescence intensity of the sensor showed a gradual and consistent decrease with the addition of 2,4-D in increasing concentrations. According to the Stern-Volmer plot of the solid ZnO@MIP shown in the inset of Fig. 3-10A, Ksv which is a measure of sensor sensitivity was calculated as 0.0233 with the correlation coefficient of 0.98. The limit of detection, calculated using the IUPAC criteria $3\sigma/S$ was 2.36 μM, where σ is the standard deviation of the blank solution and S is the slope of the calibration curve.[134]

In comparison, the ZnO@NIP solid sensor was not able to show distinguishable changes in the fluorescence intensity to the increasing concentration of 2,4-D, which can be seen more clearly in the Stern-Volmer plot shown in the inset of Fig. 3-10B. The response of ZnO@MIP to 10 μM of 2,4-D was 10 times higher than that of ZnO@NIP; the overall sensitivity of ZnO@MIP was 14 times higher than the ZnO@NIP, which is the imprinting factor of the sensor. This large difference in the sensor performance is considered to be due to the imprinted sites on ZnO@MIP; the presence of imprinted sites facilitated the binding of 2,4-D to the sensor and enabled the recognition of 2,4-D in different concentrations. Thus, the ZnO@MIP sensor was able to show consistent and concentration-specific quenching.

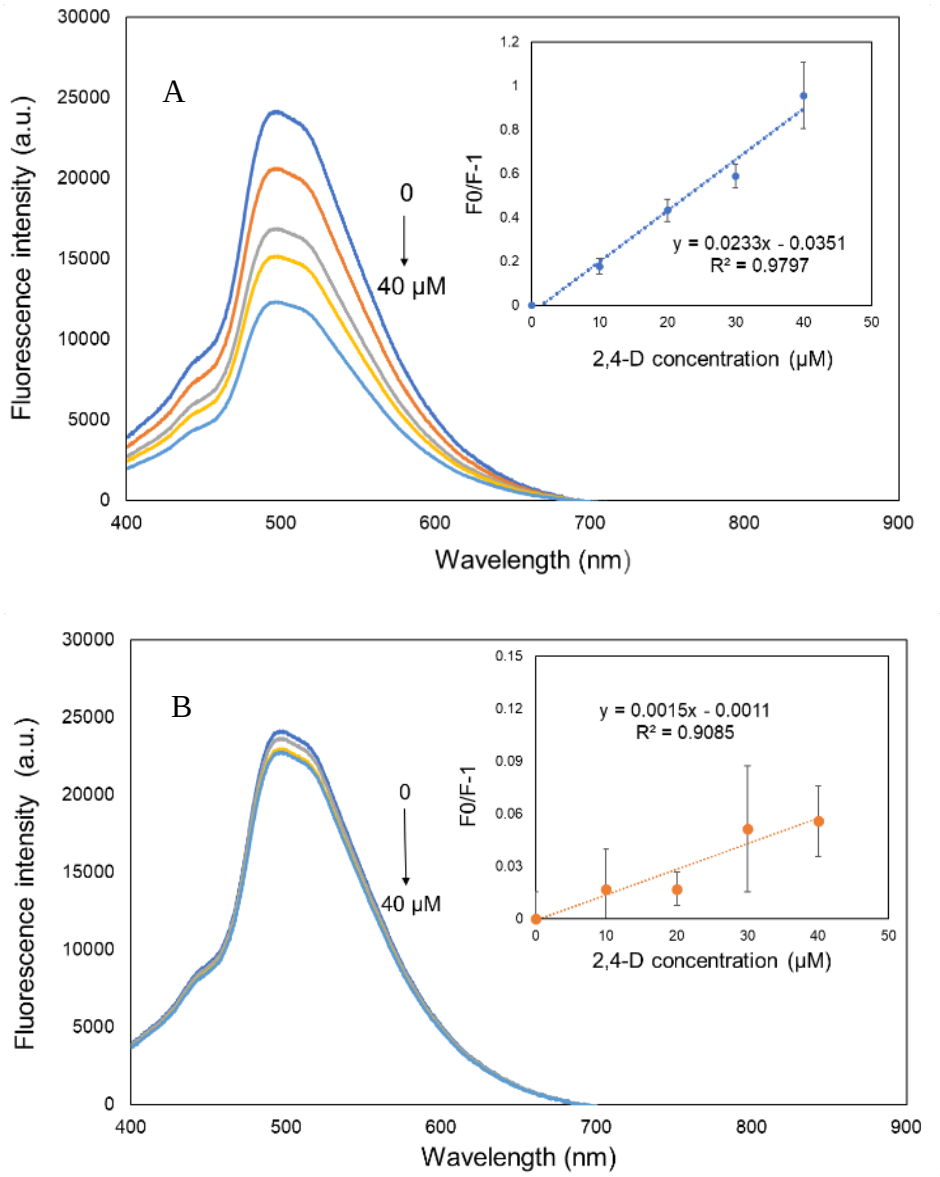

Figure 3-10: Response of the (A) ZnO@MIP and (B) ZnO@NIP solid sensors to 0–40 µM of 2,4-D. The response of the sensor was represented with fluorescence spectra and Stern-Volmer plot (inset).

The selectivity of the sensor is an important parameter to determine the effect of interfering molecules and highlight the sensor's capability of detecting 2,4-D in actual water samples, where other organic molecules may present. The widely used herbicides MCPB and glyphosate as well

as 2,4-D's structure analogous 2,4-DCP were selected as the main interfering molecules for this study. These molecules might cause the sensor to generate a false-positive response which is normally expected when there are no recognition materials. To investigate the sensor's reliability in detecting 2,4-D, the same concentrations of the target molecule and the interfering molecules were added to the sensing layer, and their fluorescence responses were recorded. The highest quenching was shown by 2,4-D which is the molecule that exactly matched the imprinted sites (Fig. 3-11), while the response to other molecules was equally low and similar to that of DI water. Therefore, we concluded that the response shown to the interference molecules was mainly because of the DI water, and the response induced by the interfering molecules was negligible.

In contrast, responses of ZnO@NIP to the interfering molecule were not differentiable from the response to 2,4-D. Since all the responses for the NIP-based sensor were slightly higher than its response to DI water, the added organic molecules were accountable for the fluorescence quenching. We concluded that whether the molecule is the target molecule or not, ZnO@NIP would generate sensor response at the same level as 2,4-D which indicates the inability of the ZnO@NIP to recognize 2,4-D. A comparison of the results for ZnO@MIP and ZnO@NIP, indicated that the recognition of the target molecule by the sensor was attributed to the molecularly imprinted sites. During the polymer formation, the carboxyl functional group of 2,4-D was bound to the amino functional group of the monomer APTES so the specificity of the MIPs was determined by the shape, size and functional group of the target molecule. If one of these criteria did not match with the imprinted sites, the ZnO@MIP sensor would not show sensor response. Therefore, the target molecule's structure analogous 2,4-DCP was not recognized by the sensor despite the similarity in their size, shape and side groups because it lacked the acidic group that binds to the sensing unit.

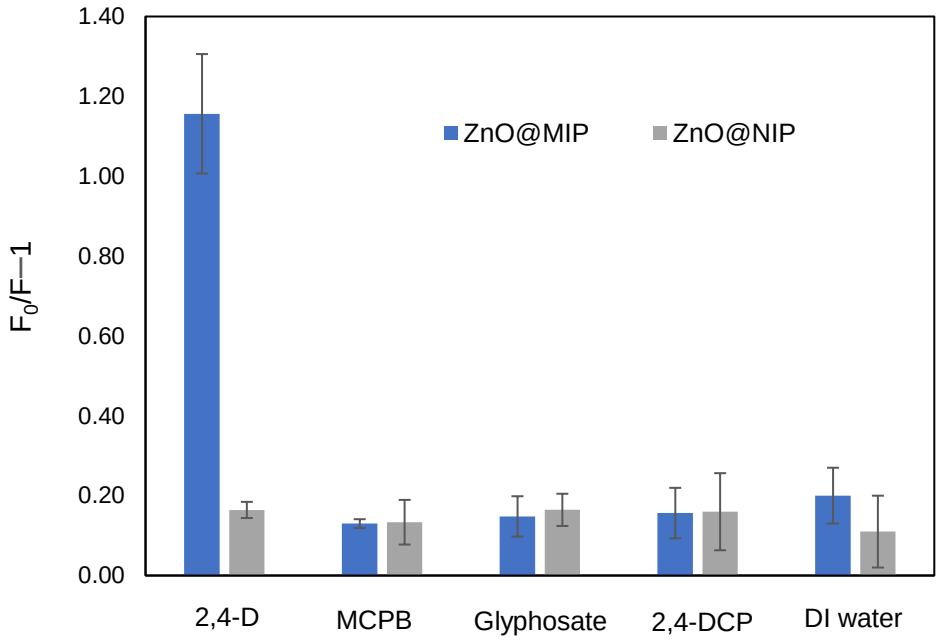

Figure 3-11: Response of the ZnO@MIP (blue bars) and ZnO@NIP sensors (gray bars) to 40 µM of 2,4-D, MCPB, glyphosate, 2,4-DCP and the blank solution.

3.3.7 Comparison of Solid and Liquid Sensing Performance

The solid phase ZnO@MIP sensor has superiority in its ease of operation and simple sample preparation procedure compared with the liquid phase sensor. To completely transform to the solid phase, the detection performance of the ZnO@MIP solid sensor should be at the same or preferably a higher level than that of the liquid response. According to the overall performance comparison of sensors prepared in the solid and the liquid phases shown in Fig. 3-12, sensor response was enhanced 12 times when transformed to the solid phase. The inferior sensing performance of the liquid phase compared with the solid phase was likely due to the following drawbacks of the liquid sensor. First, the sample was diluted when added to the liquid sensor which reduced the mass-transfer efficiency; there might have been less 2,4-D bound to the polymer in the liquid phase than

the solid phase because of the dilution, resulting in a low sensor response level. Second, the binding of the target molecule in the liquid phase might be associated with higher entropy than in the solid phase which resulted in higher activation energy for the reaction mechanism. The foundation for such a hypothesis is that the entropy of the solvent, especially for a charge transfer process might be dominating source of a high entropy that is limiting the reaction.[137–139] Third, the concentration of the ZnO@MIP in the liquid phase, in general, was too low to respond to the higher concentration of 2,4-D. Even though a lower amount of sensing material was beneficial to detect lower concentrations, the limited imprinted sites were not able to accommodate higher concentrations of target molecule thus reducing the overall sensitivity of the sensor. When a higher concentration of ZnO@MIP was used in the liquid phase, the sensing material precipitated over time and caused a fluctuation in the fluorescence intensity because of the low solubility of the polymer even in ethanol, so it was not appropriate to use a high ZnO@MIP concentration. The abovementioned problems were avoided when the sensing layer was transformed to the solid phase; there was not any dilution of the sample and a larger amount of sensing material could be deposited on the solid sensor without the effect of sedimentation. Therefore, sensor response was improved overall when immobilized on the quartz chip.

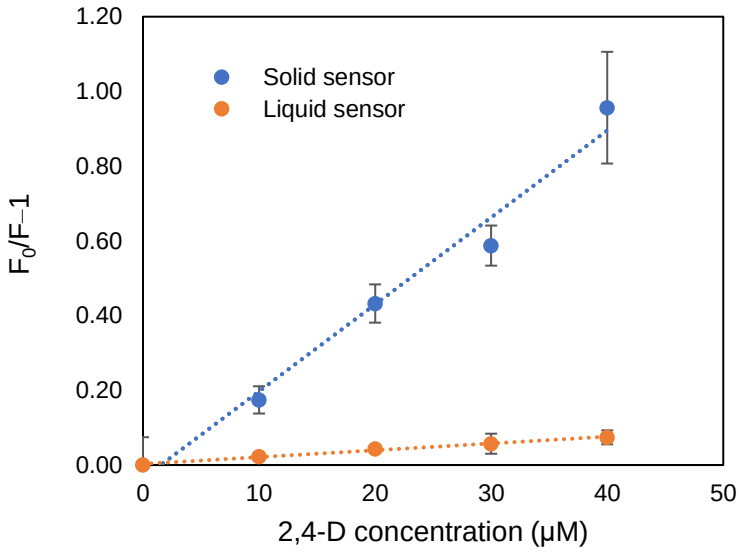

Figure 3-12: Comparison of the solid and the liquid ZnO@MIP sensors' response to 0–40 µM of 2,4-D.

3.3.8 Sensor Working Mechanism

Fluorescence sensors respond to the target molecule by quenching. Typically, there are two main working mechanisms for quenching: RET and PET. RET is induced when there is an alignment between the emission band of the fluorescence molecule and the absorption band of the target molecule. PET is triggered when there is a complex formed between the fluorescence molecules and the target molecule.[140] RET cannot be the quenching mechanism because 2,4-D is not able to absorb light in the 400 to 600 nm range which, in this case, was the emission band of the prepared QDs (Fig. 3-13A). PET, on the other hand, can be the working mechanism because of the Meisenheimer complex formed between APTES and 2,4-D.[141] The binding reaction was assumed to be taking place between the carboxyl functional group of 2,4-D and the amino functional group of APTES. Since APTES was also grown on the ZnO QDs, the complex can also be formed on the QDs' surface which is capable of accepting the excited electrons of the QDs. To evaluate this hypothesis, UV-Vis spectra of 2,4-D were taken and the peaks at 285 nm and 230 nm

were assigned to the two light-absorbing groups, the benzene and carboxyl group, respectively.[142,143] To see the binding effect, different amounts of APTES were added to the 2,4-D solution and the changes in the two light-absorbing groups were recorded in a way similar to that reported by Shaobo Han et al.[144] As shown in Fig. 3-13B, with the addition of APTES, the peak belonging to the carboxyl functional group of 2,4-D (230 nm) gradually decreased while the peak belonging to the benzene group of 2,4-D (280 nm) remained the same. This shows that the carboxyl group of 2,4-D was binding to APTES resulting in the formation of Meisenheimer complexes.[71,134] Therefore, we concluded that the quenching shown to 2,4-D is the result of electron transfer from QDs to the target molecule.

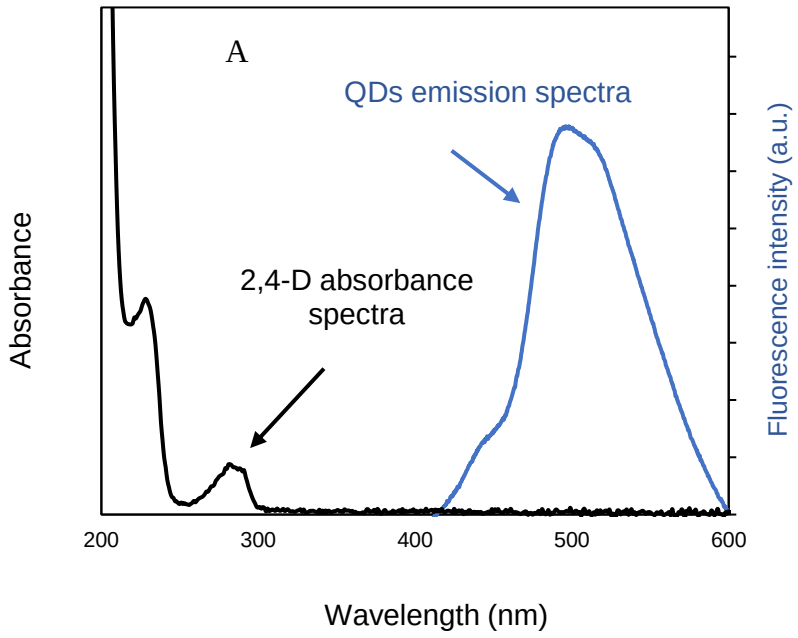

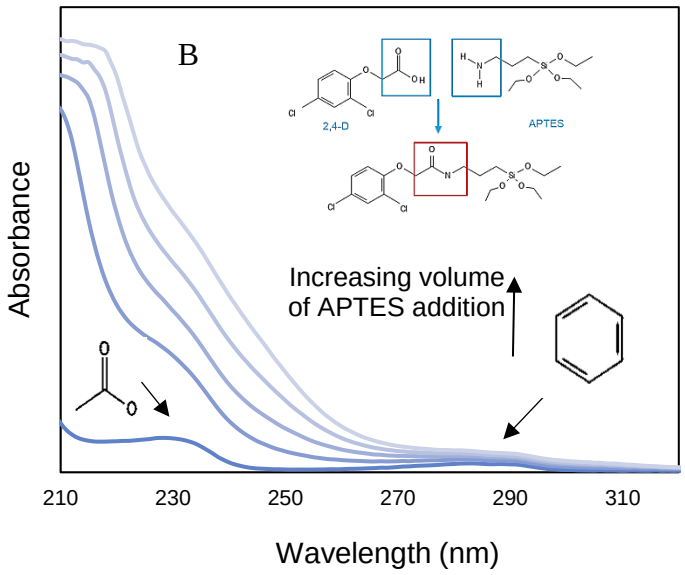

Figure 3-13: (A) Emission spectra of ZnO QDs and absorbance spectra of 2,4-D (B) measurements of the absorbance spectra of 2,4-D with the addition of APTES in increasing volume; the peaks at 285 nm and 230 nm were assigned to the two light-absorbing groups: benzene and carboxyl group; the binding mechanism of 2,4-D to APTES is shown in the inset of (B).

3.3.9 MCLR Measurement

The results obtained for 2,4-D detection revealed the advantages of detection in the solid phase and the potentials of measurement with the portable fluorescence probes. In principle, both the sensing materials and the immobilization method can be applied for different target molecules and various purposes of detection. To demonstrate the applicability of the developed sensing platform to the measurement of other contaminants, the sensor was modified for MCLR detection. Unlike 2,4-D, MCLR is a cyclic biomolecule produced by cyanobacteria that consist of seven amino acids. The molecular volume of MCLR can reach 2.63 nm^3 which is comparable with the size of the QDs. The large particle size of MCLR is reflected on the molar mass of the molecule

which is almost five times higher than the molar mass of 2,4-D; thus, modifications were made to the synthesis process to accommodate the large molecule size (Fig. 3-14A). First, L-arginine, one of the signature amino acid constituents of MCLR, was used to form imprinted sites; this way the danger of MCLR leaking during the imprinting process was avoided, and a more stable polymer structure was obtained. Then, mesoporous was introduced to the MIP to facilitate MCLR binding to the imprinted sites. Fig. 3-14B shows the performances of sensors with and without pores, it can be seen that the pores enhanced the consistency of the sensor response for 1–20 µg/L.

A

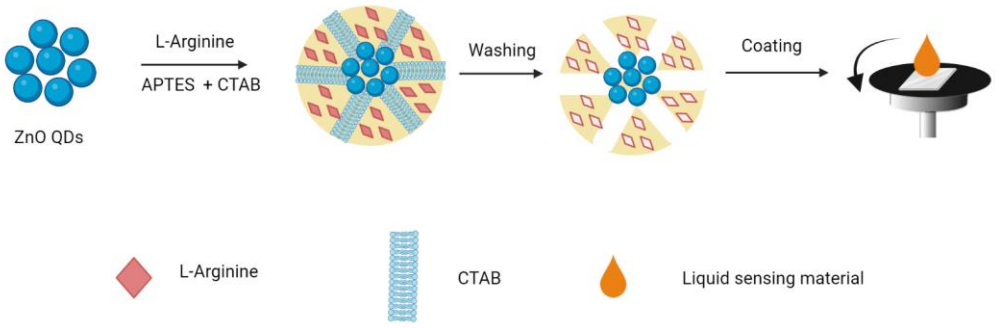

B

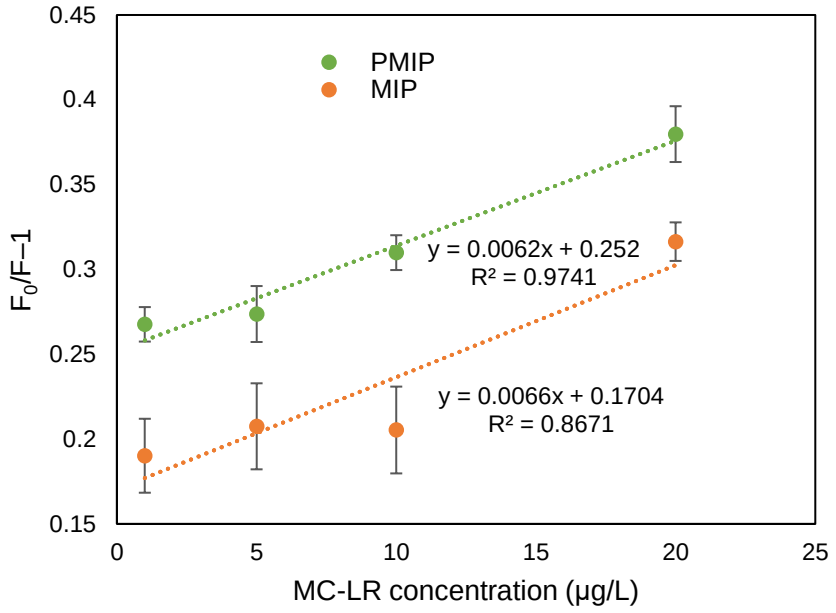

Figure 3-14: (A) Synthesis process of porous MIFS (ZnO@PMIPs) for MCLR detection, (B) Fluorescence response of the MCLR sensors prepared with and without porous to 1–20 µg/L of MCLR.

The porous molecularly imprinted ZnO QDs fluorescence sensor (ZnO@PMIP) was further evaluated using the same procedure as that of the 2,4-D sensor. As shown in Fig. 3-15A, the fluorescence intensity of the sensor gradually decreased with the increasing concentration of MCLR, proving the ability of the sensor to detect MCLR. According to the Stern-Volmer plot of the sensor (inset of Fig. 3-15A), for 0–20 µg/L of MCLR, ZnO@PMIP showed a sensor sensitivity of 0.0076 and a detection limit of 1 µg/L, indicating its applicability to determine if the drinking water is contaminated by MCLR according to WHO regulations. Porous non-imprinted polymer (ZnO@PNIP) also showed slight quenching to MCLR (Fig. 3-15B). However, the changes in the fluorescence intensity were not significant and the results were poorly consistent compared with the ZnO@PMIP sensor. Also, the large error bar associated with each response point of ZnO@PNIP made it difficult to distinguish between the MCLR concentrations. The imprinting

was calculated to be 1.6 under optimum conditions, thus highlighting the importance of imprinted sites to sensor sensitivity.

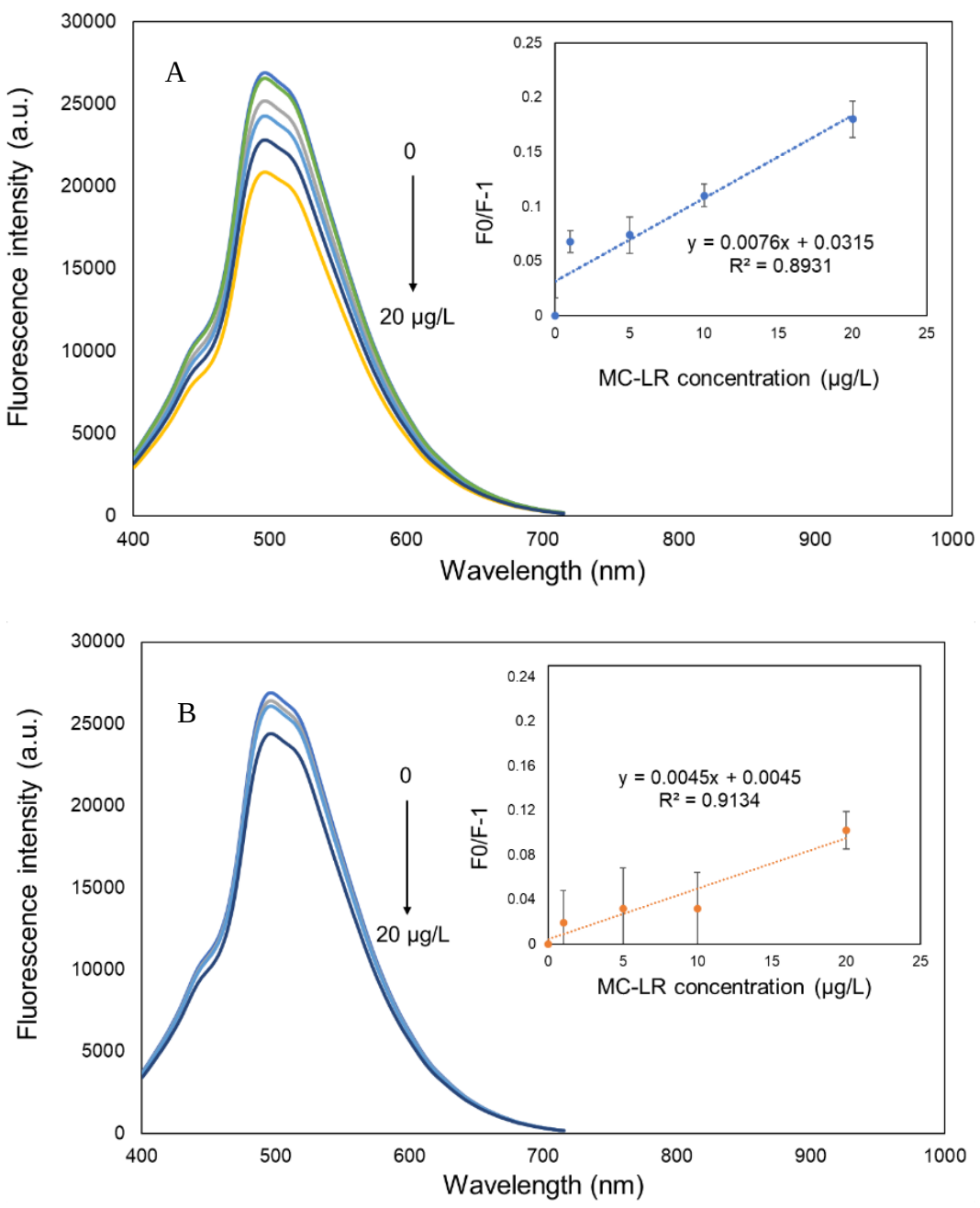

Figure 3-15: Response of the (A) ZnO@PMIP and (B) ZnO@PNIP sensor chips to 0–20 µg/L of MCLR represented with fluorescence spectra and Stern-Volmer plot (inset).

The selectivity of the MCLR sensors was evaluated by recording the sensors' response to the molecules commonly found in polluted water including PNP, glyphosate, MCPB, and 2,4-D. As shown in Fig. 3-16, MCLR induced the highest response of ZnO@PMIP because of the complementary imprinted sites. It is also worth mentioning that ZnO@PMIP's response to interfering molecules was at a similar level to its response to DI water and even the presence of 1 µg/L of MCLR could be differentiated from other molecules. It can be said that the ZnO@PMIP sensor's response to the interference molecules was mainly due to the quenching effect of DI water; organic molecules other than MCLR were not capable of inducing sensor response. In comparison, responses of ZnO@PNIP to the interfering molecules were very similar to the response to MCLR which indicated the low selectivity of the non-imprinted sensor. The contribution of the molecularly imprinted sites to sensor selectivity was made clear by comparing the results of ZnO@PMIP and ZnO@PNIP sensors; the existence of the imprinted sites assured that only the target molecule MCLR can bind to the PMIP and induce sensor response. For ZnO@PNIP that lacks imprinted sites, organic molecules would either bind to the non-selective polymer surface or pores, so MCLR could not be differentiated from other molecules.

Overall, a few simple modifications of the 2,4-D sensor allowed the detection of a different molecule with high sensitivity and selectivity. Compared with 2,4-D, MCLR is a cyclic biomolecule with a larger size, so the successful application of the sensor for both chemical and biological water contaminants shows the prospect of the developed sensing system to detect various types of water contaminants with a simple modification of the sensing layer. Also, given the flexibility of the physical immobilization method proposed and successfully tested in our study, any type of sensing material can in principle be transformed to the solid phase to obtain portable sensors with minimum effort.

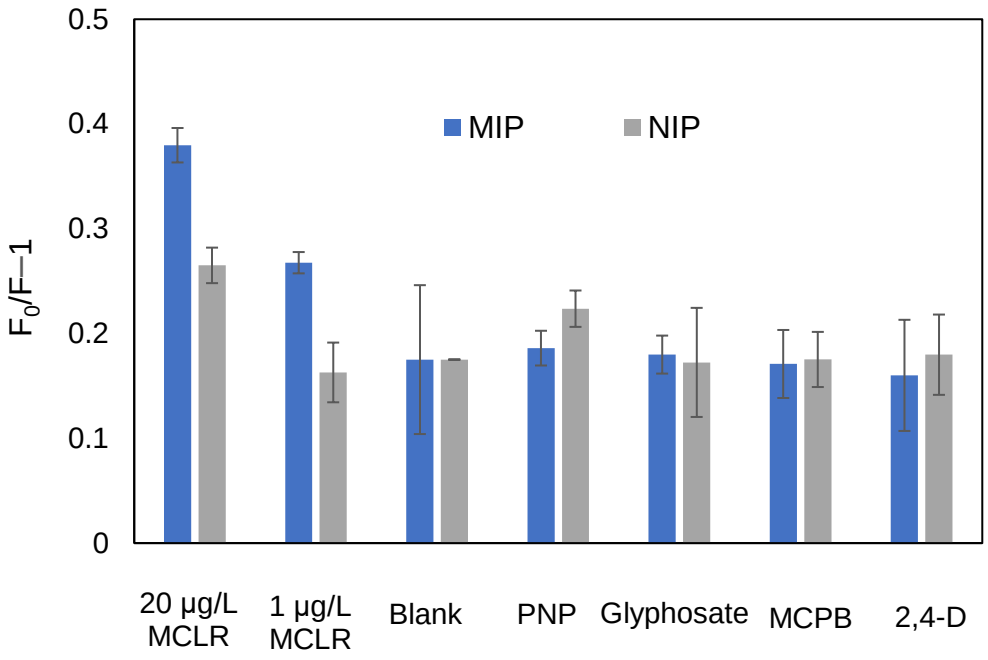

Figure 3-16: Response of the ZnO@PMIP and ZnO@PNIP sensors to MCLR, 60 µg/L of PNP, 70 µg/L 2,4-D, 280 µg/L Glyphosate, 20 µg/L MCPB, and the blank solution. The concentrations of the interfering molecules were selected according to their limit set by the WHO.

3.4 Conclusion

In summary, the first reported solid-phase ZnO@MIP fluorescence sensor that combines the high sensitivity of ZnO QDs and the high selectivity of MIPs showed a superior performance in the detection of the herbicide 2,4-D and algae-bloom toxin MCLR. The sensor showed a stable emission and high sensitivity for target detection, which indicates the potential of using cost-efficient, environmentally and biologically friendly ZnO QDs as the fluorescence sensing material. The developed sensing materials could respond to the target molecule when transformed to the solid phase and a portable detector could reliably measure the changes in the fluorescence intensity of these solid sensors. This demonstrated that sensors prepared by physical attachment methods

like spin coating can be used to deposit fluorescence materials in a simple and time-efficient way without impairing the sensing properties. Moreover, the successful detection of two different model contaminants of vastly different sizes and nature, 2,4-D and MCLR, shows that the developed system can be easily adapted for the detection of different types of target molecules. The next step would be collecting contaminated water samples to detect 2,4-D and MCLR in natural resources and evaluating the sensor performance according to the standard protocols of measuring these contaminants in water, such as the ones proposed by the Environmental Protection Agency (EPA).

The ease of use and high performances of the fluorescence solid sensor for detecting organic contaminants in water demonstrated in our study can bring the sensor's development a step closer to the realization of lab-on-chip devices by overcoming the limitations of time-consuming sample preparation and the necessity of using sophisticated detection equipment.

Chapter 4: Solid-Phase Molecularly Imprinted Fluorescence Sensor for Lactate Measurement in Sweat

4.1 Introduction

It was mentioned in Chapter 2 that lactate, the anion form of lactic acid, is a biochemical formed by anaerobic glycolysis, and its concentration is relevant to sports performance, condition of patients and the quality of food products.[99–104] Compared with the conventional laboratory analysis of lactate concentration, detection through biosensors is more efficient and convenient. Various biosensors have been reported for measuring lactate in blood,[109,110] sweat,[111,112] and tears,[113,114] using the enzymatic reaction between lactate and lactate oxidase. Since enzymes are made from protein, the orientation, and the folding of peptides are critical for enzymes to show catalytic activity. So, the conjugation of enzymes with the transducers and the changes in the temperature and PH cause significant loss in enzyme activity.[111,115] Therefore, biological receptors like enzymes should be avoided for future sensor development.

As an alternative, MIFS offers high sensitivity, selectivity and a straightforward detection method. The direct quenching mechanisms of fluorescent sensors including PET and RET enable target detection without an intermediate such as enzyme. The recognition ability of MIPs can be comparable to enzymes by forming stable and well-defined imprinted sites. Although there are previous examples of forming lactate imprinted polymers, there is no precedence of forming MIFS to detect lactate, to the best of our knowledge. Also, the portable MIFS chips presented in Chapter 3 were proven to be promising sensing platforms to measure target molecules with high sensitivity and selectivity. Therefore, in this chapter, I investigated the possibility of forming MIFS for lactate

measurement and the applicability of the sensing platform developed in Chapter 3 for lactate analysis in sweat.

Similar to the sensor components reported in chapter 3, sensing material was formed with ZnO QDs and MIPs, fluorescence chips were generated using spin coating and the fluorescence signals were evaluated with a portable detector. Since there is no previous example of MIFS formation for lactate, the developed biosensor chips were first evaluated for measuring lactic acid in DI water to prove the feasibility of the detection concept and then for measuring lactate in PBS, which is a water-based salt solution commonly used in biological research to represent sweat. In addition, two different monomers were used to form MIFS to optimize sensor selectivity. The commonly used monomer APTES, which is expected to bind with the carboxyl group of lactic acid, and 5-indolylboronic, which is expected to bind with the *cis*-diol group of lactic acid. The developed biosensor chips exhibited the capability of target detection in both DI water and PBS with high sensitivity and selectivity, thus proving the ability of MIFS for lactate analysis and the potential applicability of the developed sensing platform for biological targets.

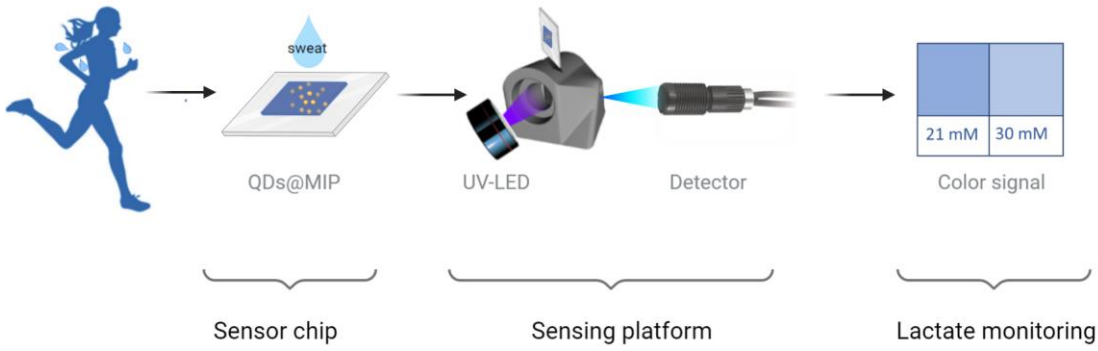

Figure 4-1: Graphical abstract of the sensing platform for lactate measurement in sweat. As presented, the sensing material was formed with QDs and MIPs and coated on quartz chips; UV-LED and a portable detector were used to detect sensor signals and the intensity of fluorescence signals were used to analyze lactate concentration.

4.2 Methodology

Similar to the sensing material reported in Chapter 3, the lactate sensing material was formed using ZnO QDs and MIPs. MIPs were synthesized with the monomers APTES and 5-indolylboronic acid using the reported synthesis methods with some modifications. NIP-based sensors were prepared using the same method except for the addition of the template molecule. Several characterization methods were applied to examine the structure, composition, and optical properties of the sensing materials.

4.2.1 Materials and Synthesis Method

5-Indolylboronic acid, hydrogen peroxide (H_2O_2), iron (II) chloride, lactic acid, ascorbic acid (AA), uric acid (UA), and glucose were purchased from Sigma-Aldrich (Ontario, Canada).

4.2.1.1 Synthesis of APTES Functionalized ZnO QDs

The synthesis and the functionalization of ZnO QDs are explained in detail in Chapter 3, section 3.2.

4.2.1.2 Synthesis of MIFS with APTES

The MIFS was formed with APTES monomer using the procedure presented in Chapter 3, section 3.2 with lactic acid as the template molecule.

4.2.1.3 Synthesis of MIFS With 5-Indolylboronic Acid

Molecularly imprinted poly(indolylboronic acid) (MIP@Pin-BAc) was prepared according to the previously reported methods[145,146] with some modifications. The 5-indolylboronic

acid/lactic acid/ $FeCl_2$ (0.1 g/0.1 g/0.05 g) mixture was first dissolved in 50 ml of DI water and the PH of the solution was set to 8 with the addition of NaOH. After the formation of a homogenous solution, 2.5 ml H_2O_2 was added to start the polymerization. After 6 h of reaction at room temperature, the polymer was collected and washed with DI water to remove the unreacted monomer and the template molecule. The NIP was prepared using the same procedure without the addition of lactic acid.

To form molecularly imprinted Pin-BAc and ZnO QDs composite (MIP@PIn-BAc/ZnO), 0.26 g of centrifuged Pin-BAc dissolved in 32 ml of DI water and 0.7 g of ZnO QDs dissolved in 18 ml of ethanol were vigorously mixed for 3 h. The composite was washed with ethanol to remove unattached QDs. The product was dissolved in ethanol to prepare the sole for spin coating.

4.2.1.4 Solid Sensors Preparation Method

The preparation and the detection of the solid sensors are the same as the process presented in detail in Chapter 3, section 3.2.1.

4.2.2 Characterization and Evaluation Methods

The characterization and the evaluation of the sensors are discussed in detail in Chapter 3, section 3.2.2. The sensitivity of the sensors was determined by recording sensor response to lactic acid in DI water then with lactate in PBS; selectivity of the sensors was determined by measuring the sensor response to 0.3 mM glucose, 0.03 mM AA and 0.05 mM UA which are the concentrations of these molecules commonly found in sweat.

4.3 Results and Discussion

The morphology and topography of the sensing material were examined using TEM, and the chemical composition was determined using FT-IR spectra. The sensors formed with two different monomers were evaluated with lactic acid in DI water to prove the concept of detection and optimize the MIP composition. The monomer that led to better sensing performance was further adjusted to measure lactate in PBS to prove the applicability of the sensor to sweat analysis.

4.3.1 Characterization of ZnO@MIP

According to the UV-Vis spectra, ZnO QDs absorbed UV radiation between 290 and 340 nm, with a peak value of 320 nm (Fig. 4-2). To allow QDs to generate higher emission intensity, a commercial UV-LED at a wavelength of 310 nm was used to excite the solid sensing material. The excited ZnO QDs exhibited symmetric emission spectra with a peak emission around 500 nm.

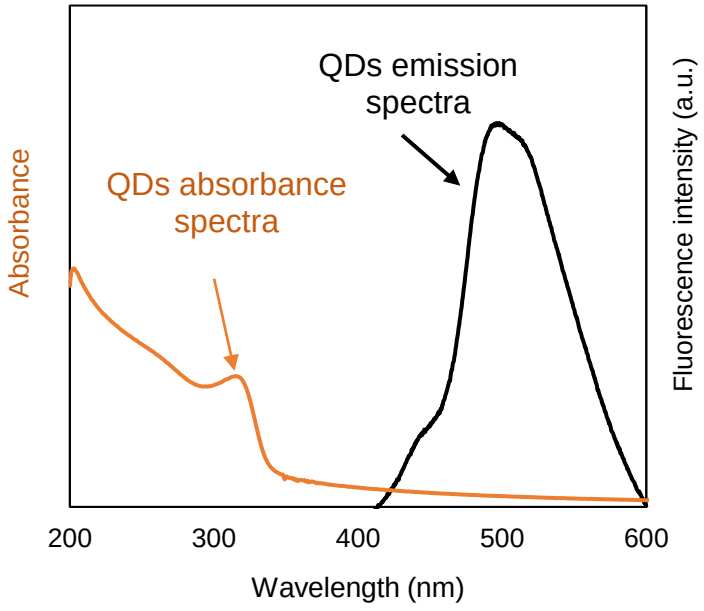

Figure 4-2: Absorbance and the emission spectra of ZnO QD recorded with UV-Vis spectroscopy and fluorescence spectroscopy respectively.

The TEM image of ZnO QDs (Fig. 4-3A) exhibited that QDs were well dispersed and ranged from 3 to 5 nm in diameter. The high-resolution TEM images of MIP@PIn-Bac (Fig. 4-3B&C) showed that the PIn-BAc nanoparticles appeared in spherical shapes with a diameter of approximately 30 nm. A similar structure was observed when the ZnO QDs were linked to the MIP@PIn-BAc (Fig. 4-3D); part of the QDs was at the periphery of the polymer and part of them was inside the polymer, as shown in the inset of Fig. 4-3D. The observation that QDs residing on the margin of the polymer spheres might be due to the π-π interaction between the PIn-BAc and the $sp^2\pi$ clouds of the QDs.[39]

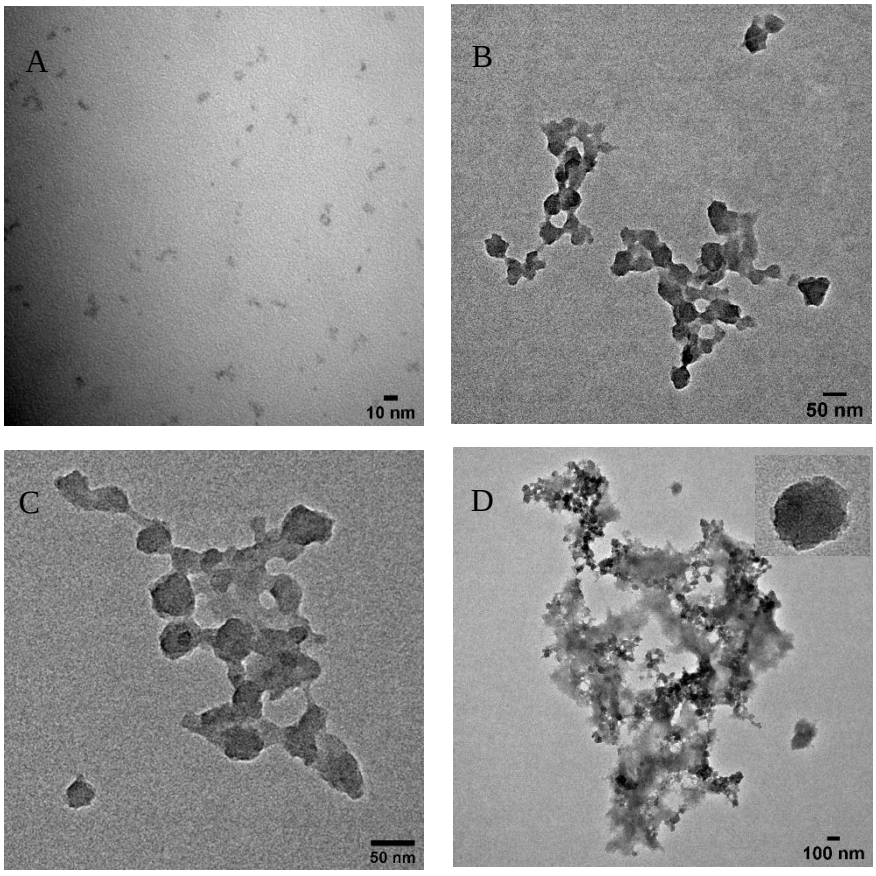

Figure 4-3: (A) TEM images of ZnO QDs, (B, C) high-resolution TEM images of MIP@PIn-BAc, (D) MIP@PIn-BAc/ZnO composite, and the QDs contained in the polymer (D-inset).

FT-IR spectrums of silica-coated ZnO QDs, MIP@PIn-BAc, and MIP@PIn-BAc/ZnO composite are shown in Fig. 4-4. The asymmetrical absorption peaks of silica-coated ZnO QDs at 1504 cm^{-1} and 1423 cm^{-1} are due to the stretching of the C-H and O-H groups attached to the QDs from the reactant acetate during the synthesis; the peaks at 866 cm^{-1} and 672 cm^{-1} are assigned to C-H vibration, especially the peak at 672 cm^{-1} is assigned to the C-H group of alcohols that resulted from the repeated washing with ethanol. The Si-O-Si stretching peak that appeared on 1000 cm^{-1} and 1030 cm^{-1} was evidence of growing APTES functional groups on the surface of QDs.[128–130] For the MIP@PIn-BAc, the broad peak from 3625 cm^{-1} to 2990 cm^{-1} is assigned to the N-H stretching, the peak at 1603 cm^{-1} is ascribed to the carbon-carbon double-bound of the cyclic structure, and the peak at 1327 cm^{-1} is attributed to the C-N stretching for aromatic amines.[147] The FT-IR spectrum of the MIP@PIn-BAc/ZnO composite is predominated by the peaks belonging to the QDs. The peaks assigned to C-H, O-H, and Si-O-Si for the QDs can be seen in the composite, thus proving the successful incorporation of the QDs to the MIP structure.

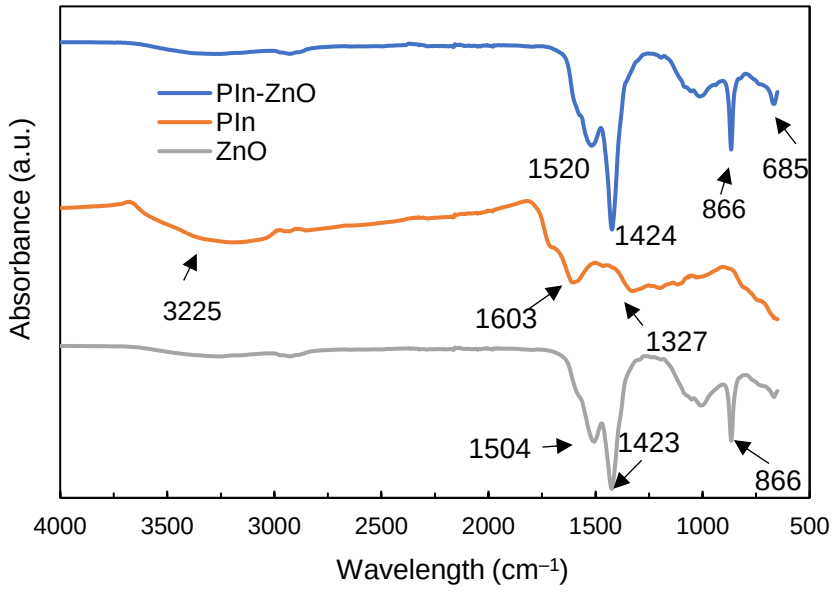

Figure 4-4: FT-IR spectrum of silica-coated ZnO QDs, MIP@PIn-BAc and MIP@PIn-BAc/ZnO composite.

4.3.2 Evaluation of Lactic Acid Imprinted Polymer

Optimizing the monomer to enable a strong monomer and template binding is critical for the selectivity of molecularly imprinted fluorescence sensors, especially since this is the first study to apply MIFS for measuring lactic acid, to the best of our knowledge. We evaluated the effects of two different monomers on lactic acid detection; APTES and 5-indolylboronic acid were selected to form the imprinted polymer by binding to the carboxyl functional group and *cis*-diol functional group of the template respectively. APTES is commonly used for MIP formation[66,76,134] and parametric studies have been conducted for APTES-MIP in Chapter 3; in contrast, there is very little information on the MIP@PIn-BAc formation[38,118] and we found no research that reported the incorporation of ZnO QDs to MIP@PIn-BAc. Therefore, efforts were made to determine the optimum synthesis method for MIP@PIn-BAc/ZnO before examining the sensor's performance on lactic acid detection. The fluorescence quenching of both sensors was evaluated using the Stern-Volmer equation (Equ. 1).

4.3.3 Formation of MIP with APTES

The previous APTES-based fluorescence sensor to detect 2,4-D in chapter 3 exhibited high sensitivity and selectivity. The superior sensor performance was contributed to the imprinted sites that were formed between the amino functional group of the monomer and the carboxyl functional group of the target molecule. We anticipated that a similar high sensor performance could be obtained for lactic acid using APTES monomer because of the carboxyl functional group of lactic acid. So, lactic acid imprinted polymer was prepared using APTES as the functional monomer and TEOS as the cross-linking agent following the synthesis procedure shown in Fig. 4-5.

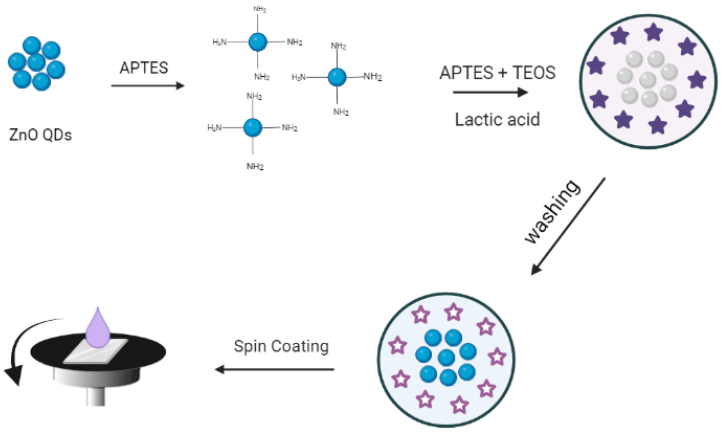

Figure 4-5: Schematic representation of lactic acid MIP synthesis procedure with APTES monomer. First, ZnO QDs were functionalized with APTES to increase the stability, then an imprinted polymer layer was formed on the surface of the QDs. After removing the template molecules from the polymer, the sensing material was coated on quartz to form MIFS chips.

The ability of the APTES-MIP solid sensor to detect lactic acid was evaluated by recording its response to 0 to 5 mM of lactic acid. As shown in Fig. 4-6A, the APTES-MIP showed fluorescence quenching proportional to lactic acid concentration and a linear Stern-Volmer relation with a sensor sensitivity of 0.1456. To determine the effect of interfering molecules and evaluate the sensor's capability to selectively measure lactic acid in actual biological samples, several commonly seen interfering molecules in sweat including glucose, UA, and AA were added to the APTES-MIP sensor to record the sensor's response. The APTES-MIP sensor failed to show selectivity toward lactic acid by demonstrating a similar level of response to the interference molecules (Fig. 4-6B). Since sensor selectivity is an important factor in preventing false-positive response, we concluded that this sensor was not capable of measuring lactic acid in actual samples. The poor selectivity of the MIP to lactic acid molecules was attributed to the unsuccessful formation of the imprinted sites.

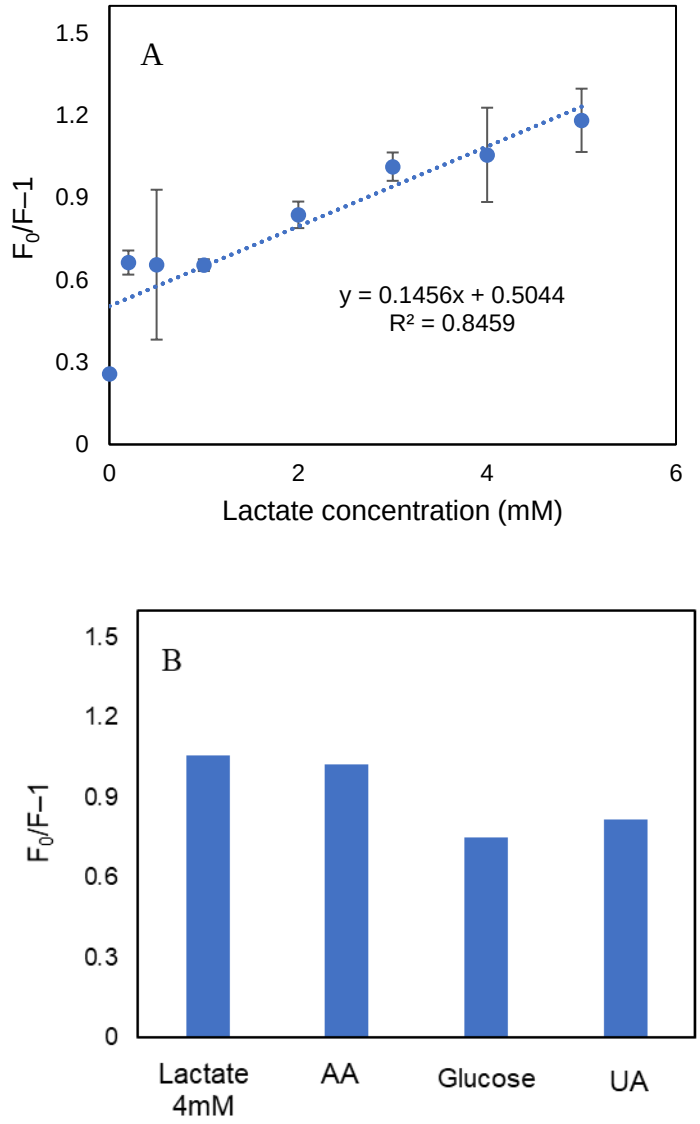

Figure 4-6: Response of APTES-MIP to (A) lactic acid and to (B) interfering molecules.

4.3.4 Formation of MIP With 5-Indolylboronic Acid

It has been found that 5-indolylboronic acid contains a boronic acid functional group that is known to have a high binding affinity to compounds with *cis*-diol functional groups such as carbohydrates, glycoproteins and nucleosides.[148,149] MIP formed by 5-indolylboronic acid was

first reported by Fuxiang Chu et al.[38,145]; the MIPs were formed with the polymerization of the indole group (Fig. 4-7A) and the selectivity of the MIPs was attributed to the boronic acid side chain that binds with the target molecule (Fig. 4-7B). The formed polymer has been successfully combined with carbon-based QDs for the fluorescence detection of dopamine[145] and glucose.[38] Since lactic acid contains a *cis*-diol group similar to dopamine and glucose, 5-indolylboronic acid was used as the functional monomer to develop MIFS to detect lactic acid.

To adapt the synthesis process of MIP@PIn-BAc for ZnO QDs and thin-film coating, modifications were made to the reported method. [38,145] As schematically represented in Fig. 4-7C, the non-fluorescence MIP@PIn-BAc was formed first, and then ZnO QDs were attached to obtain MIP@PIn-BAc/ZnO fluorescence sensors. We used the two-step fluorescence sensor formation approach to protect ZnO QDs against alkaline and oxidative polymerization conditions. This has also been shown to reduce the emission damage caused by the repeated template washing process.[150] In addition, optimization was made on the solvent selection to increase the sensor's net response.

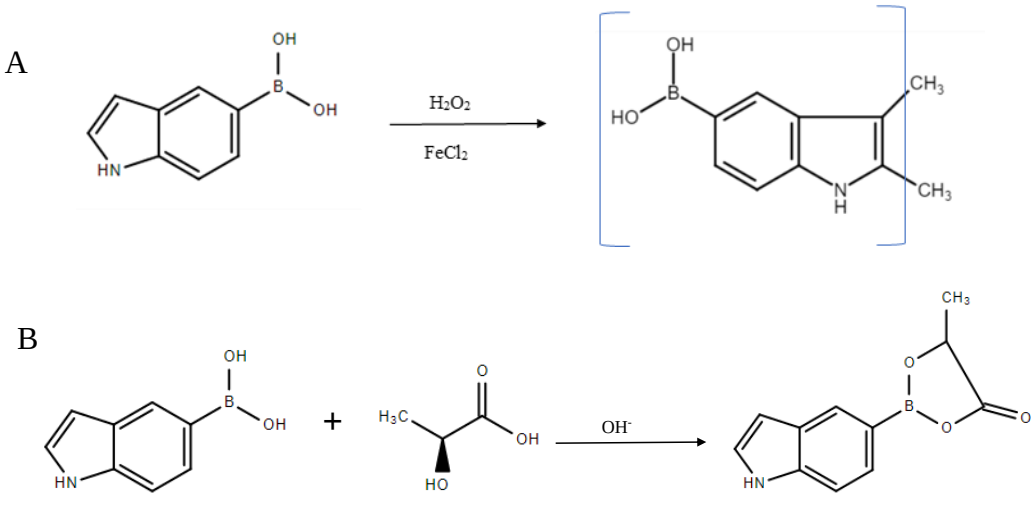

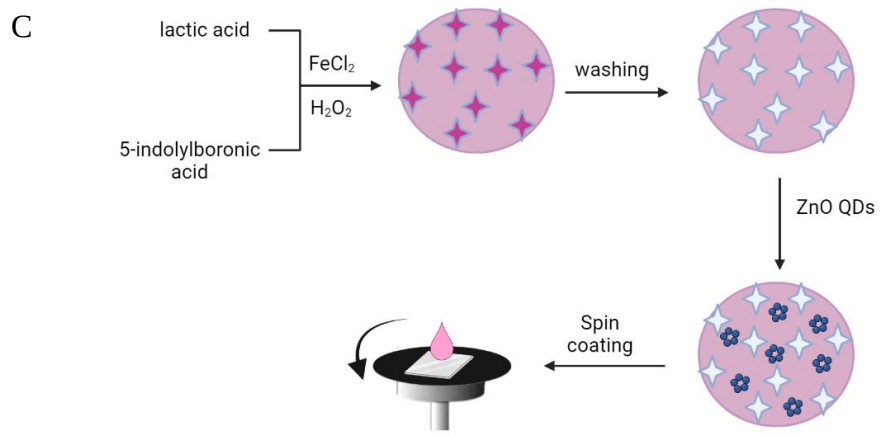

Figure 4-7: Chemical reaction of (A) indolyl group polymerization, (B) binding between boronic acid and lactic acid. (C) Schematic representation of MIP@PIn-BAc/ZnO synthesis process.

4.3.4.1 Studying the Effect of Solvent

ZnO QDs demonstrate a higher solubility and fluorescence intensity when dissolved in ethanol, while MIPs show better target recognizability when dissolved in DI water. Therefore, the attachment of QDs to MIP was performed in DI water, DI water-ethanol mixture and pure ethanol to evaluate the effect of solvent on the sensor performance. The MIP@PIn-BAc/ZnO sensor prepared with ethanol showed the highest fluorescence intensity (~70,000 a.u.) because of the compatibility between ethanol and ZnO QDs. Fluorescence intensity of around 20,000 a.u. and 10,000 a.u. were detected for sensors prepared with DI water–ethanol mixture and DI water, respectively, which indicated that the sensor's initial fluorescence intensity decreased with the addition of water (Fig. 4-8A). The difference in the initial fluorescence intensities indicated the different solvent relaxation of ZnO in ethanol and DI water, where DI water caused quenching of the QDs.[151] These sensors were then treated with the blank solution and 4 mM lactic acid to

evaluate the net sensor response to lactic acid (Fig. 4-8B). Despite the high response of the sensor prepared with ethanol, the net response was only 0.14 because of the equally high response to the blank solution. For the sensor prepared with pure DI water, although the response to the blank solution was low, the comparably low response to lactic acid resulted in a net response of around 0.07. The highest net response was realized by the sensor prepared with the DI water–ethanol mixture, which had a comparable high response to lactic acid and a low response to the blank solution. If only the response to lactic acid was taken into consideration, the sensor prepared with ethanol was the best choice. However, the equally high response to the blank solution shows that the response shown to lactic acid was mainly because of the quenching induced by DI water, so the changes in the lactic acid concentration would not be adequately reflected on the quenching amount; in other words, sensor sensitivity would be low. Therefore, the sensor with the highest net response would be the optimum candidate to obtain a high sensor sensitivity. The observed high net response is because the solvent mixture buffered the quenching effect of water compared with the sensor prepared with pure ethanol and allowed more active QDs to remain in the sensor compared with the sensor prepared DI water, which in turn enhanced the lactic acid recognition.

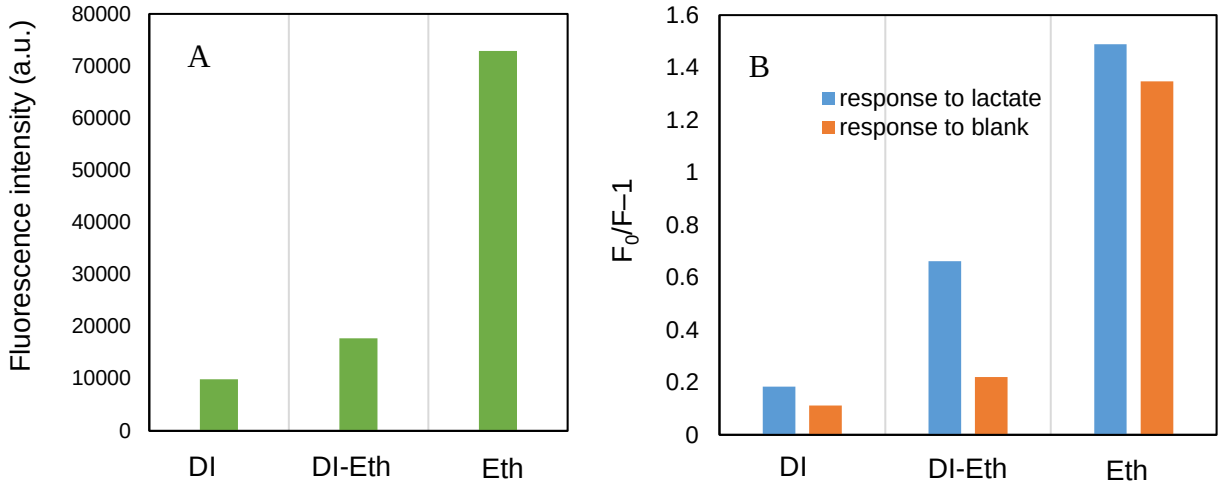

Figure 4-8: (A) Initial fluorescence intensity of the sensors prepared with DI water, ethanol and the mixture of ethanol and DI water and, (B) response of these sensors to 4 mM of lactic acid (blue bars) and the blank solution (orange bar).

4.3.4.2 Evaluation of Sensor Performance

Under the optimum preparation conditions, the MIP@PIn-BAc/ZnO solid sensor was further evaluated by analyzing its response to various concentrations of lactic acid. The response of the NIP@PIn-BAc/ZnO sensor was also analyzed and compared with the MIP@PIn-BAc/ZnO sensor to evaluate the effect of imprinted sites. For 0–4 mM of lactic acid, the fluorescence intensity of the MIP@PIn-BAc/ZnO sensor showed a gradual and consistent decrease with increasing concentrations of lactic acid (Fig. 4-9A). According to the Stern-Volmer plot, the sensor maintained a linear response curve for 0–4 mM of lactic acid with a sensor sensitivity of 0.12 and a correlation coefficient of 0.99 (inset of Fig. 4-9A).

The NIP@PIn-BAc/ZnO fluorescence sensor was not able to show distinguishable changes in the fluorescence intensity to the increasing concentration of lactic acid, as shown clearly in the

Stern–Volmer plot in the inset of Fig. 4-9B; the sensitivity of the sensor was calculated as 0.0207 with a correlation coefficient of 0.88. The imprinting factor, which is the ratio of imprinted and non-imprinted sensors' sensitivity, was 5.5. This difference in the sensor performance was due to the imprinted sites embedded in MIP@PIn-BAc/ZnO. The presence of imprinted sites facilitated the binding of lactic acid to the sensor and enabled the recognition of the target molecule in different concentrations; therefore, allowing the sensor to exhibit consistent and concentration-specific quenching. In contrast, lactic acid can only bind to the surface boronic acid groups of NIP@PIn-BAc/ZnO and quench the QDs near the surface. When the surface binding sites were saturated, despite the addition of lactic acid in a higher concentration, the response level remained at a similar level.

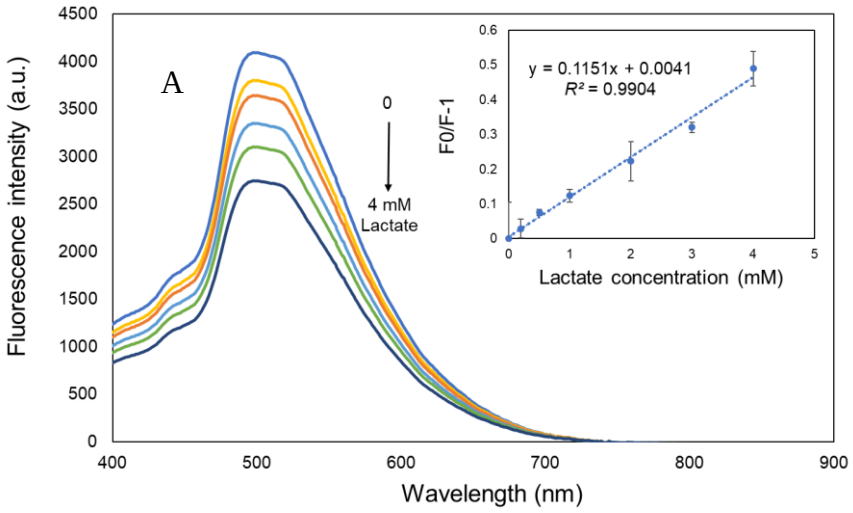

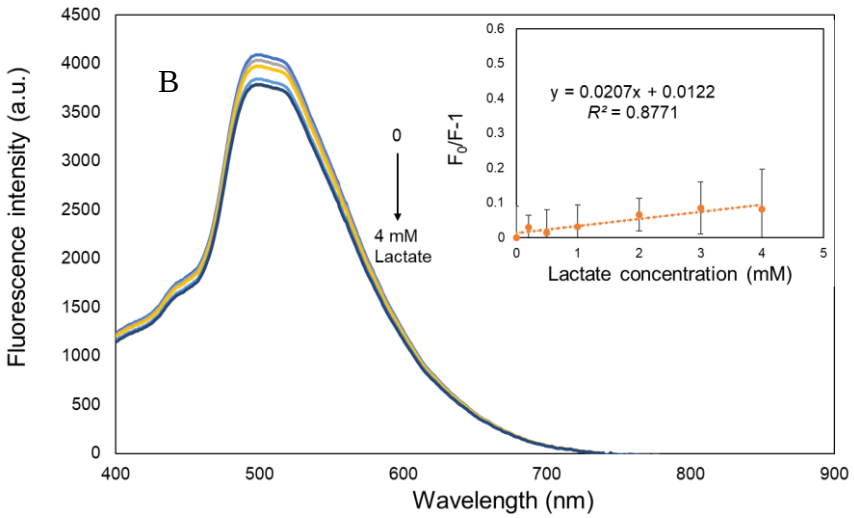

Figure 4-9: Response of the solid (A) MIP@PIn-BAc/ZnO and (B) NIP@PIn-BAc/ZnO sensors to increasing concentrations of lactic acid in DI water represented with fluorescence spectra and Stern-Volmer plot (inset)

To determine the effect of interfering molecules and evaluate the sensor's capability of detecting lactic acid in actual samples, the fluorescence response of the MIP@PIn-BAc/ZnO and NIP@PIn-BAc/ZnO sensors to the common interference molecules in sweat such as glucose, UA, and AA was evaluated (Fig. 4-10). These molecules were studied because they can bind with either the boronic acid group of the polymer or the amino-functionalized QDs to interfere with the sensor response. For the MIP@PIn-BAc/ZnO sensor, the highest quenching was shown by lactic acid, while the response to other molecules was equally low and similar to that of DI water. Therefore, it could be concluded that the response shown to the interference molecules by the MIP@PIn-BAc/ZnO sensor was mainly because of the sensor response to DI water and that the response induced by the interfering molecules was negligible.

In comparison, the responses of NIP@PIn-BAc/ZnO sensor to the interfering molecule and the blank sample were not differentiable from those of lactic acid. As a result, it can be concluded that the NIP-based sensor was not capable of either detecting or recognizing the target molecule.

Comparing the results of the MIP@PIn-BAc/ZnO and NIP@PIn-BAc/ZnO sensors indicated that the recognition of the target molecule by the sensors was due to the molecularly imprinted sites. During the polymer formation, the *cis*-diol functional group of lactic acid was bound to the boronic acid group of the monomer 5-indolylboronic acid so the specificity of the MIP@PIn-BAc/ZnO sensor was determined by the shape, size and functional group of the target molecule. All these criteria need to match the imprinted sites to achieve a high sensor response. Therefore, even though both glucose and AA contain more than one *cis*-diol group, the differences in other criteria prevented these molecules from binding with the boronic acid groups on the imprinted sites to induce a high sensor response. For the NIP@PIn-BAc/ZnO sensor, molecules bonded to the functional groups on the polymer surface, which does not display selectivity; therefore, the NIP@PIn-BAc/ZnO sensor could not differentiate lactic acid.

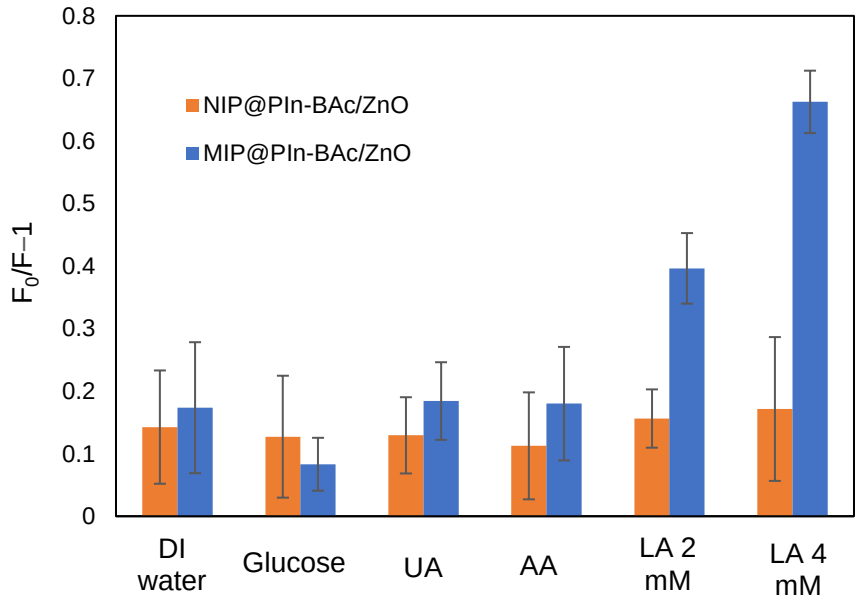

Figure 4-10:The NIP@PIn-BAc/ZnO and MIP@PIn-BAc/ZnO sensor response to glucose, uric acid and ascorbic acid with the reference response to DI water and lactic acid.

4.3.5 Performance Comparison of Sensors Formed With Different Monomers

Differences in the sensitivity and selectivity of APTES-MIP and MIP@PIn-BAc/ZnO sensors revealed the effect of monomer on sensor performance. In terms of sensor sensitivity, the APTES-MIP sensor had a higher response to lactic acid and the sensitivity was 37% higher than that of the MIP@PIn-BAc/ZnO sensor. However, the consistency of the response was better for the MIP@PIn-BAc/ZnO sensor with a linear coefficient of 0.99 compared to the 0.86 shown by the APTES-MIP sensor. In terms of sensor selectivity, the MIP@PIn-BAc/ZnO sensor could recognize lactic acid by showing negligible response to the interfering molecules, whereas the APTES-MIP sensor could not recognize lactic acid by showing similar responses to lactic acid and the interfering molecules. Therefore, it can be concluded that the MIP@PIn-BAc/ZnO sensor, which showed a comparable high sensitivity, and a significantly higher selectivity is more suitable for lactic acid detection.

The differences in lactic acid recognition ability are attributed to the differences in the binding affinity of lactic acid with the monomers. It can be interpreted from the sensor response that although both monomers contain functional groups that can bind with the target (Fig. 4-11), the imprinted sites were only formed when the monomer was binding to the *cis*-diol group of lactic acid. The unsuccessful formation of imprinted sites with APTES might be because lactic acid was presented in the deprotonated state during the synthesis process.[152] It is assumed that lactic acid lost a proton to form lactate during the synthesis because of the addition of ammonia and NaOH. Therefore, the anticipated binding between the amino functional group of APTES and the carboxyl functional group of lactic acid could not take place, given that the lactic acid was presented in its salt form lactate. In comparison, higher PH was favourable for the binding between the *cis*-diol

group and the boronic acid group so the imprinted sites were formed successfully with the 5-indolylboronic acid monomer.

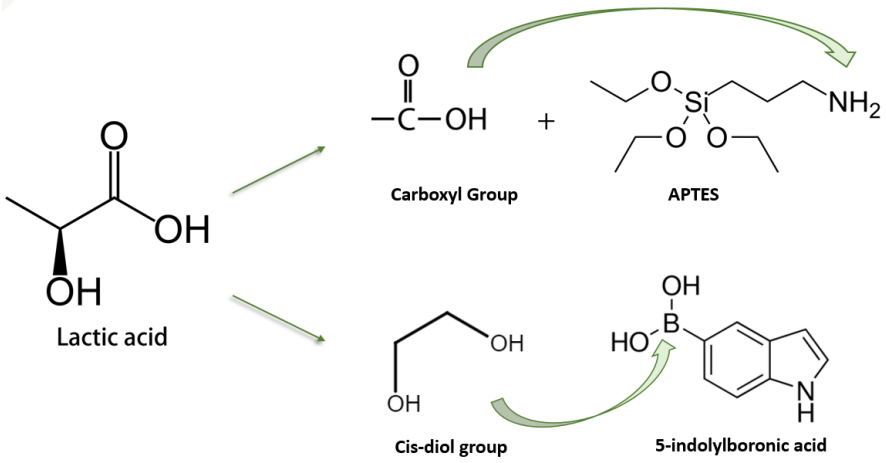

Figure 4-11: Representation of the two functional groups of lactic acid and the monomers chosen in this study, the arrows show the binding sites between the functional group and the monomer.

4.3.6 Detection of Lactate in PBS

The successful measurement of lactic acid in DI water with high sensitivity and selectivity using the MIP@PIn-BAc/ZnO sensor encouraged the evaluation of the sensor in an environment similar to that of sweat. In anaerobic glycolysis, lactate which is the anion form of lactic acid is produced by the Cori cycle. Therefore, sample solutions were prepared using PBS to mimic the ion-rich saline content of sweat where lactic acid loses a proton to form lactate, and the MIP@PIn-BAc/ZnO sensor was used to detect lactate in these samples. The sensor's response to DI water and PBS samples was significantly different (Fig. 4-12); an enhancement in the fluorescence intensity was detected for PBS in contrast to the quenching shown in the DI water samples. In

addition, the response of the sensor to lactate in PBS did not act in accordance with the Stern–Volmer relation which indicated that the sensor cannot detect lactate in a saline environment.

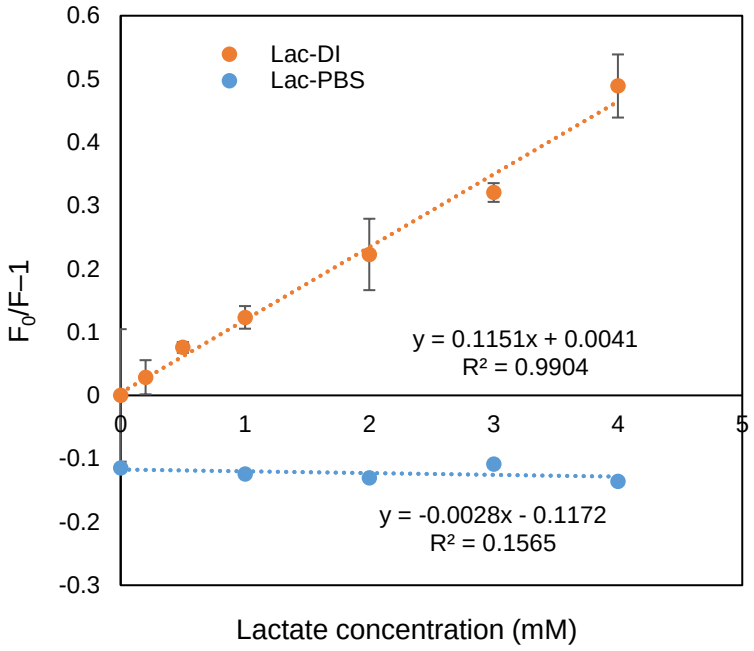

Figure 4-12: Response of the MIP@PIn-BAc/ZnO sensor to lactic acid in DI water (Lac-DI) and lactate in PBS (Lac-PBS).

Previously, it was observed that the addition of DI water during the composite formation process enhanced the target recognition of the MIP@PIn-BAc/ZnO sensor by adapting the sensing material to the sensing condition. Since the sensing condition changed for lactate in PBS samples, the adaptation of the sensing material with DI water was no longer suitable. Therefore, it was assumed that adding PBS during the synthesis might be the key to overcoming the negative impact of the saline solution. Similar to DI water, PBS also affects the fluorescence intensity of the QDs, so optimization was needed on the amount of PBS to prepare the sensor for the saline environment while preserving its fluorescence intensity. Fig. 4-13 shows the response of sensors prepared with

different amounts of PBS. When 25% PBS was added during composite formation, the response was more positive than the sensor prepared without PBS but there still was no traceable pattern on the fluorescence quenching. When the amount of PBS was increased to 50%, the zero point (the response to PBS) was negative, but the quenching effect started to take place with the addition of lactate. The increased quenching with target concentration resulted in a linear Stern–Volmer response curve for 0–20 mM of lactate. The sensor prepared with 75% PBS also showed quenching to lactate and the degree of quenching for the 0–10 mM of lactate was higher than the sensor prepared with 50% PBS. However, the sensor prepared with 75% PBS failed to maintain the high response curve and showed saturation in the sensor response for concentrations higher than 10 mM. Finally, when the amount of PBS was increased to 100%, quenching could still be observed but the degree of quenching was much lower than the sensor prepared with 50% and 75% PBS. This is because there were fewer active QDs left in the sensor when ethanol was eliminated from the synthesis process.

Overall, adding PBS during the synthesis was beneficial to adapt the sensor for the saline environment and the amount of PBS was critical to tune the response level and the linear range. The sensor prepared with 75% and 100% PBS showed saturation in the response for concentrations higher than 10 mM because of the limited active QDs in the fluorescence sensor. For the sensor prepared with 50% PBS, the sensing material was well adjusted for the saline environment while preserving more active QDs to respond to the target. Therefore, the sensor prepared with 50% PBS showed fluorescence quenching proportional to lactate concentration.

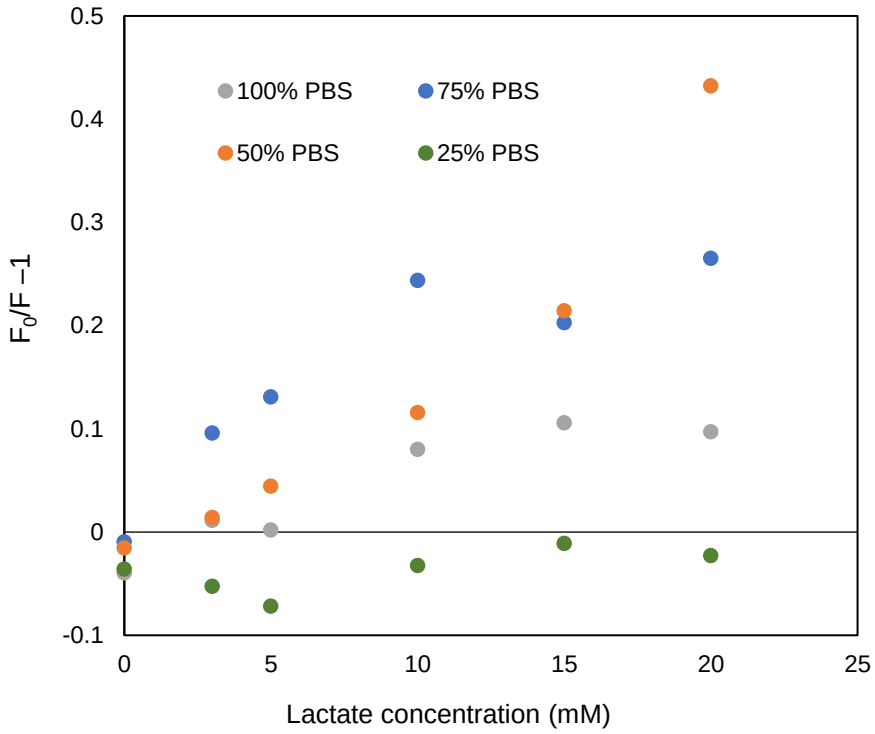

Figure 4-13: Response of @PIn-BAc/ZnO sensors prepared by adding 25%, 50%, 75% and 100% PBS during the synthesis.

The MIP@PIn-BAc/ZnO sensor prepared with 50% PBS was further evaluated on its sensitivity and selectivity for lactate measurement. By recording the sensor response with a wide range of lactate concentrations, the sensor showed an increasing amount of quenching for 0–30 mM of lactate (Fig. 4-14A), with a sensitivity of 0.0217, a correlation coefficient of 0.97 and a detection limit of 3.38 mM. The selectivity of the sensor was evaluated by recording the response to AA, UA and glucose dissolved in PBS. As shown in Fig. 4-14B, the sensor's response to 20 mM of lactate which is the lactate concentration in sweat at rest[153], was much higher than the response to the interfering molecules thus proving a high sensor selectivity.

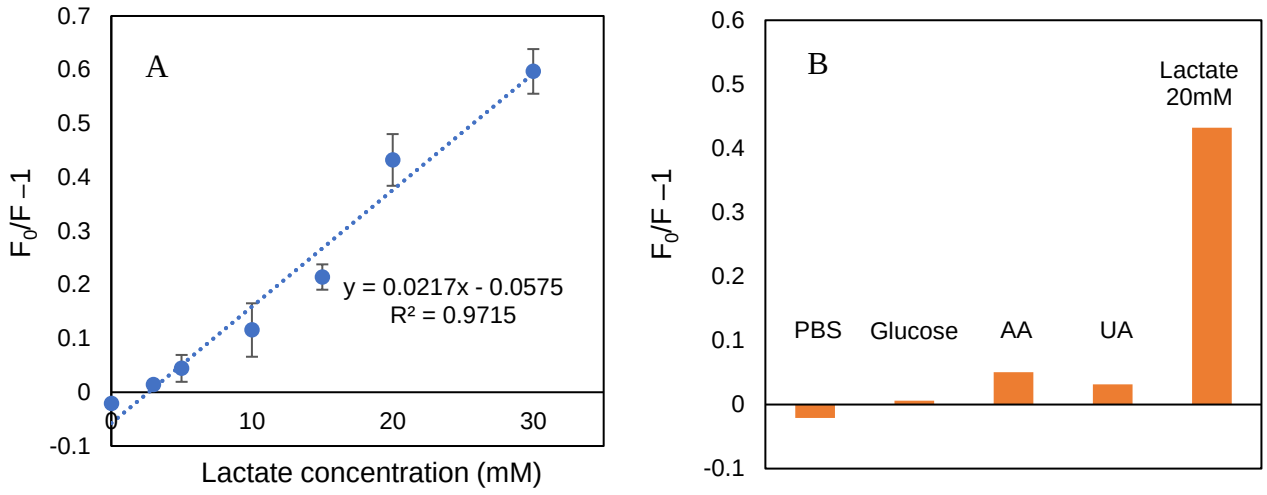

Figure 4-14: Response of the MIP@PIn-BAc/ZnO sensor prepared with 50% PBS to (A) lactate in PBS and (B) to glucose, uric acid and ascorbic acid with the reference response to PBS and lactate.

The sensing response to lactate in PBS indicates the capability of the developed sensor to measure lactate concentration in sweat with high sensitivity and selectivity. Compared to the sensor's response to lactic acid in DI water, the sensor showed a wider linear range for lactate in PBS, which is beneficial for capturing large changes in lactate concentration during exercise. This is also the first time ZnO QDs have been successfully applied to detect the target molecule in a saline environment, to the best of our knowledge.

To assess the MIP@PIn-BAc/ZnO sensor's applicability for long-term use, the response of the sensor was measured after a month of storage. The results demonstrated that the sensor maintained 60% of its original response to lactate after a month. Optimizing the sensor to attain good stability was beyond the scope of this study, whose focus was evaluating the possibility of lactate measurement with MIFS chips. However, long-term storability can be attained by further improving the sensing material. The adsorbed ions during the adaptation step, which might have

impaired QDs over time, most likely lowered the sensor response. Applying a protective layer on the QDs may help to achieve a more stable structure and increase the storability of the QDs. In addition, the passivation step may be eliminated with the core–shell QDs structure since the QDs are sheltered from the saline environment. Therefore, long-term stability can be obtained with some modification of the developed sensing system.

4.4 Conclusion

The first account of a solid fluorescence sensor that combined the high sensitivity of ZnO QDs and the high selectivity of MIPs showed superior performance in detecting lactic acid in DI water and lactate in PBS. The ability of the developed sensor to show concentration-dependent quenching revealed the potential of using cost-efficient, environmentally and biologically friendly MIFS to detect lactate. Between the sensors formed with APTES and 5-indolylboronic acid monomers, only the latter showed high sensitivity and selectivity in detecting lactic acid, highlighting the importance of the selected monomer. It was concluded that monomers should be selected according to their ability to interact with the template molecule, and this interaction should not be sensitive to easily changeable physical parameters, such as temperature and PH, to make the sensor more applicable to actual sample detection.

The successful application of the sensor formed with 5-indolylboronic acid to detect lactate in PBS with a large linear range and a high selectivity proved the viability of using the sensor to measure lactate in actual sweat samples. The next step recommended for the research is to detect lactate in simulated sweat solutions or real sweat samples and compare the results with the standard measurement techniques to evaluate the applicability of the sensing material to actual samples.

The convenient formation of the solid sensor and the detection with the portable detector can avoid the limitations of the liquid fluorescence sensors and help realize the development of lab-on-chip image-based sensing devices to monitor biomarkers that are critical to bodily functions. In addition to the experimental results obtained in Chapter 3, this work also highlighted the target flexibility and the wide-range applicability of the developed sensing platform thanks to the high sensitivity of ZnO QDs and tailor-made synthetic receptor MIP.

Chapter 5: Conclusion and Recommendations

5.1 Conclusions

The ultimate goal of this study was to show the proof-of-concept for the development of a highly sensitive, selective, portable and wide range applicable ZnO QDs based MIFS chips. The goal was realized by first proposing an optimum synthesis method for ZnO QDs based MIFS that permits a high sensitivity and selectivity to the model target molecule 2,4-D. Commonly used herbicide 2,4-D was chosen as the first model contaminant to study the feasibility of forming MIFS sensing material with biologically compatible ZnO QDs and generating MIFS chips with facile and robust physical immobilization method. The formed sensor chips were studied regarding the effect of physical parameters such as coating area and layers and evaluated on their emission stability and response time. Further, the solid ZnO@MIP sensor was assessed and compared to the liquid sensor under the operating conditions that enabled their highest sensor response. Finally, to demonstrate the wide-range applicability, efforts were made to adapt the sensing material to detect algae bloom toxin MCLR and biochemical target lactate. MCLR represents large-sized biological water contaminants and lactate represents small-sized biomarkers; for which the successful application of the developed sensor chips will indicate the flexibility of the system with respect to detection environment, molecular size and nature. The main conclusions derived from the experimental and theoretical work performed in this research are highlighted here:

For **CHAPTER 3:**

- As the first step, the most suitable MIFS composition and detection environment were studied because of the insufficient information in the open literature regarding ZnO QDs based MIFSs. It was observed that the amount of quenching is directly related to

the MIFS solvent and concentration. The solvent should allow high solubility and high initial fluorescence intensity to permit a better sensor response. The concentration of the sensing material should be decided according to the balance between the response level and the response range. A lower amount of sensing material displays a higher response level but narrows the linear detection range; a larger amount of sensing material reduces the response level but enables a wider target measurement range.

- Solid sensors prepared with various physical coating methods showed that spin coating was the desired immobilization technique that forms a robust and uniform sensing layer. Compared with spin coating, drop coating resulted in weak attachment and blade coating gave rise to inconsistent layer thickness.
- The parametric study on the spin coating process showed that the thickness of the layer (number of the sensing layers produced by spin coating) affects the response level and the linear range. Moreover, the coating layer should be more than one to ensure deposition consistency. So, the solid sensors were formed using three layers of coating (equivalent to 1.7 µm layer thickness) that enabled a uniform dispersion, comparable high sensor response and a good linear range.
- The ZnO@MIP solid sensor formed with thin-film coating was evaluated concerning emission stability, response time, sensor sensitivity and selectivity. The solid sensor was able to maintain a stable emission over 1 h and respond to the target within 10 min. In addition, the sensor showed a sensitivity of 0.0233 and a high selectivity with an imprinting factor of 14 for 2,4-D measurement, which demonstrated the ability of ZnO QD-based MIFS to detect 2,4-D.

- The comparison of the liquid and solid sensors' performance exhibited that the solid sensor detected the target more conveniently and with much higher sensitivity. Therefore, it was proven that spin coating is capable of forming MIFS chips while maintaining the integrity of the sensing material.
- The solid sensing system developed for 2,4-D was further adapted to detect algae bloom toxin MCLR. MCLR molecules are different from 2,4-D in terms of molecular nature and size. To accommodate the large size of MCLR, mesoporous were formed on the polymer shell and imprinted sites were shaped using one of the amino acids of MCLR. The incorporation of mesoporous was proven to increase the consistency of the sensor response.
- The porous solid sensor formed for MCLR detection was evaluated regarding the sensor sensitivity and selectivity. The sensor showed a sensitivity of 0.0076 with a detection limit of 1 μg/L, highlighting the applicability of the sensor to detect drinking water safety according to the WHO regulations. This was the first study to measure MCLR using a MIFS chip, to the best of our knowledge.
- The successful detection of 2,4-D and MCLR proved the flexibility of the sensing system and the capability of portable detectors to measure fluorescence signals reliably and efficiently.

For **CHAPTER 4:**

- To evaluate if the sensing system developed in Chapter 3 could detect biomarkers in biological fluids, efforts were made to adapt the sensing platform for lactate detection in sweat to monitor sports performance.

- Since no study in the open literature reported lactate detection with MIFSs, two monomers were used to optimize sensor selectivity. The sensor formed with APTES monomer could not recognize lactic acid by showing similar responses to lactic acid and the interfering molecules. It was assumed that the low selectivity was caused by the poorly formed imprinted sites; during the synthesis process, the alkaline solution facilitated the formation of lactate from template lactic acid. Therefore, the anticipated binding between the amino functional group of APTES and the carboxyl functional group of lactic acid could not take place to shape the imprinted sites.
- The sensor prepared with the 5-indolylboronic acid monomer was capable of showing high sensitivity and selectivity to lactic acid samples under the optimal sensing condition. The sensor sensitivity was 0.12 with a correlation coefficient of 0.99. In addition, sensor response to the interfering molecules was negligible compared to sensor response to lactic acid. The performance of the sensor prepared with the 5-indolylboronic acid showed the feasibility of using MIFS to measure lactic acid with high sensitivity and selectivity.
- The effect of the monomer on the sensor selectivity was highlighted by comparing the performances of the sensor prepared with APTES and 5-indolylboronic acid. It was concluded that monomers should be chosen according to their ability to interact with the template molecule and this interaction should not be sensitive to environmental parameters.
- The sensor formed with 5-indolylboronic acid was further evaluated using lactate samples prepared with PBS to investigate the sensor's applicability for sweat analysis. It was realized that PBS solution needed to be added during the synthesis process to

measure target in the saline environment and the amount of PBS affected the linear range and the response level of the sensor. We concluded that for ZnO QDs based MIFS prepared with post modification method, a passivation step is needed to increase the net response to the target. This adaptation can be realized by adding an appropriate amount of the sample solvent during the synthesis and the amount should be optimized to be enough to passivate the exposed QDs without harming the QDs residing in the imprinted sites. To the best of our knowledge, it is the first time ZnO QDs based MIFS was successfully applied to detect molecules in the saline environment.

- The solvent addition step was not necessary for the sensor prepared for 2,4-D and MCLR because the sensing material was formed using a one-step method that includes the QDs within the polymer structure. Therefore, there were no QDs exposed and unprotected by the polymer that needed to be passivated.
- The final lactate sensor showed a linear response to 0–30 mM of lactate with a detection limit of 3.38 mM, proving for the first time that lactate can be measured with MIFS chips. Moreover, the sensor was insensitive to the interfering molecules commonly found in sweat such as glucose, ascorbic acid, and uric acid, and was capable of generating sensor response with a small amount of sample (10 µL). These results highlighted the practicality of using the sensing platform to perform sweat analysis.

The extended application area of the sensing system developed in chapter 3 to biological fluid presented in Chapter 4 indicated the comprehensiveness of the developed sensing platform. This flexibility of the sensing system was imparted by the wide-range applicability of the fluorescence sensors, target-flexibility of MIPs and the generality of the thin-film coating method. The

performances of the sensing system showed the ability of fluorescence sensor chips to provide sensitive, selective, and reliable signals. The successful application for lactate analysis in PBS demonstrated the potential of the sensing platform to measure target molecules in actual samples including sweat, biological fluids and seawaters. The robustness of the sensing material, the convenient formation of the solid sensor, and the detection with a portable detector established in this thesis exhibited the great prospects of fluorescence sensors to be used for various purposes, thus supporting the realization of the lab-on-chip image-based sensing devices. This, in turn, is anticipated to draw the interest among researchers and entrepreneurs in developing sensing devices for environmental analysis and health monitoring.

5.2 Recommendations

- The experimental results presented in chapters 3 and 4 showed the target flexibility and the ability of the sensor to detect target molecules with high selectivity and sensitivity. To further prove the capability of the sensor, the next step of the research would be detecting the target molecules using the actual samples and adapting the sensing material to the actual detecting environment.
- As mentioned in the literature review, one of the signals demonstrated by the fluorescence sensors is the ratiometric signal. A ratiometric fluorescence sensor is formed with two or more emissive molecules in different wavelengths. The working principle of this type of fluorescence sensor is that when one of the emissions is quenched by the target molecule the others stay stable regardless of the chemical environment (like the yellow emissive ZnO QDs in Chapter 3 section 3.4); the sensitivity of the sensor is then evaluated with the ratio of different fluorescence peaks. This unique property of the ratiometric sensor enables

a higher sensitivity than the monochromatic fluorescence sensors and displays a colour change in accordance with the target concentration. Therefore, ratiometric sensors provide a possibility of eliminating the dependency on fluorescence detectors by tracking the colour change of the sensor by our eyes.

- As shown in Chapter 3, the sensitivity of the MCLR sensor was lower than that of the 2,4-D sensor. A possible solution could be using a core-shell structure to further adjust the sensing material to the large particle size. The sensor's core can be formed with silica nanoparticles and QDs can be anchored to the nanoparticle's surface by covalent attachment. With the following imprinted layer formation on the surface of the silica nanoparticle, a thin polymer layer can be obtained. This core-shell structure will help with obtaining higher sensor sensitivity by easily reachable imprinted sites.
- To further enhance the sensing material's accuracy and recognition ability, machine learning and data analysis can be used. Implementing different sensing materials and recognizing the signal pattern through mega data analysis can also realize the detection of a few target molecules simultaneously with high selectivity.
- In this research, a portable light detector was applied to detect the fluorescence signals of the solid sensors. The capability of this type of detector to record the signal and differentiate a small change in the emission open many more opportunities to substitute laboratory equipment. For example, a similar detector attachable to smartphones or even detection through cellphone cameras can be attainable with comprehensive studies.

Bibliography

(1) Van Grieken, R.; Bruin, M. Nomenclature for Radioanalytical Chemistry (IUPAC Recommendations 1994). *Pure and Applied Chemistry* **1994**, *66* (12), 2513–2526. https://doi.org/10.1351/PAC199466122513/MACHINEREADABLECITATION/RIS.

(2) Fleming, K. G. Fluorescence Theory. *Encyclopedia of Spectroscopy and Spectrometry* **2017**, 647–653. https://doi.org/10.1016/B978-0-12-803224-4.00357-5.

(3) Wu, P.; Hou, X.; Xu, J. J.; Chen, H. Y. Ratiometric Fluorescence, Electrochemiluminescence, and Photoelectrochemical Chemo/Biosensing Based on Semiconductor Quantum Dots. *Nanoscale* **2016**, *8* (16), 8427–8442. https://doi.org/10.1039/C6NR01912A.

(4) Algar, W. R.; Massey, M.; Rees, K.; Higgins, R.; Krause, K. D.; Darwish, G. H.; Peveler, W. J.; Xiao, Z.; Tsai, H. Y.; Gupta, R.; Lix, K.; Tran, M. v.; Kim, H. Photoluminescent Nanoparticles for Chemical and Biological Analysis and Imaging. *Chemical Reviews* **2021**, *121* (15), 9243–9358. https://doi.org/10.1021/ACS.CHEMREV.0C01176/SUPPL_FILE/CR0C01176_SI_001.PDF.

(5) Neikov, O. D.; Yefimov, N. A. Nanopowders. *Handbook of Non-Ferrous Metal Powders* **2019**, 271–311. https://doi.org/10.1016/B978-0-08-100543-9.00009-9.

(6) Sumanth Kumar, D.; Jai Kumar, B.; Mahesh, H. M. Quantum Nanostructures (QDs): An Overview. *Synthesis of Inorganic Nanomaterials* **2018**, 59–88. https://doi.org/10.1016/B978-0-08-101975-7.00003-8.

(7) Rossetti, R.; Nakahara, S.; Brus, L. E. Quantum Size Effects in the Redox Potentials, Resonance Raman Spectra, and Electronic Spectra of CdS Crystallites in Aqueous Solution. *The Journal of Chemical Physics* **1998**, *79* (2), 1086. https://doi.org/10.1063/1.445834.

(8) Xu, G.; Zeng, S.; Zhang, B.; Swihart, M. T.; Yong, K. T.; Prasad, P. N. New Generation Cadmium-Free Quantum Dots for Biophotonics and Nanomedicine. *Chemical Reviews* **2016**, *116* (19), 12234–12327. https://doi.org/10.1021/ACS.CHEMREV.6B00290.

(9) Asok, A.; Gandhi, M. N.; Kulkarni, A. R. Enhanced Visible Photoluminescence in ZnO Quantum Dots by Promotion of Oxygen Vacancy Formation. *Nanoscale* **2012**, *4* (16), 4943–4946. https://doi.org/10.1039/C2NR31044A.

(10) Li, S.; Ye, S.; Liu, T.; Guo, Z.; Wang, H.; Wang, D. Dual Role of the Reactant MOH (M=Li, Na or K) in the Growth of ZnO Quantum Dots under a Sol-Gel Process: Promoter and Inhibitor. *RSC Advances* **2016**, *6* (55), 50173–50179. https://doi.org/10.1039/c6ra06660g.

(11) Liu, X.; Xing, X.; Li, Y.; Chen, N.; Djerdj, I.; Wang, Y. Controllable Synthesis and Change of Emission Color from Green to Orange of ZnO Quantum Dots Using Different Solvents. *New Journal of Chemistry* **2015**, *39* (4), 2881–2888. https://doi.org/10.1039/c5nj00070j.

(12) Belbruno, J. J. Molecularly Imprinted Polymers. *Chemical Reviews* **2018**, *119* (1), 94–119. https://doi.org/10.1021/ACS.CHEMREV.8B00171.

(13) Ruela, A. L. M.; Figueiredo, E. C.; Pereira, G. R. Molecularly Imprinted Polymers as Nicotine Transdermal Delivery Systems. *Chemical Engineering Journal* **2014**, *248*, 1–8. https://doi.org/10.1016/J.CEJ.2013.12.106.

(14) Ansari, S.; Karimi, M. Recent Progress, Challenges and Trends in Trace Determination of Drug Analysis Using Molecularly Imprinted Solid-Phase Microextraction Technology. *Talanta* **2017**, *164*, 612–625. https://doi.org/10.1016/J.TALANTA.2016.11.007.

(15) Bakas, I.; Oujji, N. ben; Moczko, E.; Istamboulie, G.; Piletsky, S.; Piletska, E.; Ait-Addi, E.; Ait-Ichou, I.; Noguer, T.; Rouillon, R. Computational and Experimental Investigation of Molecular Imprinted Polymers for Selective Extraction of Dimethoate and Its Metabolite Omethoate from Olive Oil. *Journal of Chromatography A* **2013**, *1274*, 13–18. https://doi.org/10.1016/J.CHROMA.2012.11.061.

(16) Pourfarzib, M.; Dinarvand, R.; Akbari-Adergani, B.; Mehramizi, A.; Rastegar, H.; Shekarchi, M. Water-Compatible Molecularly Imprinted Polymer as a Sorbent for the Selective Extraction and Purification of Adefovir from Human Serum and Urine. *Journal of Separation Science* **2015**, *38* (10), 1755–1762. https://doi.org/10.1002/JSSC.201401492.

(17) Tang, W.; Li, G.; Row, K. H.; Zhu, T. Preparation of Hybrid Molecularly Imprinted Polymer with Double-Templates for Rapid Simultaneous Purification of Theophylline and Chlorogenic Acid in Green Tea. *Talanta* **2016**, *152*, 1–8. https://doi.org/10.1016/J.TALANTA.2016.01.046.

(18) Barahona, F.; Díaz-álvarez, M.; Turiel, E.; Martín-Esteban, A. Molecularly Imprinted Polymer-Coated Hollow Fiber Membrane for the Microextraction of Triazines Directly from Environmental Waters. *Journal of Chromatography A* **2016**, *1442*, 12–18. https://doi.org/10.1016/J.CHROMA.2016.03.004.

(19) Wang, S.; Ge, L.; Li, L.; Yan, M.; Ge, S.; Yu, J. Molecularly Imprinted Polymer Grafted Paper-Based Multi-Disk Micro-Disk Plate for Chemiluminescence Detection of Pesticide.

Biosensors and Bioelectronics **2013**, *50*, 262–268. https://doi.org/10.1016/J.BIOS.2013.07.003.

(20) Chen, J.; Bai, L.; Tian, M.; Zhou, X.; Zhang, Y. Hollow-Fiber Membrane Tube Embedded with a Molecularly Imprinted Monolithic Bar for the Microextraction of Triazine Pesticides. *Analytical Methods* **2013**, *6* (2), 602–608. https://doi.org/10.1039/C3AY41455H.

(21) Bakas, I.; Oujji, N. ben; Moczko, E.; Istamboulie, G.; Piletsky, S.; Piletska, E.; Ait-Addi, E.; Ait-Ichou, I.; Noguer, T.; Rouillon, R. Computational and Experimental Investigation of Molecular Imprinted Polymers for Selective Extraction of Dimethoate and Its Metabolite Omethoate from Olive Oil. *Journal of Chromatography A* **2013**, *1274*, 13–18. https://doi.org/10.1016/J.CHROMA.2012.11.061.

(22) Mustafa, G.; Lieberzeit, P. A. Molecularly Imprinted Polymer–Ag2S Nanoparticle Composites for Sensing Volatile Organics. *RSC Advances* **2014**, *4* (25), 12723–12728. https://doi.org/10.1039/C3RA44208J.

(23) González-Vila, Á.; Debliquy, M.; Lahem, D.; Zhang, C.; Mégret, P.; Caucheteur, C. Molecularly Imprinted Electropolymerization on a Metal-Coated Optical Fiber for Gas Sensing Applications. *Sensors and Actuators B: Chemical* **2017**, *244*, 1145–1151. https://doi.org/10.1016/J.SNB.2017.01.084.

(24) Alizadeh, T.; Hamedsoltani, L. Graphene/Graphite/Molecularly Imprinted Polymer Nanocomposite as the Highly Selective Gas Sensor for Nitrobenzene Vapor Recognition. *Journal of Environmental Chemical Engineering* **2014**, *2* (3), 1514–1526. https://doi.org/10.1016/J.JECE.2014.07.007.

(25) Cecchini, A.; Raffa, V.; Canfarotta, F.; Signore, G.; Piletsky, S.; Macdonald, M. P.; Cuschieri, A. In Vivo Recognition of Human Vascular Endothelial Growth Factor by Molecularly Imprinted Polymers. *Nano Letters* **2017**, *17* (4), 2307–2312. https://doi.org/10.1021/ACS.NANOLETT.6B05052/SUPPL_FILE/NL6B05052_SI_002.PDF.

(26) Pandey, I.; Jha, S. S. Molecularly Imprinted Polyaniline-Ferrocene-Sulfonic Acid-Carbon Dots Modified Pencil Graphite Electrodes for Chiral Selective Sensing of D-Ascorbic Acid and L-Ascorbic Acid: A Clinical Biomarker for Preeclampsia. *Electrochimica Acta* **2015**, *182*, 917–928. https://doi.org/10.1016/J.ELECTACTA.2015.10.005.

(27) Hashemi-Moghaddam, H.; Rahimian, M.; Niromand, B. Molecularly Imprinted Polymers for Solid-Phase Extraction of Sarcosine as Prostate Cancer Biomarker from Human Urine. *Bull Korean Chem Soc* **2013**, *34* (8), 2330–2334. https://doi.org/10.5012/BKCS.2013.34.8.2330.

(28) Lian, W.; Liu, S.; Wang, L.; Liu, H. A Novel Strategy to Improve the Sensitivity of Antibiotics Determination Based on Bioelectrocatalysis at Molecularly Imprinted Polymer Film Electrodes. *Biosensors and Bioelectronics* **2015**, *73*, 214–220. https://doi.org/10.1016/J.BIOS.2015.06.006.

(29) Diouf, A.; Motia, S.; el Alami El Hassani, N.; el Bari, N.; Bouchikhi, B. Development and Characterization of an Electrochemical Biosensor for Creatinine Detection in Human Urine Based on Functional Molecularly Imprinted Polymer. *Journal of Electroanalytical Chemistry* **2017**, *788*, 44–53. https://doi.org/10.1016/J.JELECHEM.2017.01.068.

(30) Chantada-Vázquez, M. P.; Sánchez-González, J.; Peña-Vázquez, E.; Tabernero, M. J.; Bermejo, A. M.; Bermejo-Barrera, P.; Moreda-Piñeiro, A. Simple and Sensitive

Molecularly Imprinted Polymer – Mn-Doped ZnS Quantum Dots Based Fluorescence Probe for Cocaine and Metabolites Determination in Urine. *Analytical Chemistry* **2016**, *88* (5), 2734–2741. https://doi.org/10.1021/ACS.ANALCHEM.5B04250.

(31) Xu, Z.; Deng, P.; Li, J.; Tang, S. Fluorescent Ion-Imprinted Sensor for Selective and Sensitive Detection of Copper (II) Ions. *Sensors and Actuators B: Chemical* **2018**, *255*, 2095–2104. https://doi.org/10.1016/J.SNB.2017.09.007.

(32) Qi, J.; Li, B.; Wang, X.; Zhang, Z.; Wang, Z.; Han, J.; Chen, L. Three-Dimensional Paper-Based Microfluidic Chip Device for Multiplexed Fluorescence Detection of Cu2+ and Hg2+ Ions Based on Ion Imprinting Technology. *Sensors and Actuators B: Chemical* **2017**, *251*, 224–233. https://doi.org/10.1016/J.SNB.2017.05.052.

(33) Ng, S. M.; Narayanaswamy, R. Fluorescence Sensor Using a Molecularly Imprinted Polymer as a Recognition Receptor for the Detection of Aluminium Ions in Aqueous Media. *Anal Bioanal Chem* **2006**, *386* (5), 1235–1244. https://doi.org/10.1007/S00216-006-0736-3.

(34) Zhang, Z.; Ma, X.; Li, B.; Zhao, J.; Qi, J.; Hao, G.; Jianhui, R.; Yang, X. Fluorescence Detection of 2,4-Dichlorophenoxyacetic Acid by Ratiometric Fluorescence Imaging on Paper-Based Microfluidic Chips. *Analyst* **2020**, *145* (3), 963–974. https://doi.org/10.1039/C9AN01798D.

(35) Liu, G.; Chen, Z.; Jiang, X.; Feng, D. Q.; Zhao, J.; Fan, D.; Wang, W. In-Situ Hydrothermal Synthesis of Molecularly Imprinted Polymers Coated Carbon Dots for Fluorescent Detection of Bisphenol A. *Sensors and Actuators B: Chemical* **2016**, *228*, 302–307. https://doi.org/10.1016/J.SNB.2016.01.010.

(36) Nsibande, S. A.; Forbes, P. B. C. Development of a Quantum Dot Molecularly Imprinted Polymer Sensor for Fluorescence Detection of Atrazine. *Luminescence* **2019**, *34* (5), 480–488. https://doi.org/10.1002/BIO.3620.

(37) Luo, L.; Zhang, F.; Chen, C.; Cai, C. Visual Simultaneous Detection of Hepatitis A and B Viruses Based on a Multifunctional Molecularly Imprinted Fluorescence Sensor. *Analytical Chemistry* **2019**, *91* (24), 15748–15756. https://doi.org/10.1021/ACS.ANALCHEM.9B04001.

(38) Zhou, X.; Gao, X.; Liu, M.; Wang, C.; Chu, F. A Poly(5-Indolylboronic Acid) Based Molecular Imprint Doped with Carbon Dots for Fluorometric Determination of Glucose. *Microchimica Acta 2017 184:10* **2017**, *184* (10), 4175–4181. https://doi.org/10.1007/S00604-017-2448-0.

(39) Zhou, X.; Ma, P.; Wang, A.; Yu, C.; Qian, T.; Wu, S.; Shen, J. Dopamine Fluorescent Sensors Based on Polypyrrole/Graphene Quantum Dots Core/Shell Hybrids. *Biosensors and Bioelectronics* **2015**, *64*, 404–410. https://doi.org/10.1016/J.BIOS.2014.09.038.

(40) Peng, L.; Xu, Y.; Huang, T.; Liu, X.; Yang, X.; Meng, M.; Yan, Y. Molecularly Imprinted Fluorescent Sensors Based on Nitrogen-Doped CDs for Highly Selective Detection of Aspirin. *https://doi.org/10.1142/S1793292021500193* **2021**, *16* (2). https://doi.org/10.1142/S1793292021500193.

(41) Cui, C.; Lei, J.; Yang, L.; Shen, B.; Wang, L.; Zhang, J. Carbon-Dot-Encapsulated Molecularly Imprinted Mesoporous Organosilica for Fluorescent Sensing of Rhodamine 6G. *Research on Chemical Intermediates* **2018**, *44* (8), 4633–4640. https://doi.org/10.1007/S11164-018-3279-2/FIGURES/5.

(42) Xu, S.; Lu, H. One-Pot Synthesis of Mesoporous Structured Ratiometric Fluorescence Molecularly Imprinted Sensor for Highly Sensitive Detection of Melamine from Milk Samples. *Biosensors and Bioelectronics* **2015**, *73*, 160–166. https://doi.org/10.1016/J.BIOS.2015.05.064.

(43) Nikazar, S.; Sivasankarapillai, V. S.; Rahdar, A.; Gasmi, S.; Anumol, P. S.; Shanavas, M. S. Revisiting the Cytotoxicity of Quantum Dots: An in-Depth Overview. *Biophysical Reviews* **2020**, *12* (3), 703. https://doi.org/10.1007/S12551-020-00653-0.

(44) Zhu, C.; Chen, Z.; Gao, S.; Goh, B. L.; Samsudin, I. bin; Lwe, K. W.; Wu, Y.; Wu, C.; Su, X. Recent Advances in Non-Toxic Quantum Dots and Their Biomedical Applications. *Progress in Natural Science: Materials International* **2019**, *29* (6), 628–640. https://doi.org/10.1016/J.PNSC.2019.11.007.

(45) DeVolder, R. J.; Kong, H. Quantifying Integrin–Ligand Engagement and Cell Phenotype in 3D Scaffolds. *Comprehensive Biomaterials* **2011**, *5*, 65–71. https://doi.org/10.1016/B978-0-08-055294-1.00268-3.

(46) Zhu, J. J.; Huang, H.; Wang, W.; Liang, G. Preparation and Analytical Applications of Quantum Dots. *Comprehensive Sampling and Sample Preparation* **2012**, *3*, 169–187. https://doi.org/10.1016/B978-0-12-381373-2.00072-7.

(47) Lakowicz, J. R. Principles of Fluorescence Spectroscopy. *Principles of Fluorescence Spectroscopy* **2006**, 1–954. https://doi.org/10.1007/978-0-387-46312-4.

(48) Goldman, E. R.; Medintz, I. L.; Whitley, J. L.; Hayhurst, A.; Clapp, A. R.; Uyeda, H. T.; Deschamps, J. R.; Lassman, M. E.; Mattoussi, H. A Hybrid Quantum Dot - Antibody Fragment Fluorescence Resonance Energy Transfer-Based TNT Sensor. *J Am Chem Soc*

2005, *127* (18), 6744–6751. https://doi.org/10.1021/JA043677L/SUPPL_FILE/JA043677LSI20050224_111350.PDF.

(49) Matsushita, M.; Yoshida, K.; Yamamoto, N.; Wirsching, P.; Lerner, R. A.; Janda, K. D. High-Throughput Screening by Using a Blue-Fluorescent Antibody Sensor. *Angewandte Chemie International Edition* **2003**, *42* (48), 5984–5987. https://doi.org/10.1002/ANIE.200352793.

(50) Lin, Y.; Yang, Z.; Lake, R. J.; Zheng, C.; Lu, Y. Enzyme-Mediated Endogenous and Bioorthogonal Control of a DNAzyme Fluorescent Sensor for Imaging Metal Ions in Living Cells. *Angewandte Chemie* **2019**, *131* (47), 17217–17223. https://doi.org/10.1002/ANGE.201910343.

(51) Dai, N.; Kool, E. T. Fluorescent DNA-Based Enzyme Sensors. *Chemical Society Reviews* **2011**, *40* (12), 5756–5770. https://doi.org/10.1039/C0CS00162G.

(52) Yang, Q.; Li, J.; Wang, X.; Peng, H.; Xiong, H.; Chen, L. Strategies of Molecular Imprinting-Based Fluorescence Sensors for Chemical and Biological Analysis. *Biosensors and Bioelectronics* **2018**, *112*, 54–71. https://doi.org/10.1016/J.BIOS.2018.04.028.

(53) Chen, J. L. Determination of Tetracycline Using Imprinted Polymethacrylates along with Fluorescent CdTe Quantum Dots on Plastic Substrates. *Microchimica Acta* **2017**, *184* (5), 1335–1343. https://doi.org/10.1007/S00604-017-2118-2/TABLES/1.

(54) Harz, S.; Schimmelpfennig, M.; Tse Sum Bui, B.; Marchyk, N.; Haupt, K.; Feller, K. H. Fluorescence Optical Spectrally Resolved Sensor Based on Molecularly Imprinted Polymers and Microfluidics. *Engineering in Life Sciences* **2011**, *11* (6), 559–565. https://doi.org/10.1002/ELSC.201000222.

(55) Li, B.; Zhang, Z.; Qi, J.; Zhou, N.; Qin, S.; Choo, J.; Chen, L. Quantum Dot-Based Molecularly Imprinted Polymers on Three-Dimensional Origami Paper Microfluidic Chip for Fluorescence Detection of Phycocyanin. *ACS Sensors* **2017**, *2* (2), 243–250. https://doi.org/10.1021/acssensors.6b00664.

(56) Zhang, Z.; Ma, X.; Li, B.; Zhao, J.; Qi, J.; Hao, G.; Jianhui, R.; Yang, X. Fluorescence Detection of 2,4-Dichlorophenoxyacetic Acid by Ratiometric Fluorescence Imaging on Paper-Based Microfluidic Chips. *Analyst* **2020**, *145* (3), 963–974. https://doi.org/10.1039/c9an01798d.

(57) Liu, H.; Wu, D.; Liu, Y.; Zhang, H.; Ma, T.; Aidaerhan, A.; Wang, J.; Sun, B. Application of an Optosensing Chip Based on Molecularly Imprinted Polymer Coated Quantum Dots for the Highly Selective and Sensitive Determination of Sesamol in Sesame Oils. *Journal of Agricultural and Food Chemistry* **2015**, *63* (9), 2545–2549. https://doi.org/10.1021/JF505790C/SUPPL_FILE/JF505790C_SI_001.PDF.

(58) Wang, S.; Ge, L.; Li, L.; Yan, M.; Ge, S.; Yu, J. Molecularly Imprinted Polymer Grafted Paper-Based Multi-Disk Micro-Disk Plate for Chemiluminescence Detection of Pesticide. *Biosensors and Bioelectronics* **2013**, *50*, 262–268. https://doi.org/10.1016/J.BIOS.2013.07.003.

(59) Boivin, A.; Amellal, S.; Schiavon, M.; van Genuchten, M. T. 2,4-Dichlorophenoxyacetic Acid (2,4-D) Sorption and Degradation Dynamics in Three Agricultural Soils. *Environmental Pollution* **2005**, *138* (1), 92–99. https://doi.org/10.1016/J.ENVPOL.2005.02.016.

(60) Smith, A. M.; Smith, M. T.; la Merrill, M. A.; Liaw, J.; Steinmaus, C. 2,4-Dichlorophenoxyacetic Acid (2,4-D) and Risk of Non-Hodgkin Lymphoma: A Meta-

Analysis Accounting for Exposure Levels. *Ann Epidemiol* **2017**, *27* (4), 281-289.e4. https://doi.org/10.1016/J.ANNEPIDEM.2017.03.003.

(61) Gobi, K. V.; Tanaka, H.; Shoyama, Y.; Miura, N. Highly Sensitive Regenerable Immunosensor for Label-Free Detection of 2,4-Dichlorophenoxyacetic Acid at Ppb Levels by Using Surface Plasmon Resonance Imaging. In *Sensors and Actuators, B: Chemical*; Elsevier, 2005; Vol. 111–112, pp 562–571. https://doi.org/10.1016/j.snb.2005.03.118.

(62) Guidelines for THIRD EDITION Drinking-Water Quality. **2004**.

(63) Wilmer, M.; Trau, D.; Renneberg, R.; Spener, F. Amperometric Immunosensor for the Detection of 2,4-Dichlorophenoxyacetic Acid (2,4-D) in Water. *http://dx.doi.org/10.1080/00032719708001798* **2006**, *30* (3), 515–525. https://doi.org/10.1080/00032719708001798.

(64) Ozkan, D.; Kerman, K.; Meric, B.; Kara, P.; Demirkan, H.; Polverejan, M.; Pinnavaia, T. J.; Ozsoz, M. Heterostructured Fluorohectorite Clay as an Electrochemical Sensor for the Detection of 2,4-Dichlorophenol and the Herbicide 2,4-D. *Chemistry of Materials* **2002**, *14* (4), 1755–1761. https://doi.org/10.1021/CM011529D.

(65) Hall, J. C.; Deschamps, R. J. A.; Krieg, K. K. Immunoassays for the Detection of 2,4-D and Picloram in River Water and Urine. *Journal of Agricultural and Food Chemistry* **2002**, *37* (4), 981–984. https://doi.org/10.1021/JF00088A035.

(66) Zhang, Z.; Ma, X.; Jia, M.; Li, B.; Rong, J.; Yang, X. Deposition of CdTe Quantum Dots on Microfluidic Paper Chips for Rapid Fluorescence Detection of Pesticide 2,4-D. *Analyst* **2019**, *144* (4), 1282–1291. https://doi.org/10.1039/C8AN02051E.

(67) Yang, M.; Wang, C.; Liu, E.; Hu, X.; Hao, H.; Fan, J. A Novel Ascorbic Acid Ratiometric Fluorescent Sensor Based on ZnCdS Quantum Dots Embedded Molecularly Imprinted

Polymer and Silica-Coated CdTeS Quantum Dots. *Journal of Molecular Liquids* **2021**, *337*, 116438. https://doi.org/10.1016/J.MOLLIQ.2021.116438.

(68) Prusty, A. K.; Bhand, S. A Capacitive Sensor for 2,4-D Determination in Water Based on 2,4-D Imprinted Polypyrrole Coated Pencil Electrode. *Materials Research Express* **2017**, *4* (3), 035306. https://doi.org/10.1088/2053-1591/AA6386.

(69) Jia, J.-L.; Xu, H.-H.; Zhang, G.-R.; Hu, Z.; Xu, B.-Q. High Quality Gold Nanorods and Nanospheres for Surface-Enhanced Raman Scattering Detection of 2,4-Dichlorophenoxyacetic Acid. *Nanotechnology* **2012**, *23* (49), 495710. https://doi.org/10.1088/0957-4484/23/49/495710.

(70) Sheng, L.; Jin, Y.; He, Y.; Huang, Y.; Yan, L.; Zhao, R. Well-Defined Magnetic Surface Imprinted Nanoparticles for Selective Enrichment of 2,4-Dichlorophenoxyacetic Acid in Real Samples. *Talanta* **2017**, *174*, 725–732. https://doi.org/10.1016/j.talanta.2017.07.002.

(71) Jia, M.; Zhang, Z.; Li, J.; Yang, X.; Chen, L. A Molecular Imprinting Fluorescence Sensor Based on Quantum Dots and a Mesoporous Structure for Selective and Sensitive Detection of 2,4-Dichlorophenoxyacetic Acid. *Sensors and Actuators B: Chemical* **2017**, *252*, 934–943. https://doi.org/10.1016/J.SNB.2017.06.090.

(72) Wang, X.; Yu, J.; Wu, X.; Fu, J.; Kang, Q.; Shen, D.; Li, J.; Chen, L. A Molecular Imprinting-Based Turn-on Ratiometric Fluorescence Sensor for Highly Selective and Sensitive Detection of 2,4-Dichlorophenoxyacetic Acid (2,4-D). *Biosensors and Bioelectronics* **2016**, *81*, 438–444. https://doi.org/10.1016/J.BIOS.2016.03.031.

(73) Chianella, I.; Lotierzo, M.; Piletsky, S. A.; Tothill, I. E.; Chen, B.; Karim, K.; Turner, A. P. F. Rational Design of a Polymer Specific for Microcystin-LR Using a Computational Approach. *Anal Chem* **2002**, *74* (6), 1288–1293. https://doi.org/10.1021/AC010840B.

(74) Tian, X.; She, C.; Qi, Z.; Xu, X. Magnetic-Graphene Oxide Based Molecularly Imprinted Polymers for Selective Extraction of Microsystin-LR Prior to the Determination by HPLC. *Microchemical Journal* **2019**, *146*, 1126–1133. https://doi.org/10.1016/J.MICROC.2019.02.033.

(75) Teng, W.; Wu, Z.; Feng, D.; Fan, J.; Wang, J.; Wei, H.; Song, M.; Zhao, D. Rapid and Efficient Removal of Microcystins by Ordered Mesoporous Silica. *Environmental Science and Technology* **2013**, *47* (15), 8633–8641. https://doi.org/10.1021/ES400659B/SUPPL_FILE/ES400659B_SI_001.PDF.

(76) Qi, Z.; Lu, R.; Wang, S.; Xiang, C.; Xie, C.; Zheng, M.; Tian, X.; Xu, X. Selective Fluorometric Determination of Microcystin-LR Using a Segment Template Molecularly Imprinted by Polymer-Capped Carbon Quantum Dots. *Microchemical Journal* **2021**, *161*, 105798. https://doi.org/10.1016/J.MICROC.2020.105798.

(77) Chen, K.; Liu, M.; Zhao, G.; Shi, H.; Fan, L.; Zhao, S. Fabrication of a Novel and Simple Microcystin-LR Photoelectrochemical Sensor with High Sensitivity and Selectivity. *Environmental Science and Technology* **2012**, *46* (21), 11955–11961. https://doi.org/10.1021/ES302327W/SUPPL_FILE/ES302327W_SI_001.PDF.

(78) 23 Million Salmon Dead Due to Toxic Algal Bloom in Chile - EcoWatch https://www.ecowatch.com/23-million-salmon-dead-due-to-toxic-algal-bloom-in-chile-1882188276.html (accessed 2022 -02 -05).

(79) Botswana: Mystery elephant deaths caused by cyanobacteria - BBC News https://www.bbc.com/news/world-africa-54234396 (accessed 2022 -02 -05).

(80) Nobre, A. C. L.; Jorge, M. C. M.; Menezes, D. B.; Fonteles, M. C.; Monteiro, H. S. A. Effects of Microcystin-LR in Isolated Perfused Rat Kidney. *Braz J Med Biol Res 32* (8), 1999.

(81) Li, G.; Cai, F.; Yan, W.; Li, C.; Wang, J. A Proteomic Analysis of MCLR-Induced Neurotoxicity: Implications for Alzheimer's Disease. *Toxicological Sciences* **2012**, *127* (2), 485–495. https://doi.org/10.1093/TOXSCI/KFS114.

(82) Ding, X. S.; Li, X. Y.; Duan, H. Y.; Chung, I. K.; Lee, J. A. Toxic Effects of Microcystis Cell Extracts on the Reproductive System of Male Mice. *Toxicon* **2006**, *48* (8), 973–979. https://doi.org/10.1016/J.TOXICON.2006.07.039.

(83) Soares, R. M.; Cagido, V. R.; Ferraro, R. B.; Meyer-Fernandes, J. R.; Rocco, P. R. M.; Zin, W. A.; Azevedo, S. M. F. O. Effects of Microcystin-LR on Mouse Lungs. *Toxicon* **2007**, *50* (3), 330–338. https://doi.org/10.1016/J.TOXICON.2007.04.003.

(84) Epa, U.; of Water, O. Drinking Water Health Advisory for the Cyanobacterial Microcystin Toxins. **2015**.

(85) Han, M.; Li, Q.; Chen, H.; Xiao, J.; Jiang, F. Spatial and Temporal Variations in Cyanobacteria and Microcystins in Aha Reservoir, Southwest China. *Journal of Oceanology and Limnology 2018 36:4* **2018**, *36* (4), 1126–1131. https://doi.org/10.1007/S00343-018-7178-6.

(86) Chen, Y. C.; Ao, Y. T.; Ding, W. H. Determination of Microcystins in Water Samples by Deep Eutectic Solvent-Based Vortex-Assisted Liquid–Liquid Microextraction Coupled with Ultrahigh-Performance Liquid Chromatography-High Resolution Mass Spectrometry. *RSC Advances* **2019**, *9* (66), 38669–38676. https://doi.org/10.1039/C9RA07544E.

(87) Saito, K.; Sei, Y.; Miki, S.; Yamaguchi, K. Detection of Microcystin–Metal Complexes by Using Cryospray Ionization-Fourier Transform Ion Cyclotron Resonance Mass Spectrometry. *Toxicon* **2008**, *51* (8), 1496–1498. https://doi.org/10.1016/J.TOXICON.2008.03.026.

(88) Chen, L.; Tan, R.; Zhou, Y.; Zhang, L.; Zhang, S.; Li, X.; Cong, Y.; Li, H.; Sun, P.; Ueda, H.; Dong, J. Development of an Open Sandwich ELISA for the Detection of Microcystin-LR. *Microchemical Journal* **2020**, *158*, 105325. https://doi.org/10.1016/J.MICROC.2020.105325.

(89) Almeida de Oliveira, R.; Zanato, N.; Cruz Vieira, I. Label-Free Immunosensor for the Determination of Microcystin-LR in Water. *Electroanalysis* **2020**, *32* (10), 2166–2173. https://doi.org/10.1002/ELAN.202060041.

(90) Wang, L.; Chen, W.; Xu, D.; Shim, B. S.; Zhu, Y.; Sun, F.; Liu, L.; Peng, C.; Jin, Z.; Xu, C.; Kotov, N. A. Simple, Rapid, Sensitive, and Versatile SWNT-Paper Sensor for Environmental Toxin Detection Competitive with ELISA. *Nano Letters* **2009**, *9* (12), 4147–4152. https://doi.org/10.1021/NL902368R/SUPPL_FILE/NL902368R_SI_001.PDF.

(91) Chen, K.; Liu, M.; Zhao, G.; Shi, H.; Fan, L.; Zhao, S. Fabrication of a Novel and Simple Microcystin-LR Photoelectrochemical Sensor with High Sensitivity and Selectivity. *Environmental Science and Technology* **2012**, *46* (21), 11955–11961. https://doi.org/10.1021/ES302327W/SUPPL_FILE/ES302327W_SI_001.PDF.

(92) Li, X.; Cheng, R.; Shi, H.; Tang, B.; Xiao, H.; Zhao, G. A Simple Highly Sensitive and Selective Aptamer-Based Colorimetric Sensor for Environmental Toxins Microcystin-LR

in Water Samples. *Journal of Hazardous Materials* **2016**, *304*, 474–480. https://doi.org/10.1016/J.JHAZMAT.2015.11.016.

(93) Kim, M.; Ko, S. M.; Lee, C.; Son, J.; Kim, J.; Kim, J. M.; Nam, J. M. Hierarchic Interfacial Nanocube Assembly for Sensitive, Selective, and Quantitative Dna Detection with Surface-Enhanced Raman Scattering. *Analytical Chemistry* **2019**, *91* (16), 10448–10457. https://doi.org/10.1021/ACS.ANALCHEM.9B00750/SUPPL_FILE/AC9B00750_SI_002.AVI.

(94) Chianella, I.; Piletsky, S. A.; Tothill, I. E.; Chen, B.; Turner, A. P. F. MIP-Based Solid Phase Extraction Cartridges Combined with MIP-Based Sensors for the Detection of Microcystin-LR. *Biosensors and Bioelectronics* **2003**, *18* (2–3), 119–127. https://doi.org/10.1016/S0956-5663(02)00165-3.

(95) Herranz, S.; Bocková, M.; Marazuela, M. D.; Homola, J.; Moreno-Bondi, M. C. An SPR Biosensor for the Detection of Microcystins in Drinking Water. *Analytical and Bioanalytical Chemistry* **2010**, *398* (6), 2625–2634. https://doi.org/10.1007/S00216-010-3856-8/TABLES/3.

(96) Long, F.; He, M.; Shi, H. C.; Zhu, A. N. Development of Evanescent Wave All-Fiber Immunosensor for Environmental Water Analysis. *Biosensors and Bioelectronics* **2008**, *23* (7), 952–958. https://doi.org/10.1016/J.BIOS.2007.09.013.

(97) Zhang, G.; Li, C.; Wu, S.; Zhang, Q. Label-Free Aptamer-Based Detection of Microcystin-LR Using a Microcantilever Array Biosensor. *Sensors and Actuators B: Chemical* **2018**, *260*, 42–47. https://doi.org/10.1016/J.SNB.2017.12.112.

(98) Bakker, J.; Nijsten, M. W. N.; Jansen, T. C. Clinical Use of Lactate Monitoring in Critically Ill Patients. *Annals of Intensive Care* **2013**, *3* (1), 1–8. https://doi.org/10.1186/2110-5820-3-12/FIGURES/4.

(99) Bollella, P.; Sharma, S.; Cass, A. E. G.; Antiochia, R. Microneedle-Based Biosensor for Minimally-Invasive Lactate Detection. *Biosensors and Bioelectronics* **2019**, *123*, 152–159. https://doi.org/10.1016/J.BIOS.2018.08.010.

(100) Parra, A.; Casero, E.; Vázquez, L.; Pariente, F.; Lorenzo, E. Design and Characterization of a Lactate Biosensor Based on Immobilized Lactate Oxidase onto Gold Surfaces. *Analytica Chimica Acta* **2006**, *555* (2), 308–315. https://doi.org/10.1016/J.ACA.2005.09.025.

(101) Kucherenko, I. S.; Topolnikova, Y. V.; Soldatkin, O. O. Advances in the Biosensors for Lactate and Pyruvate Detection for Medical Applications: A Review. *TrAC Trends in Analytical Chemistry* **2019**, *110*, 160–172. https://doi.org/10.1016/J.TRAC.2018.11.004.

(102) Kruse, O.; Grunnet, N.; Barfod, C. Blood Lactate as a Predictor for In-Hospital Mortality in Patients Admitted Acutely to Hospital: A Systematic Review. *Scandinavian Journal of Trauma, Resuscitation and Emergency Medicine* **2011**, *19* (1), 1–12. https://doi.org/10.1186/1757-7241-19-74/TABLES/3.

(103) Zhang, Z.; Xu, X. Lactate Clearance Is a Useful Biomarker for the Prediction of All-Cause Mortality in Critically Ill Patients: A Systematic Review and Meta-Analysis. *Critical Care Medicine* **2014**, *42* (9), 2118–2125. https://doi.org/10.1097/CCM.0000000000000405.

(104) Satomura, T.; Hayashi, J.; Sakamoto, H.; Nunoura, T.; Takaki, Y.; Takai, K.; Takami, H.; Ohshima, T.; Sakuraba, H.; Suye, S. ichiro. D-Lactate Electrochemical Biosensor Prepared by Immobilization of Thermostable Dye-Linked d-Lactate Dehydrogenase from

Candidatus Caldiarchaeum Subterraneum. *Journal of Bioscience and Bioengineering* **2018**, *126* (4), 425–430. https://doi.org/10.1016/J.JBIOSC.2018.04.002.

(105) Alizadeh, T.; Nayeri, S.; Mirzaee, S. A High Performance Potentiometric Sensor for Lactic Acid Determination Based on Molecularly Imprinted Polymer/MWCNTs/PVC Nanocomposite Film Covered Carbon Rod Electrode. *Talanta* **2019**, *192*, 103–111. https://doi.org/10.1016/J.TALANTA.2018.08.027.

(106) Ewaschuk, J. B.; Zello, G. A.; Naylor, J. M.; Brocks, D. R. Metabolic Acidosis: Separation Methods and Biological Relevance of Organic Acids and Lactic Acid Enantiomers. *Journal of Chromatography B* **2002**, *781* (1–2), 39–56. https://doi.org/10.1016/S1570-0232(02)00500-7.

(107) Paik, M. J.; Cho, E. Y.; Kim, H.; Kim, K. R.; Choi, S.; Ahn, Y. H.; Lee, G. Simultaneous Clinical Monitoring of Lactic Acid, Pyruvic Acid and Ketone Bodies in Plasma as Methoxime/Tert-Butyldimethylsilyl Derivatives by Gas Chromatography–Mass Spectrometry in Selected Ion Monitoring Mode. *Biomedical Chromatography* **2008**, *22* (5), 450–453. https://doi.org/10.1002/BMC.966.

(108) Tan, L.; Wang, Y.; Liu, X.; Ju, H.; Li, J. Simultaneous Determination of L- and d-Lactic Acid in Plasma by Capillary Electrophoresis. *Journal of Chromatography B* **2005**, *814* (2), 393–398. https://doi.org/10.1016/J.JCHROMB.2004.10.059.

(109) Nishiyama, K.; Mizukami, R.; Kuki, S.; Ishida, A.; Chida, J.; Kido, H.; Maeki, M.; Tani, H.; Tokeshi, M. Electrochemical Enzyme-Based Blood ATP and Lactate Sensor for a Rapid and Straightforward Evaluation of Illness Severity. *Biosensors and Bioelectronics* **2022**, *198*, 113832. https://doi.org/10.1016/J.BIOS.2021.113832.

(110) Nishiyama, K.; Mizukami, R.; Kuki, S.; Ishida, A.; Chida, J.; Kido, H.; Maeki, M.; Tani, H.; Tokeshi, M. Electrochemical Enzyme-Based Blood ATP and Lactate Sensor for a Rapid and Straightforward Evaluation of Illness Severity. *Biosensors and Bioelectronics* **2022**, *198*, 113832. https://doi.org/10.1016/J.BIOS.2021.113832.

(111) Zhang, Q.; Jiang, D.; Xu, C.; Ge, Y.; Liu, X.; Wei, Q.; Huang, L.; Ren, X.; Wang, C.; Wang, Y. Wearable Electrochemical Biosensor Based on Molecularly Imprinted Ag Nanowires for Noninvasive Monitoring Lactate in Human Sweat. *Sensors and Actuators B: Chemical* **2020**, *320*, 128325. https://doi.org/10.1016/J.SNB.2020.128325.

(112) Promphet, N.; Rattanawaleedirojn, P.; Siralertmukul, K.; Soatthiyanon, N.; Potiyaraj, P.; Thanawattano, C.; Hinestroza, J. P.; Rodthongkum, N. Non-Invasive Textile Based Colorimetric Sensor for the Simultaneous Detection of Sweat PH and Lactate. *Talanta* **2019**, *192*, 424–430. https://doi.org/10.1016/J.TALANTA.2018.09.086.

(113) Lin, C. E.; Hiraka, K.; Matloff, D.; Johns, J.; Deng, A.; Sode, K.; La Belle, J. Development toward a Novel Integrated Tear Lactate Sensor Using Schirmer Test Strip and Engineered Lactate Oxidase. *Sensors and Actuators B: Chemical* **2018**, *270*, 525–529. https://doi.org/10.1016/J.SNB.2018.05.061.

(114) Lin, C. E.; Hiraka, K.; Matloff, D.; Johns, J.; Deng, A.; Sode, K.; la Belle, J. Development toward a Novel Integrated Tear Lactate Sensor Using Schirmer Test Strip and Engineered Lactate Oxidase. *Sensors and Actuators B: Chemical* **2018**, *270*, 525–529. https://doi.org/10.1016/J.SNB.2018.05.061.

(115) Zhu, X.; Ju, Y.; Chen, J.; Liu, D.; Liu, H. Nonenzymatic Wearable Sensor for Electrochemical Analysis of Perspiration Glucose. *ACS Sensors* **2018**, *3* (6), 1135–1141.

https://doi.org/10.1021/ACSSENSORS.8B00168/SUPPL_FILE/SE8B00168_SI_001.PDF
.

(116) Manju, S.; Hari, P. R.; Sreenivasan, K. Fluorescent Molecularly Imprinted Polymer Film Binds Glucose with a Concomitant Changes in Fluorescence. *Biosensors and Bioelectronics* **2010**, *26* (2), 894–897. https://doi.org/10.1016/J.BIOS.2010.07.025.

(117) Zhao, D.; Song, H.; Hao, L.; Liu, X.; Zhang, L.; Lv, Y. Luminescent ZnO Quantum Dots for Sensitive and Selective Detection of Dopamine. *Talanta* **2013**, *107*, 133–139. https://doi.org/10.1016/j.talanta.2013.01.006.

(118) Zhou, X.; Gao, X.; Song, F.; Wang, C.; Chu, F.; Wu, S. A Sensing Approach for Dopamine Determination by Boronic Acid-Functionalized Molecularly Imprinted Graphene Quantum Dots Composite. *Applied Surface Science* **2017**, *423*, 810–816. https://doi.org/10.1016/J.APSUSC.2017.06.199.

(119) Zhou, X.; Gao, X.; Song, F.; Wang, C.; Chu, F.; Wu, S. A Sensing Approach for Dopamine Determination by Boronic Acid-Functionalized Molecularly Imprinted Graphene Quantum Dots Composite. *Applied Surface Science* **2017**, *423*, 810–816. https://doi.org/10.1016/J.APSUSC.2017.06.199.

(120) Mao, Y.; Bao, Y.; Han, D.; Li, F.; Niu, L. Efficient One-Pot Synthesis of Molecularly Imprinted Silica Nanospheres Embedded Carbon Dots for Fluorescent Dopamine Optosensing. *Biosensors and Bioelectronics* **2012**, *38* (1), 55–60. https://doi.org/10.1016/J.BIOS.2012.04.043.

(121) Zhou, X.; Wang, A.; Yu, C.; Wu, S.; Shen, J. Facile Synthesis of Molecularly Imprinted Graphene Quantum Dots for the Determination of Dopamine with Affinity-Adjustable. **2015**. https://doi.org/10.1021/am5078478.

(122) Ahmadpour, H.; Hosseini, S. M. M. A Solid-Phase Luminescence Sensor Based on Molecularly Imprinted Polymer-CdSeS/ZnS Quantum Dots for Selective Extraction and Detection of Sulfasalazine in Biological Samples. *Talanta* **2019**, *194*, 534–541. https://doi.org/10.1016/J.TALANTA.2018.10.053.

(123) Qi, J.; Li, B.; Wang, X.; Fu, L.; Luo, L.; Chen, L. Rotational Paper-Based Microfluidic-Chip Device for Multiplexed and Simultaneous Fluorescence Detection of Phenolic Pollutants Based on a Molecular-Imprinting Technique. *Analytical Chemistry* **2018**, *90* (20), 11827–11834. https://doi.org/10.1021/ACS.ANALCHEM.8B01291.

(124) Asok, A.; Gandhi, M. N.; Kulkarni, A. R. Enhanced Visible Photoluminescence in ZnO Quantum Dots by Promotion of Oxygen Vacancy Formation. *Nanoscale* **2012**, *4* (16), 4943–4946. https://doi.org/10.1039/c2nr31044a.

(125) Abdullah, M.; Shibamoto, S.; Okuyama, K. Synthesis of ZnO/SiO2 Nanocomposites Emitting Specific Luminescence Colors. *Opt Mater (Amst)* **2004**, *26* (1), 95–100. https://doi.org/10.1016/j.optmat.2004.01.006.

(126) Vahid, B. Specific Fluorescence Probe for Direct Recognition of Dimethoate Using Molecularly Imprinting Polymer on ZnO Quantum Dots. *Journal of Fluorescence* **2017**, *27* (4), 1339–1347. https://doi.org/10.1007/s10895-017-2068-4.

(127) Fan, J. Z.; Vafaie, M.; Bertens, K.; Sytnyk, M.; Pina, J. M.; Sagar, L. K.; Ouellette, O.; Proppe, A. H.; Rasouli, A. S.; Gao, Y.; Baek, S. W.; Chen, B.; Laquai, F.; Hoogland, S.; Arquer, F. P. G. De; Heiss, W.; Sargent, E. H. Micron Thick Colloidal Quantum Dot Solids. *Nano Letters* **2020**, *20* (7), 5284–5291. https://doi.org/10.1021/acs.nanolett.0c01614.

(128) Pérez-Cuapio, R.; Alvarado, J. A.; Pacio, M.; Arce-Plaza, A.; Santoyo-Salazar, J.; Liang, L. H.; Sue, H. J. Enhanced Green Photoluminescence and Dispersion of ZnO Quantum Dots Shelled by a Silica Shell. *Journal of Nanoparticle Research* **2020**, *22* (9), 1–13. https://doi.org/10.1007/S11051-020-04985-6/FIGURES/10.

(129) Huang, S.; Guo, M.; Tan, J.; Geng, Y.; Wu, J.; Tang, Y.; Su, C.; Lin, C. C.; Liang, Y. Novel Fluorescence Sensor Based on All-Inorganic Perovskite Quantum Dots Coated with Molecularly Imprinted Polymers for Highly Selective and Sensitive Detection of Omethoate. *ACS Applied Materials and Interfaces* **2018**, *10* (45), 39056–39063. https://doi.org/10.1021/ACSAMI.8B14472.

(130) Zhou, R.; Zhao, Q.; Liu, K. K.; Lu, Y. J.; Dong, L.; Shan, C. X. Europium-Decorated ZnO Quantum Dots as a Fluorescent Sensor for the Detection of an Anthrax Biomarker. *Journal of Materials Chemistry C* **2017**, *5* (7), 1685–1691. https://doi.org/10.1039/C6TC05108A.

(131) Lakowicz, J. R. Effects of Solvents on Fluorescence Emission Spectra. In *Principles of Fluorescence Spectroscopy*; Springer US, 1983; pp 187–215. https://doi.org/10.1007/978-1-4615-7658-7_7.

(132) Vasapollo, G.; Sole, R. del; Mergola, L.; Lazzoi, M. R.; Scardino, A.; Scorrano, S.; Mele, G. Molecularly Imprinted Polymers: Present and Future Prospective. *International Journal of Molecular Sciences* **2011**, *12* (9), 5908. https://doi.org/10.3390/IJMS12095908.

(133) Fan, J. Z.; Vafaie, M.; Bertens, K.; Sytnyk, M.; Pina, J. M.; Sagar, L. K.; Ouellette, O.; Proppe, A. H.; Rasouli, A. S.; Gao, Y.; Baek, S. W.; Chen, B.; Laquai, F.; Hoogland, S.; Arquer, F. P. G. de; Heiss, W.; Sargent, E. H. Micron Thick Colloidal Quantum Dot

Solids. *Nano Letters* **2020**, *20* (7), 5284–5291. https://doi.org/10.1021/acs.nanolett.0c01614.

(134) Xu, S.; Lu, H.; Li, J.; Song, X.; Wang, A.; Chen, L.; Han, S. Dummy Molecularly Imprinted Polymers-Capped CdTe Quantum Dots for the Fluorescent Sensing of 2,4,6-Trinitrotoluene. *ACS Applied Materials and Interfaces* **2013**, *5* (16), 8146–8154. https://doi.org/10.1021/AM4022076.

(135) Yang, Q.; Li, J.; Wang, X.; Xiong, H.; Chen, L. Ternary Emission of a Blue-, Green-, and Red-Based Molecular Imprinting Fluorescence Sensor for the Multiplexed and Visual Detection of Bovine Hemoglobin. **2019**. https://doi.org/10.1021/acs.analchem.9b00082.

(136) Miao, Y.; Sun, X.; Lv, J.; Yan, G. -Phosphorescent Mesoporous Surface Imprinting Microspheres: Preparation and Application for Transferrin Recognition from Biological Fluids. *ACS Applied Materials & Interfaces* **2018**, *11* (2), 2264–2272. https://doi.org/10.1021/ACSAMI.8B17772.

(137) Verteramo, M. L.; Stenström, O.; Ignjatović, M. M.; Caldararu, O.; Olsson, M. A.; Manzoni, F.; Leffler, H.; Oksanen, E.; Logan, D. T.; Nilsson, U. J.; Ryde, U.; Akke, M. Interplay between Conformational Entropy and Solvation Entropy in Protein-Ligand Binding. *J Am Chem Soc* **2019**, *141* (5), 2012–2026. https://doi.org/10.1021/JACS.8B11099/SUPPL_FILE/JA8B11099_SI_001.PDF.

(138) Kazemi, M.; Åqvist, J. Chemical Reaction Mechanisms in Solution from Brute Force Computational Arrhenius Plots. *Nature Communications 2015 6:1* **2015**, *6* (1), 1–7. https://doi.org/10.1038/ncomms8293.

(139) Åqvist, J.; Kazemi, M.; Isaksen, G. V.; Brandsdal, B. O. Entropy and Enzyme Catalysis. *Accounts of Chemical Research* **2017**, *50* (2), 199–207.

https://doi.org/10.1021/ACS.ACCOUNTS.6B00321/ASSET/IMAGES/ACS.ACCOUNTS.6B00321.SOCIAL.JPEG_V03.

(140) Mechanisms and Dynamics of Fluorescence Quenching. *Principles of Fluorescence Spectroscopy* **2006**, 331–351. https://doi.org/10.1007/978-0-387-46312-4_9.

(141) Tan, L.; Kang, C.; Xu, S.; Tang, Y. Selective Room Temperature Phosphorescence Sensing of Target Protein Using Mn-Doped ZnS QDs-Embedded Molecularly Imprinted Polymer. *Biosensors and Bioelectronics* **2013**, *48*, 216–223. https://doi.org/10.1016/J.BIOS.2013.04.024.

(142) Lambert, J. B. Organic Structural Analysis. **1976**, 596.

(143) Ziylan, A.; Dogan, S.; Agopcan, S.; Kidak, R.; Aviyente, V.; Ince, N. H. Sonochemical Degradation of Diclofenac: Byproduct Assessment, Reaction Mechanisms and Environmental Considerations. *Environmental Science and Pollution Research* **2014**, *21* (9), 5929–5939. https://doi.org/10.1007/S11356-014-2514-7.

(144) Xu, S.; Lu, H.; Li, J.; Song, X.; Wang, A.; Chen, L.; Han, S. Dummy Molecularly Imprinted Polymers-Capped CdTe Quantum Dots for the Fluorescent Sensing of 2,4,6-Trinitrotoluene. *ACS Applied Materials and Interfaces* **2013**, *5* (16), 8146–8154. https://doi.org/10.1021/AM4022076/SUPPL_FILE/AM4022076_SI_001.PDF.

(145) Zhou, X.; Gao, X.; Song, F.; Wang, C.; Chu, F.; Wu, S. A Sensing Approach for Dopamine Determination by Boronic Acid-Functionalized Molecularly Imprinted Graphene Quantum Dots Composite. *Applied Surface Science* **2017**, *423*, 810–816. https://doi.org/10.1016/J.APSUSC.2017.06.199.

(146) Zhou, X.; Gao, X.; Liu, M.; Wang, C.; Chu, F. A Poly(5-Indolylboronic Acid) Based Molecular Imprint Doped with Carbon Dots for Fluorometric Determination of Glucose.

Microchimica Acta 2017 184:10 **2017**, *184* (10), 4175–4181. https://doi.org/10.1007/S00604-017-2448-0.

(147) Hong Liu, B.; Ting Dou, L.; He, F.; Yang, J.; Peng Li, Z. A Cobalt Coordination Compound with Indole Acetic Acid for Fabrication of a High Performance Cathode Catalyst in Fuel Cells. **2016**. https://doi.org/10.1039/c5ra27558j.

(148) Srivastava, A.; Shakya, A. K.; Kumar, A. Boronate Affinity Chromatography of Cells and Biomacromolecules Using Cryogel Matrices. *Enzyme and Microbial Technology* **2012**, *51* (6–7), 373–381. https://doi.org/10.1016/J.ENZMICTEC.2012.08.006.

(149) Weith, H. L.; Wiebers, J. L.; Gilham, P. T. Synthesis of Cellulose Derivatives Containing the Dihydroxyboryl Group and a Study of Their Capacity to Form Specific Complexes with Sugars and Nucleic Acid Components. *Biochemistry* **2002**, *9* (22), 4396–4401. https://doi.org/10.1021/BI00824A021.

(150) Lu, H.; Wei, D.; Zheng, R.; Xu, S. Post-Imprinting Modification Based on Multilevel Mesoporous Silica for Highly Sensitive Molecularly Imprinted Fluorescent Sensors. *Analyst* **2019**, *144* (21), 6283–6290. https://doi.org/10.1039/C9AN01503E.

(151) Lakowicz, J. R. Effects of Solvents on Fluorescence Emission Spectra. *Principles of Fluorescence Spectroscopy* **1983**, 187–215. https://doi.org/10.1007/978-1-4615-7658-7_7.

(152) Rambow, J.; Wu, B.; Rönfeldt, D.; Beitz, E. Aquaporins with Anion/Monocarboxylate Permeability: Mechanisms, Relevance for Pathogen-Host Interactions. *Frontiers in Pharmacology* **2014**, *5 AUG*. https://doi.org/10.3389/FPHAR.2014.00199.

(153) Sakharov, D. A.; Shkurnikov, M. U.; Vagin, M. Y.; Yashina, E. I.; Karyakin, A. A.; Tonevitsky, A. G. Relationship between Lactate Concentrations in Active Muscle Sweat

and Whole Blood. *Bulletin of Experimental Biology and Medicine* **2010**, *150* (1), 83–85. https://doi.org/10.1007/S10517-010-1075-0.